HEAT AND MASS TRANSFER OF A LOW PRESSURE MARS GREENHOUSE: SIMULATION AND EXPERIMENTAL ANALYSIS

By

INKA HUBLITZ

A DISSERTATION PRESENTED TO THE GRADUATE SCHOOL
OF THE UNIVERSITY OF FLORIDA IN PARTIAL FULFILLMENT
OF THE REQUIREMENTS FOR THE DEGREE OF
DOCTOR OF PHILOSOPHY

UNIVERSITY OF FLORIDA

2006

I dedicate this dissertation to my parents, Melitta and Bruno Hublitz, who have always supported my adventures and endeavors. Their love and guidance encouraged me to follow my dreams and to reach innumerable goals.

ACKNOWLEDGMENTS

First and foremost, I would like to express my deepest gratitude to my major advisor, Dr. Ray Bucklin, for giving me the unique opportunity to complete my Ph.D. program under his guidance. Furthermore, I am thankful that Dr. Bucklin encouraged me to participate in various conferences and international events, such as the International Space University's Summer Session Program in Australia. With his help I have constantly increased my network of colleagues working in relevant fields. Dr. Bucklin's help in realizing my stay at NASA's Kennedy Space Center was also highly appreciated.

I also acknowledge the members of my supervisory committee for their huge amount of support and advice. I especially would like to thank

- Dr. Jim Leary for his positive attitude that helped me enrich my people skills.
- Dr. Khe Chau for providing me with lab space.
- Dr. Raymond Wheeler for introducing me to Dr. Bucklin during my master's thesis research and for helping to organize my stay at NASA's Kennedy Space Center.
- Dr. David Hahn for his quick responses to all my questions and for being much more involved in the project than an external committee member generally is.

I am grateful to Dr. Sencer Yeralan for sharing his great expertise in the field of microcontrollers. At NASA's Kennedy Space Center I thank Dr. Vadim Rygalov, Dr. Phil Fowler and Dr. John Sager for their support. I am thankful to Dr. Hartwell Allen for teaching me how to grow plants and providing me with the right equipment. Bob Tonkinson's, Billy Duckworth's and Steve Feagle's hard work was always greatly appreciated.

My family and my husband, Sharath Cugati, deserve special thanks for their emotional and technical support. My gratitude also extends to my friends Dr. Peter Eckart and Dr. Kristian Pauly, for introducing me to the field of space life support systems and biospherics.

TABLE OF CONTENTS

page

ACKNOWLEDGMENTS iv

LIST OF TABLES ix

LIST OF FIGURES xi

ABSTRACT xv

CHAPTER

1 INTRODUCTION 1

Low Pressure Mars Greenhouses 1
Structure of the Dissertation 3

2 LITERATURE REVIEW 4

Advanced Life Support 4
Mars Environment 6
Plant Requirements and Environment Control 10
Temperature 11
Temperature effect 11
Temperature control 12
Relative Humidity 12
Relative humidity effect 12
Relative humidity control 13
Atmospheric Pressure and Composition 13
Carbon dioxide effect 13
Carbon dioxide control 14
Oxygen effect 14
Oxygen control 15
Vapor pressure effect and control 15
Pressurizing gas 15
Ventilation 15
Radiation 16
Radiation effects 16
Radiation control 17
Growth Area 19

Low Pressure Plant Growth Studies 19

3 OBJECTIVES OF THIS STUDY 23

4 EXPERIMENTAL WORK 24

System Description 24
Instrumentation and Sensor Calibration 28
Leakage Testing 32
Leakage of Vacuum Chamber 32
Leakage of Greenhouse Dome 34
Data Acquisition and Control System 36
Greenhouse Dome Environmental Control 37
Gas Composition and Total Pressure Control Algorithm 37
Air Temperature Control Algorithm 39
Heat and Mass Transfer Experiments without Plants 41
Heat and Mass Transfer Experiments with Plants 50
Medium-term Plant Experiment involving Buttercrunch Lettuce 50
Long-term Plant Experiment involving Galactic Lettuce 56

5 MATHEMATICAL MODEL DEVELOPMENT 65

Effect of Low Pressure on Heat and Mass Transfer 65
Convection Heat Transfer 65
Laminar flow over a horizontal plate 67
Turbulent flow over a horizontal plate 68
Laminar free convection on a vertical plate 69
External free convection for a sphere 70
Mass Transfer by Evaporation 71
Development of Low Pressure Psychrometrics for Non-Standard Atmospheres 72
Gas Theory 73
Equation of state 73
Dry gas mixture 74
Water vapor component 75
Construction of Modified Psychrometric Chart 75
Saturation line 75
Humidity isolines 77
Specific enthalpy isolines 78
Specific volume isolines 78
Vapor pressure isolines 79
Adiabatic saturation temperature isolines 79
Dew-point temperature isolines 80
One–dimensional Steady State Heat Transfer Model of the Greenhouse Dome 83
Overall Thermal Resistance Model 83
Individual Thermal Resistances and Thermal Coefficients 84
Total Thermal Resistance 90
Comparison of Radiation and Convection in the Chamber at Mars Pressure 92

Transient Heat Transfer Model for Greenhouse Temperature Simulation 93

6 RESULTS AND CONCLUSION.....98

7 FUTURE WORK.....100

APPENDIX

A STRUCTURAL ANALYSIS OF DOME SHELL, BASE PLATE AND CYLINDRICAL CALIBRATION CHAMBER 102

Structural Analysis of the Spherical Greenhouse Dome 102
Structural Analysis of Base Plate for Greenhouse Dome 103
Structural Analysis of the Base Plate without Additional Bracings 104
Structural Analysis of the Base Plate with Additional Bracings 106
Structural Analysis of Cylinder used as Sensor Calibration Chamber 112
Maximum Allowable Pressure 112
Short cylinder behavior 113
Intermediate cylinder behavior 113
Long cylinder behavior 114
Axial Buckling 114
Wall Yielding 115

B SENSOR CALIBRATION 116

Pressure 116
Temperature 117
Relative Humidity 117
Carbon Dioxide Concentration 118
Oxygen Concentration 119
Load Cells 121
Radiation 122
Amplification of Low Voltage Sensors 123

LIST OF REFERENCES 124

BIOGRAPHICAL SKETCH 129

LIST OF TABLES

Table		page
2-1	Human metabolism values per crew member and per day (CM-d) for average activity level.	5
2-2	Environment properties.	8
2-3	Atmosphere composition by volume.	8
2-4	Plant environment requirements.	10
2-5	Advanced life support crop growth conditions.	11
4-1	Sensors used to measure environmental parameters, the sensor ranges and accuracies.	29
4-2	Steady state temperature distribution under different freezer temperature, light and heating power conditions.	44
4-3	Buttercrunch lettuce environmental conditions and their control.	53
4-4	Evaporation rates per scale with scales 2-5 containing two lettuce plants each.	55
4-5	Galactic lettuce environmental conditions and their control.	57
5-1	Effect of reduced pressure on convective heat transfer coefficient and mass diffusion coefficient.	71
5-2	Psychrometric parameters of a low pressure atmosphere (76% N_2, 20% O_2, 4% CO_2) with initial conditions of 20 kPa dry air at 20°C and a constant specific volume of 0.004138m^3/kg.	80
5-3	Steady state temperature data of the long-term experiment involving Galactic lettuce plants.	86
5-4	Thermal resistances and coefficients based on the data obtained of the long-term experiment involving Galactic lettuce plants.	87
5-5	Simulated temperatures based on the thermal resistance model.	89
5-6	Comparison of measured and simulated temperature values.	90

5-7 Comparison of convection heat transfer to radiation heat transfer in the chamber at a pressure of 0.6 kPa.....93

A-1 Structural analysis of base plate without and with additional bracings. 112

LIST OF FIGURES

Figure page

1-1 "Astronaut" approaching University of Florida's Mars Greenhouse Dome. 2

2-1 Martian spectral irradiance (L_s=250, 15ºS, noon) vs. terrestrial spectral irradiance 9

2-2 Average solar irradiance of Mars compared to Earth.....10

2-3 Photosynthetic efficiency 16

4-1 Dome used to protect plants from the simulated low pressure, low temperature Mars environment. A) Empty dome. B) Dome with sensors, scales and flasks installed. 25

4-2 Vacuum chamber used to simulate the low pressure Mars environment (less than 1% of Earth's atmosphere). 26

4-3 Industrial walk-in freezer ensures low temperature of the vacuum chamber (simulated Mars environment). 26

4-4 Schematic of experimental setup.....28

4-5 Cylinder used for calibration of pressure-sensitive sensors and for initial gas mixing control algorithm development. 30

4-6 Comparison of Honeywell capacitance RH sensors to the HMP 237 reference RH sensor for pressures of 0 to 25 kPa. 31

4-7 Forces on chamber window. A) Vacuum chamber at 0.6 kPa with top window bulging in. B) Gasket drawn into the chamber due to pressure difference. 33

4-8 Dome and chamber leakage with gas resupply and vacuum pumps turned off at a temperature of -10 ºC. 35

4-9 Comparison of vacuum chamber and greenhouse dome leak rates to values of other low pressure plant growth studies (leak rate is presented in logarithmic scale).....35

4-10 Gas mixing of dome greenhouse atmosphere without plants (oxygen set point at 4.0 kPa and carbon dioxide set point at 0.5 kPa). 38

4-11 Pressure control of vacuum chamber (set point 0.6 kPa) and greenhouse dome (set points 20 kPa). 39

4-12 Air temperature control of greenhouse dome (set point at 20 ºC).....40

4-13 Sensor locations for heat and mass transfer experiments without plants. 41

4-14 Preparation of the steady state experiments. A) Bottom of dome base with foam insulation. B) Side view of greenhouse dome with the sensors and scales installed. C) Top view of greenhouse dome without shell. D) Installation of greenhouse dome into the vacuum chamber. 42

4-15 Temperature readings until steady state is achieved. (0 ºC freezer temperature, 26 W heating power and light switched off). 43

4-16 Steady state temperatures versus power of heater at seven different locations (T_1-T_7). Freezer temperature is 0 ºC and the growth light is switched off. 44

4-17 Steady state temperatures versus power of heater at seven different locations (T_1-T_7). Freezer temperature is -10 ºC and the growth light is switched off. 45

4-18 Steady state temperatures versus power of heater at seven different locations (T_1-T_7). Freezer temperature is -20 ºC and the growth light is switched off. 45

4-19 Steady state temperatures versus power of heater at seven different locations (T_1-T_7). Freezer temperature is -10 ºC and the growth light is switched on. 46

4-20 Steady state temperatures versus power of heater at seven different locations (T_1-T_7). Freezer temperature is -20 ºC and the growth light is switched on. 46

4-21 Steady state air temperatures (T_3) versus power of heater for freezer temperatures of 0 ºC, -10 ºC and -20 ºC (growth light switched off).....47

4-22 Freezer temperature versus power of heater for steady state air temperatures (T_3) of 15 ºC, 20 ºC and 25 ºC. 48

4-23 Condensation inside of greenhouse shell with a greenhouse air temperature of 20 ºC. A) Freezer temperature at 0 ºC. B) Freezer temperature at -20 ºC.....50

4-24 Buttercrunch lettuce in Ehrlenmeyer flask. A) The average height of the shoot zone is 15 cm. B) Putty and a stopper prevent evaporation of the hydroponic solution as they separate the root from the shoot zone. 51

4-25 Installation of flasks containing the lettuce plants onto the scales.....52

4-26 Constant temperature distribution and varying relative humidity during the buttercrunch lettuce experiment. 53

4-27 Plant evapo-transpiration rates of plants from 5 to 10 hours after the beginning of the experiment. 55

4-28 Lettuce plants after an exposure of 36 hours to the controlled Mars greenhouse environment. Healthy plant without any visible physical damage on the left side, wilted plant with roots that do not reach water and nutrient supply on the right side. 56

4-29 Galactic lettuce plant for long-term experiments with an average height of 8 cm. .57

4-30 Sensor locations for the long-term experiments with galactic lettuce plants. 58

4-31 Temperature variations during the long-term galactic lettuce experiment. 59

4-32 Comparison of steady state temperature distribution of the day cycle to the night cycle during the long-term plant experiments. 60

4-33 Relative humidity variation during the day and night cycle. 61

4-34 Gas composition control of the greenhouse atmosphere. Set points are 20 kPa for total pressure, 4 kPa for oxygen partial pressure and 0.8 kPa for carbon dioxide partial pressure. 62

4-35 Water evaporation measured on scale 2 and 3 during the galactic lettuce plant experiment. 63

4-36 Galactic lettuce plants after exposure of seven days to the low pressure Mars greenhouse environment. 63

4-37 Visible damages of the plants. A) and B) Wilting/drying of the plant leaves..... 64

5-1 Effect of pressure on the saturation line of an open system with standard atmosphere composition..... 72

5-2 Psychrometric chart of low pressure atmosphere (76% N_2, 20% O_2, 4% CO_2) with initial conditions of 20 kPa dry air at 20°C and a constant specific volume of 0.004138m^3/kg. 82

5-3 Heat transfer of greenhouse dome and thermal resistance circuit. 84

5-4 Emissivities of the polycarbonate dome and the stainless steel chamber (light off). 87

5-5 Emissivities of the polycarbonate dome and the stainless steel chamber (light on)..... 88

5-6 Required heating power versus temperature difference of the dome air to the freezer. Slope of linear regression is the total thermal resistance (light off). 91

5-7 Required heating power versus temperature difference of the dome air to the freezer. Slope of linear regression is the total thermal resistance (light on). 91

5-8 Simulation of greenhouse atmosphere, dome and vacuum chamber temperatures (light off, 51W heating power, -10° C freezer temperature). 96

5-9 Simulation of greenhouse atmosphere, dome and vacuum chamber temperatures (light off, 77 W heating power, -10° C freezer temperature). 96

5-10 Simulation of greenhouse atmosphere, dome and vacuum chamber temperatures (light off, 103 W heating power, -10° C freezer temperature). 97

5-11 LabView front panel of overall model for simulation. 97

7-1 Ice building up on the bottom part of the greenhouse shell. A) Overview. B) Detailed view of the ice-crystals. 101

A-1 Bottom view of greenhouse dome base. 103

A-2 Triangular load over full beam. 104

A-3 Trapezoidal load over part of the beam. 106

A-4 First part of superposition: uniform load for x>a. 107

A-5 Second part of superposition: triangular load for x>a. 108

A-6 Bending moments of beam for trapezoidal load varies with the distance a of the additional bracing. 110

B-1 Pressure sensor #1 calibration. 116

B-2 Pressure sensor #2 calibration. 117

B-3 Carbon dioxide sensor calibration. 118

B-4 Carbon dioxide sensor calibration. 119

B-5 Oxygen sensor #1 calibration. 120

B-6 Oxygen sensor #1 calibration. 120

B-7 Oxygen sensor #2 calibration. 121

B-8 Oxygen sensor #2 calibration. 121

B-9 Load cell calibration. 122

B-10 Amplifier circuit. 123

Abstract of Dissertation Presented to the Graduate School
of the University of Florida in Partial Fulfillment of the
Requirements for the Degree of Doctor of Philosophy

HEAT AND MASS TRANSFER OF A LOW PRESSURE MARS GREENHOUSE:
SIMULATION AND EXPERIMENTAL ANALYSIS

By

Inka Hublitz

May 2006

Chair: Ray A. Bucklin
Major Department: Agricultural and Biological Engineering

Biological life support systems based on plant growth offer the advantage of producing fresh food for the crew during a long surface stay on Mars. Greenhouses on Mars are also used for air and water regeneration and waste treatment. A major challenge in developing a Mars greenhouse is its interaction with the thin and cold Mars environment. Operating a Mars greenhouse at low interior pressure reduces the pressure differential across the structure and therefore saves structural mass as well as reduces leakage.

Experiments were conducted to analyze the heating requirements as well as the temperature and humidity distribution within a small-scale greenhouse that was placed in a chamber simulating the temperatures, pressure and light conditions on Mars. Lettuce plants were successfully grown inside of the Mars greenhouse for up to seven days. The greenhouse atmosphere parameters, including temperature, total pressure, oxygen and

carbon dioxide concentration were controlled tightly; radiation level, relative humidity and plant evapo-transpiration rates were measured.

A vertical stratification of temperature and humidity across the greenhouse atmosphere was observed. Condensation formed on the inside of the greenhouse when the shell temperature dropped below the dew-point. During the night cycles frost built up on the greenhouse base plate and the lower part of the shell. Heat loss increased significantly during the night cycle. Due to the placement of the heating system and the fan blowing warm air directly on the upper greenhouse shell, condensation above the plants was avoided and therefore the photosynthetically active radiation at plant level was kept constant. Plant growth was not affected by the temperature stratification due to the tight temperature control of the warmer upper section of the greenhouse, where the lettuce plants were placed.

A steady state and a transient heat transfer model of the low pressure greenhouse were developed for the day and the night cycle. Furthermore, low pressure psychrometric relations for closed systems and modified atmospheres were generated to calculate the properties of the moist air in order to predict condensate formation. The results of this study improve the design of the environmental control system leading to an optimization of plant growth conditions.

CHAPTER 1
INTRODUCTION

Low Pressure Mars Greenhouses

Mars greenhouses are important components of the human Mars mission infrastructure as plant-based life support systems offer self-sufficiency and possibly cost reduction. Resupply is prohibitive for long duration Mars missions as it increases the launch mass and consequently the launch costs. Relying on frequent resupply from Earth also increases risk to the astronauts. Greenhouses produce edible biomass as well as regenerate the air and water through photosynthesis.

The atmospheric surface pressure on Mars is on average 0.61 kPa, i.e., below 1% of Earth's standard atmospheric pressure (NASA, 2004). Operating a greenhouse at low interior pressure reduces the pressure differential across the structure and therefore saves structural mass as well as reduces leakage. Studies have shown that plant growth is feasible at pressures as low as 20 kPa; plants even survive short-term exposure to pressures as low as 10 kPa (Andre and Richaud, 1986; Fowler *et al.*, 2002). Inflatable greenhouse structures are being studied as they offer the advantage of a high volume to mass ratio, and can be packed efficiently for the transit, reducing the number of launches (Clawson *et al.*, 1999; Kennedy, 1999; Hublitz, 2000).

A major challenge in developing a Mars greenhouse is its interaction with the thin and cold Mars environment. The environmental conditions inside the greenhouse have to be controlled within the ranges where plants are highly productive. Transparent structures capture day-time solar radiation that is required for photosynthesis and heating of the

greenhouse, whereas during the night they have to be covered with multi-layered insulation to avoid heat loss (Hublitz, 2000).

Most experimental Mars greenhouse studies have focused on the ability of plants to grow at reduced pressures with non-standard atmosphere compositions, but little research has been done on the thermal interactions of the greenhouse with the Mars environment. The heat and mass transfer analysis is an important step in the design of the thermal control system that provides the climatic environment essential for plant growth.

Figure 1-1. "Astronaut" approaching University of Florida's Mars Greenhouse Dome.

Structure of the Dissertation

Chapter 1 introduces the importance of research on the heat and mass transfer of low pressure Mars greenhouses and gives an outline of this dissertation. Chapter 2 states the objectives of advanced life support systems, summarizes the fundamental knowledge of the Mars environment and reviews the literature on low pressure plant growth studies. The objectives of this dissertation are discussed in Chapter 3. Chapter 4 describes the setup of the experimental work, the data acquisition and the control system. Data of the heat and mass transfer experiments with and without plants are presented. The mathematical model development and simulation results are discussed in Chapter 5. Chapter 6 gives results and conclusions; Chapter 7 states recommendations for future studies. The structural analyses of the greenhouse dome and sensor calibration cylinder as well as the sensor calibration are included in the appendices.

CHAPTER 2
LITERATURE REVIEW

Advanced Life Support

The goal of NASA's Advanced Life Support (ALS) Project (National Aeronautics and Space Administration (NASA), 2002), is to "provide life support self-sufficiency for human beings to carry out research and exploration productively in space for benefits on Earth and to open the door for extended on-orbit stays and planetary exploration."

For long-duration missions open loop life support systems have to be replaced by closed loop life support systems, in order to avoid the high costs associated with the launch and storage of consumables and high risk of relying on frequent resupply missions. Advanced life support systems should not only provide a high degree of closure of the air and water loop, but also begin to close the food loop (Eckart, 1996).

In contrast to the life support systems for the current short-duration missions, biological processes, in addition to physico-chemical processes, such as food production utilizing higher plants will be implemented for long-duration missions (Duffield, 2003). Valuable chemicals will be recovered by processing solid waste. In-situ resources, where available, may also be used to replenish life support consumables. Consumables for human space missions amount to approximately 31 kg of oxygen, water and food per astronaut and per day as listed in Table 2-1. Simultaneously, the same amount of waste is created. Physico-chemical life support systems can provide oxygen, reduce carbon dioxide and recycle water, whereas biological life support systems can fulfill all these functions and additionally produce food (Eckart, 1996).

Table 2-1. Human metabolism values per crew member and per day (CM-d) for average activity level.

Consumable	Units	Needs	Effluents
Air			
Carbon Dioxide Load	kg/CM-d		1.00
Oxygen Consumed	kg/CM-d	0.84	
Food			
Mass of Consumed Food (dry basis)	kg/CM-d	0.62	
Energy of Consumed Food	MJ/CM-d	11.82	
Potable Water Consumed (incl. water in food)	kg/CM-d	3.91	
Thermal			
Sensible Metabolic Heat Load	MJ/CM-d		6.31
Latent Metabolic Heat Load	MJ/CM-d		5.51
Waste			
Fecal Solid Waste (dry basis)	kg/CM-d		0.03
Perspiration Solid Waste (dry basis)	kg/CM-d		0.02
Urine Solid Waste (dry basis)	kg/CM-d		0.06
Water			
Fecal Water	kg/CM-d		0.09
Respiration and Perspiration Water	kg/CM-d		2.28
Urine Water	kg/CM-d		1.89
Hygiene Water			
Hygiene Water (Flush, Hand Wash, Shower, Laundry, Dish Wash)	kg/CM-d	25.58	
Greywater	kg/CM-d		25.58
Total Mass	**kg/CM-d**	**30.95**	**30.95**
Total Energy	**MJ/CM-d**	**11.82**	**11.82**

Source: Hanford, 2004.

The objectives of ALS systems based on plant growth are to (NASA, 2002)

- Produce food that meets human requirements for nutrition, sensory acceptability and food safety.
- Provide the environmental and cultural requirements to produce crops, including efficient environmental control (temperature, relative humidity, gas composition), the lighting intensity and spectral composition, the growth area, and nutrient delivery system.
- Provide post-harvest processing, materials handling and storage of harvested products.
- Utilize resources recovered from other life support systems, including carbon dioxide, waste water and solid wastes.
- Provide non-food products to other life support systems for utilization, further processing or disposal, including oxygen, transpired water, heat and inedible biomass.

- Minimize required involvement of the crew in life support operations.
- Minimize the impact of life support on planetary environments.

For the development of bioregenerative life support systems for Mars, it is critical to develop models to predict system behavior in the planetary environment and to evaluate the performance through experiments in a simulated Mars environment.

Mars Environment

The Mars environment differs from that on Earth in several significant ways including lower gravity, very low density atmosphere rich in carbon dioxide, reduced light levels and very cold ambient temperatures.

The Mars atmosphere is highly variable on a daily, seasonal and annual basis. The thinness of the atmosphere and the lower solar constant (which is 43% of the terrestrial value) guarantee a large daily temperature range at the surface under clear conditions. On an annual basis, the atmospheric pressure at the surface changed from 0.69 to 0.9 kPa at the Viking 1 lander site due to condensation and sublimation of CO_2 (NASA, 2004). The mean atmospheric pressure is estimated at 0.64 kPa.

Although Mars has no liquid water and its atmospheric pressure is approximately 1.0 percent that of Earth, many of its meteorological features are similar to the terrestrial ones. Water ice clouds, fronts with wind shifts and associated temperature changes similar in nature to those on Earth can be found. The main differences between the Earth and the Mars atmosphere are that the Mars atmosphere does not transfer as much heat by conduction and convection as the Earth atmosphere and it cools much faster by radiation. Mars' diurnal temperature cycle is larger than Earth's: 184 to 242 K during the summer but stabilized near 150 K (CO_2 frost point) during the winter (Kaplan, 1988; NASA, 2004). Water ice clouds occur due to many different causes just as on Earth. Nighttime

radiation cooling produces fogs; afternoon heating causes drafts which cool the air and cause condensation; flow over topography causes gravity clouds; and cooling in the winter polar regions causes clouds (Kaplan, 1988).

Mars has local dust storms of at least a few hundred kilometers in extent. The duration and extent of Martian dust storms vary greatly. Dust storms of planetary scale may occur each Martian year with a velocity of up to 30 m/s. Unfortunately, neither Earth based nor spacecraft observations have been systematic enough to quantify the frequency of dust storm occurrence or even the true extent of many individual storms. There is no reliable method for prediction of great dust storms. They mainly occur during southern spring and summer. Local dust storms have been observed on Mars during all seasons, but they are most likely to occur during the same periods as the great dust storms. The physical grain size of the drifting material is estimated to be 0.1 to 10 μm. It has the characteristics of very fine grained, porous materials with low cohesion (Kaplan, 1988).

The dust raised into the atmosphere by dust storms and the ordinary atmospheric dust always present in the atmosphere settle out of the atmosphere onto any horizontal surface. Measurements made by the Pathfinder Mission showed a 0.3% loss of solar array performance per day due to dust obscuration (Kaplan *et al.*, 2000). This dust deposition could be a significant problem for a greenhouse operated with solar light for long duration missions, unless a technique is developed to remove the dust periodically or prevent settled dust from coating the greenhouse surface.

The Mars atmosphere consists mainly of carbon dioxide (95.3%). Photosynthesis requires carbon dioxide which could be taken out of the planet's carbon dioxide rich

atmosphere, in case of an autonomous greenhouse that is pre-deployed before the first humans arrive.

In Table 2-2 the Mars environment properties are summarized. Table 2-3 describes the composition of the atmosphere of Mars in terms of the gases present by volume.

Table 2-2. Environment properties.

Property	Value - Mars	Value - Earth
Orbit period	687 days	365 days
Rotation period (day length)	24.62 hours	23.93 hours
Gravity	3.69 m/s²	9.81 m/s²
Surface Pressure	~ 0.64 kPa (variable, depending on season and location) 0.69 to 0.9 kPa at Viking 1 lander site (22º N lat.)	101.4 kPa (at sea level)
Surface density	~ 0.020 kg/m³	1.217 kg/m³
Average temperature	~ 210 K	288 K
Diurnal temperature range	184 to 242 K (summer) 150 K (winter)	283 to 293 K
Wind speeds	2 to 7 m/s (summer) 5 to 10 m/s (fall)	0 to 100 m/s
Solar irradiance in orbit	589 W/m²	1368 W/m²
Drifting material		
Size	0.1 to 10 μm	
Cohesion	1.6±1.2 kPa	

Source: Carr, 1981; Kaplan, 1988; NASA, 2004.

Table 2-3. Atmosphere composition by volume.

Gas	Value - Mars	Value - Earth
Carbon Dioxide (CO_2)	95.32 %	0.035 %
Nitrogen (N_2)	2.7 %	78.084%
Argon (Ar)	1.6 %	0.93%
Oxygen (O_2)	0.13%	20.946%
Carbon Monoxide (CO)	0.08%	-
Water (H_2O)	210 ppm	Highly variable (typically 1%)
Nitrogen Oxide(NO)	100 ppm	-
Neon (Ne)	2.5 ppm	18.18 ppm
Hydrogen-Deuterium-Oxygen (HDO)	0.85 ppm	-
Krypton (Kr)	0.3 ppm	1.14 ppm
Xenon (Xe)	0.08 ppm	-
Helium (He)	-	5.24 ppm
CH_4	-	1.7 ppm
Hydrogen (H_2)	-	0.55 ppm

Source: NASA, 2004.

The solar irradiance varies as a function of season, latitude, time of day and optical depth of the atmosphere. The solar irradiance incident on the surface of Mars consists of two components: the direct beam and the fuse component. The fuse component comprises the scattering by small particles in the atmosphere and the diffuse skylight. The solar radiation on Mars varies according to the eccentricity of the Mars orbit. The mean solar radiation in Mars orbit is 589 W/m². The ultraviolet radiation that reaches the Mars surface is much greater than on Earth, because the Martian atmosphere is more tenuous and there is very little ozone. The ultraviolet radiation is mainly absorbed by carbon dioxide; all ultraviolet radiation with a wavelength less than 200 nm is absorbed by the atmosphere (Kaplan, 1988). The available photosynthetically active radiation (PAR) changes throughout the Mars season. The average PAR is estimated to be 20.8 mol/(m² day) (Gertner, 1999).

Figure 2-1 depicts the spectrum of the solar radiation on Mars. Dust affects both the intensity and the spectral content of the sunlight. The solar irradiance on the surface of Mars during a global dust storm is comparable to the one of a cloudy day on Earth (see Figure 2-2).

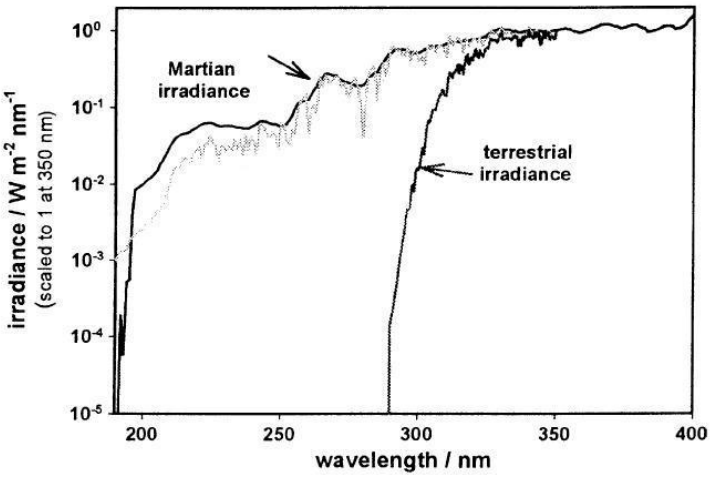

Figure 2-1. Martian spectral irradiance (L_s=250, 15ºS, noon) vs. terrestrial spectral irradiance (Rettberg *et al.*, 2004)

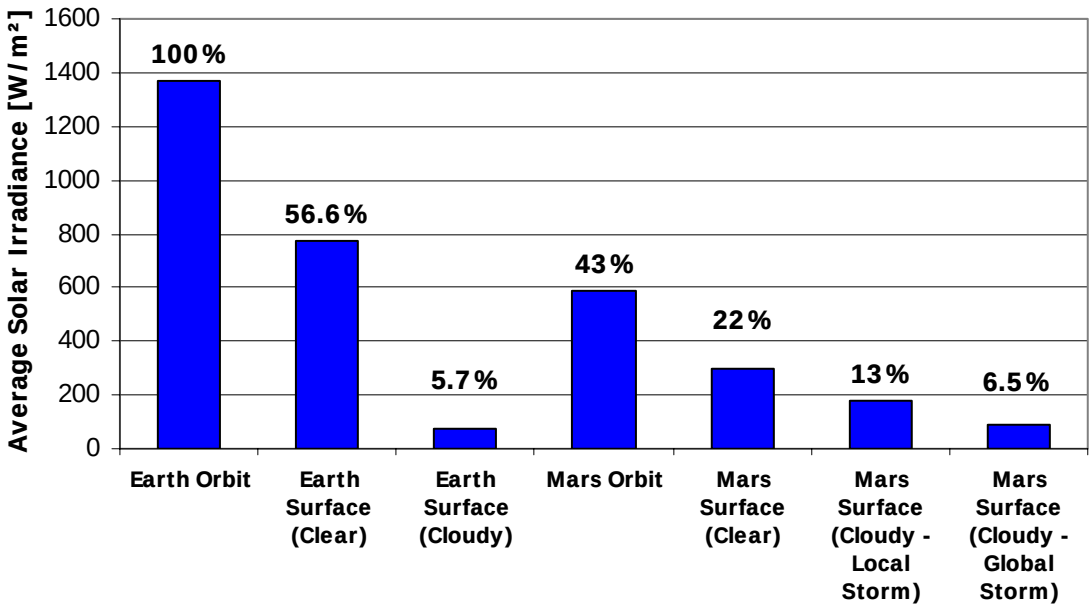

Figure 2-2. Average solar irradiance of Mars compared to Earth (Clawson *et al.*, 1999).

Plant Requirements and Environment Control

High yields in plant growth chambers can be achieved by controlling temperature, relative humidity, atmosphere pressure and composition, ventilation, light intensity and spectral quality, water and nutrient delivery. Table 2-4 lists the minimum, maximum and optimum environmental parameters. The optimal growth conditions depend on the type of crop. A list of crops identified for ALS application and the required environmental condition is shown in Table 2-5.

Table 2-4. Plant environment requirements.

Parameter	Unit	Low Value	High Value	Optimal Value
Temperature	ºC	+5.0	+35	+20 to +27
Atmospheric Pressure	kPa	10.0 (?)	100	100
Photosynthetically active radiation	W/m²	50	500	150 to 200
Partial Pressure CO_2	kPa	0.03	3.0 to 5.0	0.1 to 0.2
Partial Pressure O_2	kPa	5.0	27 to 30	10(?) to 22
Relative Humidity	%	55	100	70 to 85

Source: Rygalov *et al.*, 2000.

Table 2-5. Advanced life support crop growth conditions.

Crop	Photo-synthetic Photon Flux [mol/m²-d]	Diurnal Photoperiod [h/d]	Growth Period [days after planting]	Air Temperature - Day [ºC]	Air Temperature - Night [ºC]
Cabbage	17		85	>25	
Carrot	17		75	16-18	
Chard	17	16	45	23	23
Celery	17		75		
Dry Bean	24	18	85	28	24
Green Onion	17		50		
Lettuce	17	16	28	23	23
Onion	17		50		
Pea	24		75		
Peanut	27	12	104	26	22
Pepper	27		85		
Radish	17	16	25	23	23
Red Beet	17	16	38	23	23
Rice	33	12	85	28	24
Snap Bean	24		85	28	24
Soybean	28	12	97	26	22
Spinach	17	16	30	23	23
Strawberry	22	12	85	20	16
Sweet Potato	28	12	85	26	22
Tomato	27	12	85	24	24
Wheat	115	20-24	79	20	20
White Potato	28	12	132	20	16

Source: Hanford, 2004.

Temperature

Temperature effect

Temperature is an important physical parameter for controlling plant growth. It has a direct effect on biochemical reaction rates in the various metabolic processes and can indirectly contribute to water stress by enhancing transpiration (Downs and Hellmers, 1975). The various biochemical reactions have different minimum, maximum and optimum temperatures. Up to 30 ºC temperature affects plant growth positively by more rapid leaf expansion and increased root initiation (Albright *et al.*, 2001). In general, most plants grow well at a temperature from 10 to 30 ºC. Excessive temperatures result in heat damage; temperatures below this range lead to chilling and/or freeze damage. The

severity of the damage increases with increasing temperature difference and the time the plant spends in this unfavorable condition.

Temperature control

In order to control the air temperature of a Mars greenhouse, it is essential to analyze the heat and mass balance of the greenhouse and its environment. Heat received by the greenhouse through solar radiation or waste heat of internal electric equipment may lead to a rise of the temperature. Convective, conductive and radiative heat loss of the greenhouse to the environment may result in a decreasing internal greenhouse temperature. Furthermore, the addition and removal of latent heat by evaporation and condensation of water directly affect the plant as well as the greenhouse temperature.

Air temperature can be increased by addition of heat to the greenhouse such as by turning on the heating system. Temperature is decreased by removing heat from the greenhouse such as by utilization of cooling coils or maximizing heat emission of the greenhouse structure to the Mars environment. Temperature uniformity within a greenhouse is achieved by vertical ventilation.

Relative Humidity

Relative humidity effect

Relative humidity is an indicator of potential water loss from the plants as it is a function of the water vapor pressure. Transpiration rates of plants increase as the vapor pressure deficit between the cells of the leaf and the atmosphere increases. At a given temperature, the vapor pressure deficit increases rapidly with decreasing humidity. The balance and dynamics of water loss by transpiration and gain by root absorption determine the plant water status. Water stress and possibly wilting can be caused by a high transpiration rate and vapor pressure deficit.

Humidity also reduces the incident radiation on plants through absorption of infrared radiation leading to a higher specific heat of the air. Condensation and evaporation affect the energy balance and therefore the air temperature.

70-85% relative humidity is considered to be the optimal range for plant growth (Tibbitts, 1979). Low relative humidity levels cause wilting of the plants; high relative humidity levels lead to development of fungus and mold.

Relative humidity control

In a closed environment, humidity is increased by evaporation of open water sources or evapo-transpiration of the plants. Humidity levels are reduced by condensation. Humidity control can be achieved by studying the underlying psychrometric relationships which are explained in detail in the psychrometrics section at the end of Chapter 5.

Atmospheric Pressure and Composition

The greenhouse atmosphere is composed of essential gases required for plant growth (such as carbon dioxide, oxygen and water vapor) and some non-essential gases (such as nitrogen) for pressurizing the greenhouse structure. The total pressure of the greenhouse atmosphere is the sum of the partial pressures of the gases.

Carbon dioxide effect

Apart from light and water, carbon dioxide is required for photosynthesis and therefore plant growth. Plant response to increased/decreased carbon dioxide levels depends on plant species, development stage, irradiance, temperature and mineral nutrition (Langhans and Tibbitts, 1997). Slightly elevated carbon dioxide during the day may lead to increased biomass production, whereas highly elevated carbon dioxide levels can be toxic for plants. As net photosynthesis increases with elevated carbon dioxide

concentration (up to 0.5 kPa), transpiration may decrease due to stomatal closure and leaf temperatures could rise (Wheeler, 2000). Thus, benefits from elevated carbon dioxide concentrations can be reduced by higher leaf temperatures. On the other hand, studies showed that at super-elevated levels of carbon dioxide concentration (0.5-1.0kPa) leaf transpiration and plant water use increased significantly for some species (Wheeler, 2000). Plant photosynthesis and hence growth responses to carbon dioxide generally show near linear increases at the low concentrations (up to 0.15 kPa), after which rates either saturate or eventually taper off. Carbon dioxide concentration below terrestrial ambient levels (370 ppm) decreases photosynthesis and plant growth (Langhans and Tibbitts, 1997).

Carbon dioxide control

If carbon dioxide is not controlled in a plant growth chamber, it will decrease during the day when it is used for photosynthesis. During the night the amount of carbon dioxide increases due to plant respiration. Carbon dioxide that is taken up by the plants for photosynthesis has to be replenished to the greenhouse atmosphere. In case of an autonomous greenhouse, pre-deployed before human arrival, carbon dioxide is not available as a byproduct of the human metabolism and should be taken out of the carbon dioxide rich Mars atmosphere.

Oxygen effect

Oxygen is important for respiration, especially at night when there is no photosynthetically generated oxygen. Probably at least 5 kPa of oxygen is needed to sustain plant growth (Quebedeaux and Hardy, 1973). Partial pressure of oxygen is especially critical for the root-zone respiration. The upper limit of oxygen partial pressure

can be set at 23.5%, because above this there are safety concerns related to fire risks (Lacey *et al.*, 2000).

Oxygen control

Photosynthesis produces oxygen and therefore the oxygen levels will build up in a greenhouse over time. Thus, oxygen has to be scrubbed out of the atmosphere or used by humans in order to keep the oxygen level constant.

Vapor pressure effect and control

The effect and control of relative humidity have been described above. Under Earth atmospheric pressure in an open system, the change in vapor pressure has minimal effect on total pressure, but in a totally closed system at low pressure, fluctuations in vapor pressure will significantly influence total pressure (Bucklin *et al.*, 2004). This effect is explained in detail in the psychrometrics section in Chapter 5.

Pressurizing gas

Nitrogen and argon are two inert gases that may be used as pressurizing gases. In case of a Mars greenhouse both of the gases could be used, as they are available in the Mars atmosphere, so they could be extracted locally. Nitrogen and argon are biologically inert. They would be used as make-up gases in order to increase the total pressure required for the inflatable structure.

Ventilation

The ventilation system ensures a homogenous gas mix in terms of gas composition, temperature and humidity inside of the greenhouse. Furthermore, ventilation provides a minimum air velocity over the plants to facilitate gas exchange required for photosynthesis. On the other hand, excessive air movement through the crop canopy leads to increased transpiration and potential water stress (Albright *et al.*, 2001).

Radiation

Radiation effects

Electromagnetic radiation is the energy source for plant growth. Radiation controls photosynthesis not only through the intensity but also through the spectral distribution and photoperiod.

For photosynthesis, plants require photosynthetically active radiation in the wavelengths between 400 and 700 nm. Photosynthetic efficiency decreases in the region of 500 to 600 nm where radiation is not absorbed well by the chlorophyll, giving the plants their characteristic green appearance (see Figure 2-3).

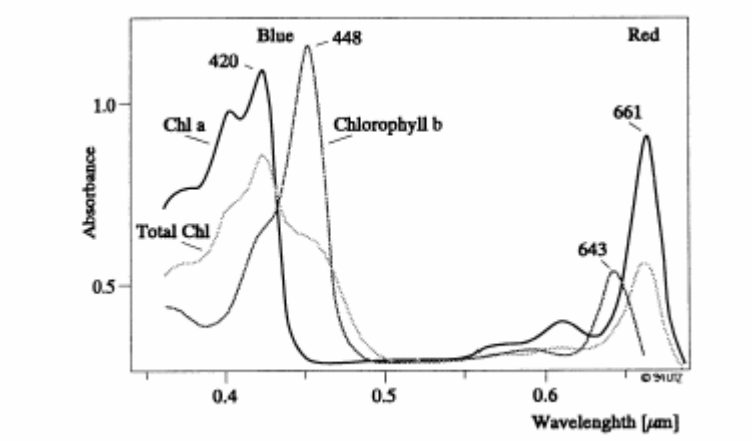

Figure 2-3. Photosynthetic efficiency (Eckart, 1996).

The radiation intensity required to saturate C-3 plants is around 300 μmol/m²-s for a daily photoperiod of 16 hours; C-4 plants require at least 500 μmol/m²-s for a daily photoperiod of 16 hours (Langhans and Tibbitts, 1997).

Shade leaves tend to be larger, thinner, and contain more chlorophyll per unit weight than do sun, i.e., bright light-grown leaves (Boardman, 1977). But sun leaves have higher photosynthetic capacities. As a consequence, low levels of photosynthetically active radiation result in bigger leaves, elongation of internodes and less dry weight,

whereas high light levels lead to stimulation of auxiliary branch growth and possibly to photodestruction of chlorophyll. Excess radiation may cause heating of the leaves and desiccation due to water loss (Langhans and Tibbitts, 1997).

Radiation control

Shading can lower radiation intensity and filters can change the spectrum. On Mars the low levels of solar radiation may have to be supplemented by light collection systems or by electric light. Options for electric lights suitable for plant growth are: Incandescent lamps, fluorescent lamps, high-intensity discharge lamps (e.g. metal halide lamps, high pressure sodium lamps), xenon lamps and light emitting diodes.

Incandescent light is blackbody radiation as it is created by a heated body. The spectrum depends on the temperature of the heated element. Most of the energy from incandescent lights is in the infrared-region. The infra-red radiation is not useful for photosynthesis and must be dissipated from the growth chamber. The spectrum can be shifted by changing the voltage to the lamp; the higher the voltage the lower the ratio of infra-red to visible radiation. Another method of altering the spectrum is the use of filters. Wavelengths not useful for photosynthesis can be filtered out. The disadvantage of this method is that the overall radiation is reduced. Incandescent lamps have a very low efficiency, not more than 10% of the output radiation is within the visible wavelengths (Langhans and Tibbitts, 1997).

Fluorescent Lamps have many advantages over incandescent lamps. The radiation output is continuous, generally uniform and the photosynthetically active radiation is high. Their optimal operation temperature is only about 38° C. In order to alter the spectrum of the fluorescent lamps the inner wall of the tubes, which emits the radiation, can be coated with different phosphors. Most fluorescent plant growth lamps are coated

with a special phosphor mix to provide an enhanced blue and red spectrum. Cool white lamps are the most efficient fluorescent lamps, with efficiencies of around 20%. Output of very high output lamps decreases to 70% after the lamps have been operated for 1 year, 16 hours per day (Langhans and Tibbitts, 1997; Schwarzkopf, 1990).

High-intensity discharge lamps excite elements in the arc in order to emit characteristic wavelengths. Their spectrum is uniform but not continuous. Irradiances are higher than those of incandescent and fluorescent lamps. Two commonly used high-intensity discharge lamps are metal halide and high-pressure sodium lights. In contrast to fluorescent lamps the output radiation of metal halide lamps is not affected by the ambient temperature. Most of the radiation output is in the 400-700 nm but output can shift with lamp age. The efficiency of metal halide lamps is around 22%. The radiation output of high pressure sodium lamps is concentrated in the 550-650 nm range, and very scarce in the 400-550 nm range. High pressure sodium lights are useful in combination with alternative lighting options such as metal halide, blue phosphor and cool-white fluorescent lamps. High pressure sodium lights are very efficient with efficiencies of 25% (Langhans and Tibbitts, 1997; Schwarzkopf, 1990).

Xenon lamps are rarely used for plant growth chambers even though they have a spectrum similar to the solar spectrum. Their disadvantages include the high cost and their emission of ultraviolet radiation, which leads to development of ozone. Furthermore, the high infra-red radiation increases the cooling load of the plant growth chamber (Langhans and Tibbitts, 1997).

Light emitting diodes (LEDs) are very useful for plant growth as certain LEDs have specific outputs required for photosynthesis. Moreover, they are solid state devices and

have a long operating life. Blue and red LEDs can be combined to fulfill the plant needs (Langhans and Tibbitts, 1997).

Growth Area

The size of the Mars greenhouse depends on the number of astronauts and the desired amount of food grown locally vs. shipped from Earth. The required plant-growth area per person can be estimated at 50 m² to fulfill 100% of the food requirements (Wheeler *et al.*, 2001). Food, if grown on-site, can regenerate some or all of the crew's air and water. If more than about 25% of the food, by dry mass, is produced locally, all the required water can be regenerated by the same process. If approximately 50% or more of the food, by dry mass, is produced on site, all the required air can be regenerated by the same process depending on the crop and growth conditions (Wheeler *et al.*, 2001; Hanford, 2004).

Low Pressure Plant Growth Studies

Operating a greenhouse on Mars at low internal pressure reduces the pressure differential across the structure and therefore saves structural mass as well as reduces leakage. The literature contains a variety of studies on the plant responses to low pressure. The lower limits of oxygen, carbon dioxide, water vapor and inert gases that plants can tolerate and thrive in are a key in the development of hypobaric Mars greenhouses.

Studies on plant responses to low pressure date back to the 1960s, when NASA first considered the implementation of biological life support systems. These studies include research at Brooks Air Force Base where the plant environment pressure was dropped to 51 and 93 kPa and other research Wright-Patterson Air Force Base with an

even lower pressure of 1/3 atmosphere. No adverse effects on plant growth due to low pressure were observed (Corey *et al.*, 2002).

Further studies focused on the effect of the different atmosphere components on the seed germination, seedling development and plant growth. Andre and Richaud (1986) and Andre and Massimino (1992) evaluated if an inert gas such as nitrogen is necessary for plant growth by studying barley at 7 kPa. They concluded that nitrogen is not necessary for plant growth. An increased transpiration rate was observed at this low pressure. Furthermore, these studies demonstrated that growth of wheat is possible at a total pressure as low as 10 kPa. Wheat growth at 20 kPa was greater than at 10 kPa and even greater than at atmospheric pressure levels.

Musgrave *at al.* (1988) found enhanced growth of mungbean at 21-24 kPa total pressure atmospheres with a low oxygen level of 5kPa. A study by Schwartzkopf and Mancinelli (1991) confirmed that an oxygen partial pressure of at least 5 kPa is necessary for seed germination and initial plant growth, as seeds failed to germinate at atmospheres with a partial pressure of oxygen lower than 5 kPa. With a total pressure of 6 kPa and therefore an oxygen concentration of 83%, this study was well above the oxygen level of 23.5% that is the upper limit considered to be safe regarding fire hazards (Lacey *et al.*, 2000). Although others have operated systems at high oxygen concentration, e.g. Goto *et al.* (2002) operated the growth chamber at a high level of 91% oxygen (21 kPa partial oxygen pressure, 23 kPa total pressure).

Spanarkel and Drew (2002) reported that lettuce grown at 70 kPa total pressure was normal in appearance, and that photosynthesis was unaffected compared to plant growth

at ambient pressure. Oxygen levels were maintained at 21 kPa and carbon dioxide at 66.5–73.5 Pa during both ambient and hypobaric conditions.

Research by Daunicht and Brinkjans (1996) compared plant growth at 100 kPa to 70 kPa and 40 kPa total pressure with equal carbon dioxide concentration. Photosynthetic rate increased at 70 kPa compared to 100 kPa and was similar at 40 kPa and 100 kPa. Furthermore, plant morphology was affected by the reduced pressures.

Experiments conducted in the variable pressure growth chambers at different NASA centers tested wheat under 70 kPa and lettuce under a progressive reduction of pressure down to 20 kPa (Corey *et al.*, 1996; Corey *et al.*, 1997b, Corey *et al.*, 2002). Lettuce, as well as the wheat experienced increased transpiration at reduced total pressures. An effect of the oxygen partial pressure on the photosynthesis was also observed. Photosynthesis increased with decreasing oxygen partial pressure and decreased if oxygen was injected into the chamber.

Studies at Texas A&M also tested the performance of wheat and lettuce at low pressures ranging from 30 to 101 kPa (He *et al.*, 2003). Low pressure increased plant growth and did not alter germination rate. Low oxygen concentration inhibited ethylene production of lettuce. Low total pressure inhibited ethylene production of wheat, whereas oxygen reduction did not have an influence on ethylene production for wheat.

The University of Tokyo performed a series of studies on spinach and maize in a reduced pressure plant growth chamber (Goto *et al.*, 1996; Iwabuchi *et al.*, 1996; Iwabuchi and Kurata, 2003). Similar to the other studies described above, they observed increased photosynthesis and transpiration rates at reduced pressures. Furthermore, stomatal size and aperture of leaves were significantly smaller at reduced total pressures.

Ferl *et al.* (2002) describes the adaptation and plant responses to low pressure environments. Plant stress includes hypoxic stress, drought stress and heat shock that may alter plant morphology. For this research genes were analyzed to understand the fundamental processes that involve gene responses to environmental signals. Genetic engineering will lead to plants that can tolerate and thrive in extreme environments.

In a study by Wilkerson (2005) evapo-transpiration rates of radishes increased significantly at a low atmospheric pressure of 12 kPa and a carbon dioxide partial pressure of 40 Pa. Furthermore, this research concluded that increasing the carbon dioxide partial pressure from 40 Pa to 150 Pa is an effective countermeasure to wilting of the plants at low atmospheric pressures because the stomata close at higher carbon dioxide concentrations and therefore transpiration rates decrease.

The studies described above indicate that plant growth is possible under low atmospheric pressure. Nevertheless, more detailed research is necessary on the response of plants to the environment properties especially for more than one life cycle. Additionally, studies on plant growth chambers exposed to the Martian environmental conditions are necessary in case of transparent greenhouse structures, as the local climate has a huge effect on the plant growth conditions. Operating a greenhouse in the Mars environment may lead to stratification of temperature and humidity, condensation resulting in lower light levels, as well as degradation of transparent greenhouse materials leading to a change of the spectrum of the photosynthetically active radiation. Last but not least, genetic engineering will play an important role in the selection of the crop suited for advanced life support.

CHAPTER 3
OBJECTIVES OF THIS STUDY

This study can be divided into the theoretical (mathematical) simulation and the experimental work.

The objectives of the experimental part were

- Design of simulated Mars environment and low pressure greenhouse for plant growth.
- Development of control-algorithm to maintain total pressure and temperature of vacuum chamber (simulated Mars environment).
- Development of control-algorithm to maintain total pressure, temperature and gas composition (CO_2, O_2 and N_2 concentration) of greenhouse dome.
- Monitoring of stratification of temperature and relative humidity in greenhouse dome.
- Monitoring of condensation pattern on interior of greenhouse dome and its effect on light reduction.
- Monitoring of plant evapo-transpiration in low pressure greenhouse that is exposed to low temperature environment.

The objectives of the simulation were

- Development of low pressure psychrometric relationships for closed systems and non-standard atmospheres.
- Prediction of temperatures of greenhouse atmosphere, greenhouse floor, interior and exterior greenhouse shell by creating a mathematical model to simulate the heat and mass transfer.
- Prediction of occurrence of condensation on interior of greenhouse dome.
- Comparison of theoretical and experimental results to deduce conclusions.

CHAPTER 4
EXPERIMENTAL WORK

System Description

A careful selection of equipment for the set-up of the experimental work was required in order to fulfill the objectives listed in Chapter 3. A polycarbonate hemispherical dome with a diameter of 1 meter served as the Mars greenhouse (see Figure 4-1). The dome was clamped to a re-inforced aluminum base with the help of a silicon rubber gasket to ensure the enclosure of the system. A 10 centimeter thick layer of polyurethane foam was fixed to the bottom of the aluminum dome base for insulation. Feed-throughs in the dome base were used for data transfer, power and gas supply. The maximum pressure differential that the dome structure could withstand without failure was estimated to be ±50 kPa. The structural analysis of the dome and its base plate is presented in Appendix A.

A dome similar to the one that was utilized as a greenhouse model for this study had been used at NASA's Kennedy Space Center as an autonomous low pressure growth chamber. In a preliminary test lettuce was grown at a pressure of 25 kPa for 45 days (Fowler *et al.*, 2002; Bucklin *et al*., 2004). However, during this lettuce growth experiment at NASA the dome was not exposed to simulated Mars conditions as in the experiments described in this document.

A large stainless steel vacuum chamber was used to simulate the Mars atmosphere of 0.6 kPa. Its interior volume was comprised by an area of 1.2 meter by 1.2 meter with a

height of 1 meter. The chamber was custom-made by Chicago Wilcox based on the following requirements:

- The vessel should be able to hold a pressure of 0.1 kPa with no significant leakage.
- It should be big enough for the greenhouse dome (0.5 m radius) to fit in.
- It should have a window on top to allow growth light to penetrate into the chamber.
- It should have 12 ports on the side for data transfer, power and gas supply.
- It should have a door to move equipment in and out.

The stainless steel chamber was braced on the bottom and on all sides (except for door) to avoid deflection of the walls because of the huge pressure difference. A 1.27 cm thick polycarbonate sheet served as a window pane. A grid of steel bars supported the polycarbonate window (see Figure 4-2).

An industrial freezer shown in Figure 4-3 ensured the low temperature of the vacuum chamber (simulated Mars environment). The interior temperature of the freezer could be dropped down to as low as –34 ºC. Initially, jacketing the vacuum chamber with a heat exchanger was discussed as an option to reduce the temperature inside of the chamber, but putting the entire vacuum chamber in a freezer had the advantage that the temperature distribution was more uniform, especially at the chamber window.

A) B)

Figure 4-1. Dome used to protect plants from the simulated low pressure, low temperature Mars environment. A) Empty dome. B) Dome with sensors, scales and flasks installed.

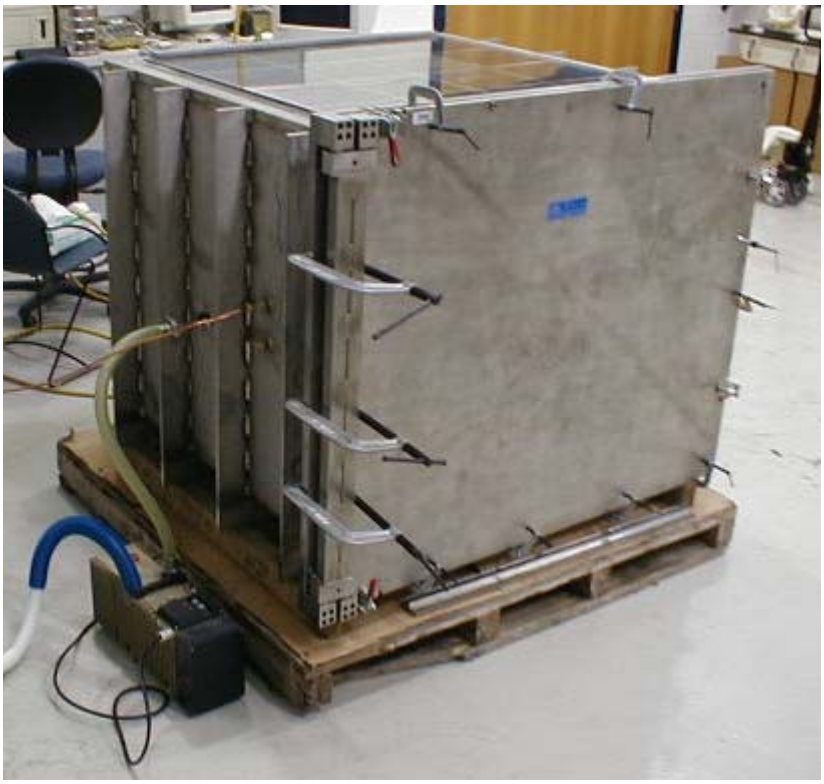

Figure 4-2. Vacuum chamber used to simulate the low pressure Mars environment (less than 1% of Earth's atmosphere).

Figure 4-3. Industrial walk-in freezer ensures low temperature of the vacuum chamber (simulated Mars environment).

Two vacuum pumps were installed outside the freezer. A powerful two-stage rotary vane vacuum pump (DUO 10, Pfeiffer Vacuum) with a volumetric flow rate of 10 m^3/hour was connected to the vacuum chamber; a two-stage vacuum pump (DV-85N, J/B Industries) with a volumetric displacement of 5 m^3/hour was connected to the greenhouse dome. During the experiments the pumps were always turned on and the air flow was controlled by two solenoid valves that were installed between the pumps and the chamber/dome. Three mass flow controllers ensured the correct gas mixture that was fed into the greenhouse dome. The mass flow controllers were connected to bottles of nitrogen, oxygen and carbon dioxide.

Scale 1 was located on the bottom of the greenhouse. It measured the amount of water that ran off the greenhouse shell and the recollection funnel. Four scales (Scale 2 to Scale 5) were installed in the upper part of the dome. They measured the amount of water that the plants evaporated and transpired. Two flasks, each containing one lettuce plant, were placed on each of these four scales, leading to a total number of 8 flasks. A 512W/110V cooking range coil was placed in the center of the greenhouse dome and served as the heater. A 24V fan ensured mixing of the air and minimized temperature, gas composition and relative humidity stratification.

A high pressure sodium growth light (1000W HPS, Hortilux) was installed above the vacuum chamber. Two I/O boards, one for data acquisition and one for control, were connected to the sensors and actuators. They were connected to the computer for programming and as user interface. Figure 4-4 gives an overview of the experimental setup.

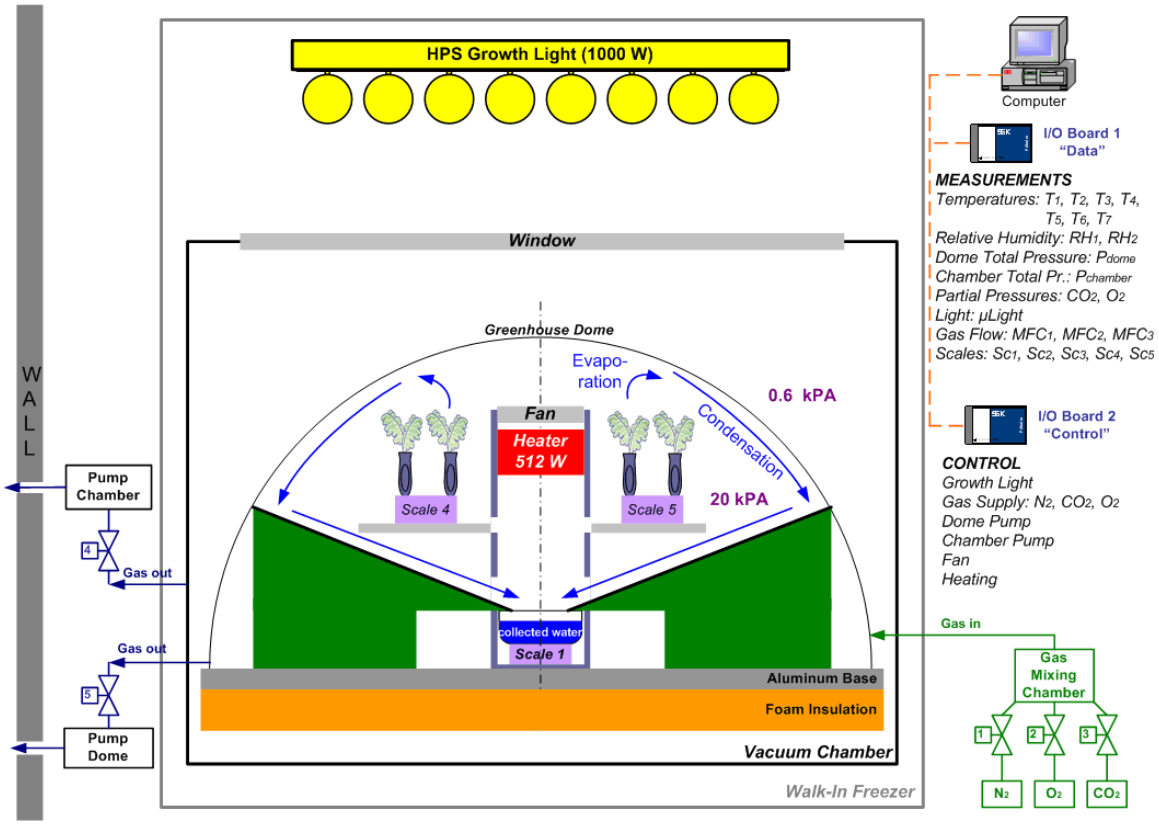

Figure 4-4. Schematic of experimental setup.

Instrumentation and Sensor Calibration

Most commercially available sensors for the measurement of environmental parameters contain a data sheet with calibration information under standard atmospheric conditions. However, in this project, the pressure and gas composition of the environment that the sensors were exposed to differed significantly from the standard atmosphere. Therefore, the sensors were carefully selected according to the environmental conditions and a re-calibration of the sensors was performed against a standard sensor that was not affected by pressure or gas composition.

DS18B20 (Dallas Semiconductor) digital thermometers were selected for temperature measurements. They were shielded to avoid measurement errors caused by direct radiation onto the sensors. Relative humidity (RH) was monitored by HIH-3602-L (Honeywell) capacitance type sensors capable of measuring RH in the range of 0-100%

(non-condensing). LI-COR's LI-190 SA quantum sensor monitored the level of photosynthetically active radiation inside the greenhouse dome. The carbon dioxide concentration was measured by Vaisala's infrared GMP 221 sensor, oxygen concentration by Maxtec's Max 250 galvanic cell type sensor. The mass of the recollected water and the masses of the individual plants were measured by Vishay Celetron's LPS-2 kg load cells. Table 4-1 lists the environmental parameters that were monitored and their corresponding sensors.

Table 4-1. Sensors used to measure environmental parameters, the sensor ranges and accuracies.

Parameter	Type	Range	Accuracy
Temperature	DS18B20 digital thermometer (Dallas Semiconductor)	-55 to +125 ºC	± 0.5 ºC
Relative Humidity	HIH-3602-L capacitance type RH sensor (Honeywell)	0 to 100%	±2%
Light	LI-190SA quantum sensor (LI-COR Inc.)	0 to 10,000 $\mu mol/m^2/s$	±5%
Pressure	ASCX15AN (Sensym ICT)	0 to 15 psi	±0.5%
Carbon Dioxide	GMP 221 (VAISALA)	0 to 10 %	0.02%
Oxygen	Max 250 (MaxTec)	0 to 100%	± 1.0 %
Water / Plant Mass	LPS-2 kg Load Cell (Vishay Celtron)	0 to 2 kg	± 0.1 g

A transparent acrylic cylinder with an aluminum base served as calibration chamber for the sensors. It had an interior diameter of 20.32 cm, a wall thickness of 0.64 cm and a height of 30.48 cm. The cylinder was supported by an aluminum base containing feed-throughs for data transfer, power and gas supply. An O-ring minimized

leakage of air into the cylinder. The structural analysis of the cylinder is presented in Appendix A. The calibration data of all sensors is found in Appendix B.

Figure 4-5. Cylinder used for calibration of pressure-sensitive sensors and for initial gas mixing control algorithm development.

The performance of the temperature sensors, light sensor and load cells was unaffected by changes in total pressure. The sensors affected by low pressure, including relative humidity (RH), carbon dioxide concentration and oxygen concentration, had to be calibrated for low pressures. Carbon dioxide and oxygen were calibrated by a method similar to the one described by Mu (2005).

Rygalov *et al.* (2002) compared various types of RH sensors under low atmospheric pressure to RH readings from a chilled mirror/dew point hygrometer that is unaffected by pressure changes. This study concluded that the dry-bulb/wet-bulb method was not adequate for low pressures as not enough air mass moves over the sensor. In

contrast to this, the readings of the capacitance type RH sensor did not change significantly at different pressures.

As the accuracy of the relative humidity measurements was of major importance to the study described in this dissertation, further experiments were conducted to confirm the independence of the output of the capacitance type RH sensor at different pressures. The RH values of the capacitance sensors were compared to the output of Vaisala's HMP 237 by exposing the sensors to a wide range of humidities and pressures. The HMP 237 is also a capacitance RH sensor, but especially designed to measure RH and temperature in both pressurized as well as vacuum chambers. The difference in RH of the Honeywell sensors from Vaisala's low pressure RH sensor never exceeded 3%. Thus, the RH values obtained by the Honeywell RH sensors were not corrected for pressure.

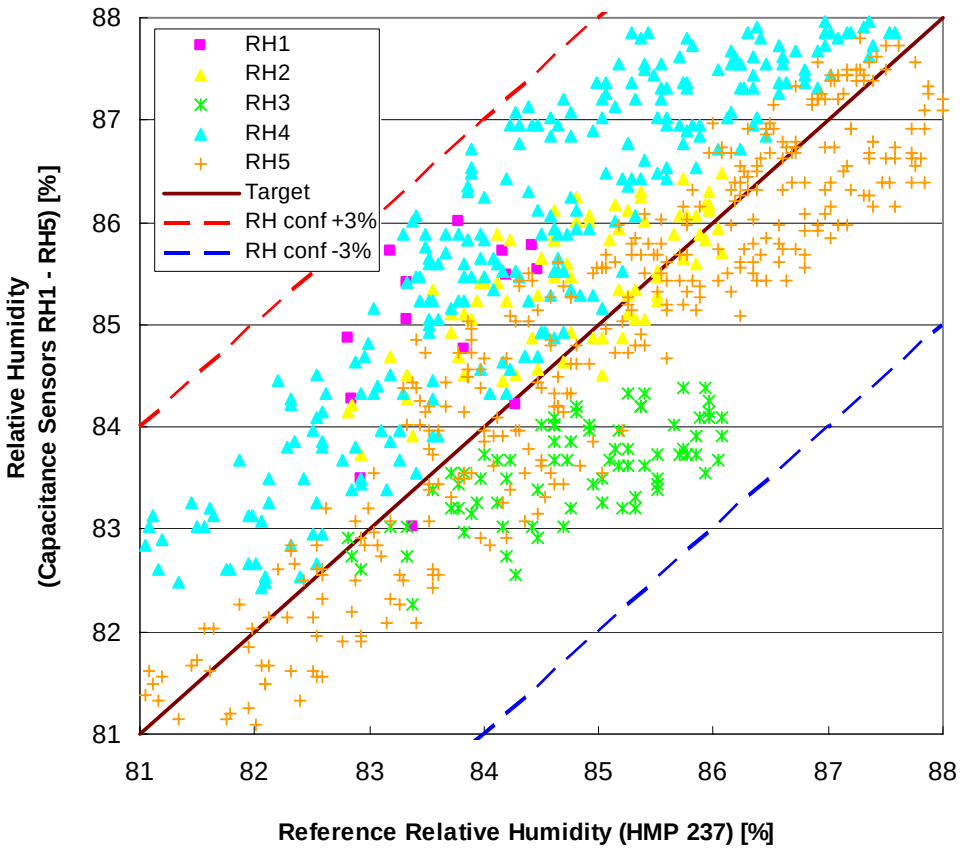

Figure 4-6. Comparison of Honeywell capacitance RH sensors to the HMP 237 reference RH sensor for pressures of 0 to 25 kPa.

Leakage Testing

In low pressure plant growth chambers, involving the measurement of gas exchange rates and evapo-transpiration, it is important to minimize the leakage and to account for the occurring leakage by making the necessary corrections (Corey, 1997a).

Leakage is defined as

$$L = \frac{P_i - P_0}{P_0} \times 100 \times \frac{1440}{t} \tag{4-1}$$

where: L = leak rate [% vol/day]

P_i = end pressure [kPa]

P_o = initial pressure [kPa]

t = time interval [min]

Leakage of Vacuum Chamber

Initial leak tests of the freshly shipped vacuum chamber, showed very high leak rates of 2.5 kPa/hour. Due to the high leak rate it was not possible to pump the chamber down to a pressure lower than 4 kPa. Changing the plastic tubing to copper tubing, attaching C-clamps to the chamber door, sealing ports additionally with Loctite glue, utilizing high vacuum rated Swaglok valves and installing a powerful new two-stage rotary vane vacuum pump (DUO 10, Pfeiffer Vacuum) with a volumetric flow rate of 10 m³/hour, led to a reduction of the leakage to 1.65 kPa/hour. Even at this lower leakage the target Mars equivalent pressure of 0.6 kPa could not be reached in the chamber. Further leak tests utilizing helium gas and a helium gas detector revealed that the gas was mainly leaking through the chamber window. Therefore, the window was taken off and a second layer of gasket was cut out and installed, so that the polycarbonate window would

be sandwiched in between the two gaskets. Thus, the window could deflect more, without causing gaps for the gas to leak in.

Figure 4-7 depicts the strong forces that act upon the window when the chamber is at low pressure: Photo A depicts the bulging of the polycarbonate window at low pressures; in Photo B the window gasket is drawn inside by the large pressure difference. Additionally, vacuum grease was applied to the window and the door. Finding the right amount of vacuum grease is the key to success: enough to fill the gaps and reduce the gas leakage but not so much, that lack of friction causes the gasket to dislocate. Finally, a pressure of 0.07 kPa was achieved, well below the required pressure of 0.6 kPa.

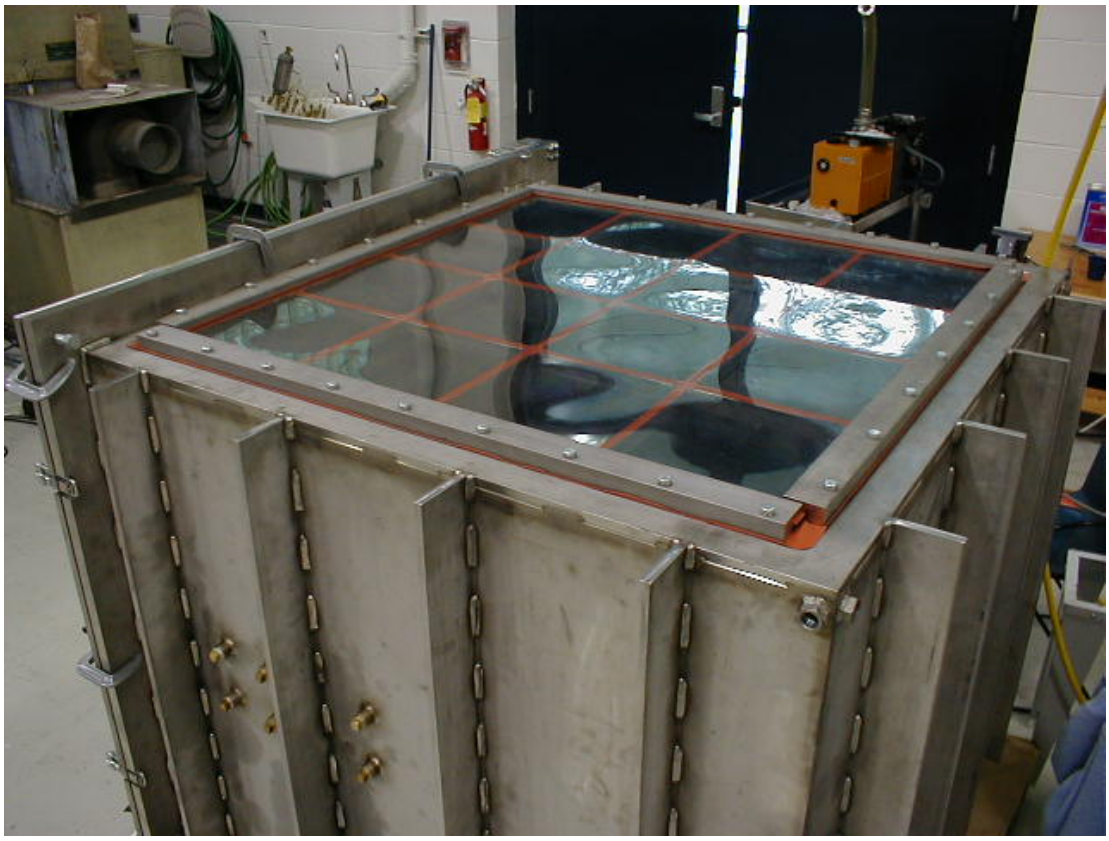

A)

Figure 4-7. Forces on chamber window. A) Vacuum chamber at 0.6 kPa with top window bulging in. B) Gasket drawn into the chamber due to pressure difference.


B)

Figure 4-7. continued

Leakage of Greenhouse Dome

The greenhouse dome was installed in the 0.6 kPa vacuum chamber. Therefore, gas leaked from the dome into the vacuum chamber, causing the dome pressure to drop. This leakage was minimized by applying vacuum grease on the dome gasket, tightening the 36 screws of the dome and sealing the feed-throughs with additional glue.

Figure 4-8 presents the data of a combined leak test of the vacuum chamber and the greenhouse dome. The dome leakage was found to be -0.375 kPa/hour (45 vol%/day) at 20 kPa; the chamber leakage 0.243kPa/hour (972 vol%/day) at 0.6 kPa. Figure 4-4 compares the leak rates of the vacuum chamber/greenhouse dome to other low pressure

plant growth systems. This comparison shows that the leak rates of this large system compared relatively well with the much smaller bell jar or tube systems.

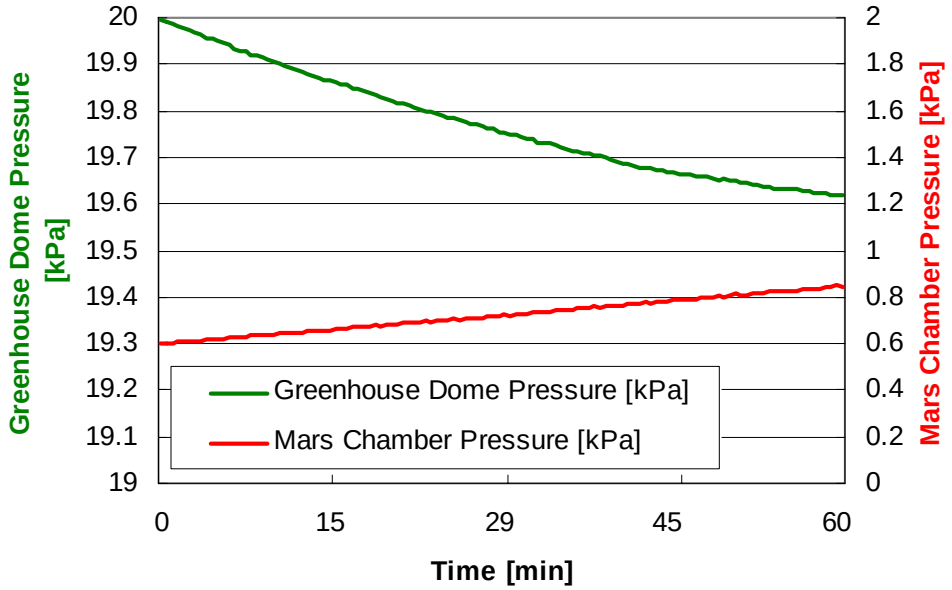

Figure 4-8. Dome and chamber leakage with gas resupply and vacuum pumps turned off at a temperature of -10 ºC.

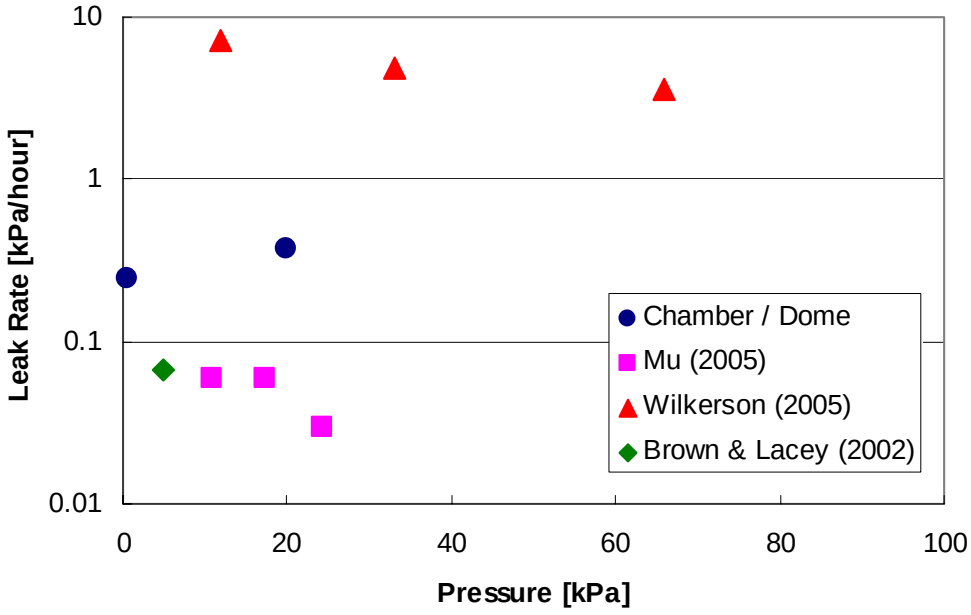

Figure 4-9. Comparison of vacuum chamber and greenhouse dome leak rates to values of other low pressure plant growth studies (leak rate is presented in logarithmic scale).

Data Acquisition and Control System

The distributed control system for this project was developed by Rigel Corporation, especially for low pressure plant growth experiments, with the aims of maximizing the inputs and outputs while being very flexible yet low cost. This control system, described in detail in Mu (2005), was modified and adapted after it had been used for previous plant growth studies. Two control boards were utilized: one for data acquisition and a second one to execute the control signals. The two boards combined had a large number of analog and digital inputs/outputs

- 16 digital inputs for temperature sensors
- 16 analog inputs especially for thermocouples
- 32 single ended (16 differential) analog inputs
- 32 digital outputs for operating the relays
- 16 analog outputs for the control of the actuators (such as mass flow controllers)
- 8 digital outputs designed for pulse width modulation (e.g. utilized for the control of the heating system)

The data board and the control board were both connected to the PC via the serial port. The data acquisition and control software was separated into two parts: The low-level programming of the microcontrollers was done by Rigel Corporation utilizing Assembly and C language. These low-level programs, loaded onto the microcontrollers, received the data from the sensors and sent out control commands to the actuators. For the high-level programming LabView was chosen as it provides an excellent user-interface and is comprised of many built-in functions. As LabView is a graphic programming language it also facilitated multi-users to work with the same program and to understand it quickly. The LabView programs communicated with the microcontrollers, contained the control logic and managed the data.

Greenhouse Dome Environmental Control

Gas Composition and Total Pressure Control Algorithm

The dry atmosphere of the greenhouse was comprised of three gases: oxygen, carbon dioxide and nitrogen. Oxygen and carbon dioxide are the essential gases required for photosynthesis and therefore plant growth. Nitrogen was used to fill up the atmosphere to the desired total pressure as total pressure is defined as the sum of the partial pressures of all gases. The oxygen and carbon dioxide concentration of the greenhouse dome were directly measured by sensors. Nitrogen was calculated by measuring the total pressure and subtracting the partial pressures of oxygen and carbon dioxide. Three mass flow controllers were utilized to control the resupply of oxygen, carbon dioxide and nitrogen separately. Resupply of the individual gas was shut off if the partial pressure of the gas was higher than the set point partial pressure. If the measured partial pressure of the gas was lower than the set point, gas was resupplied. The required mass flow of each gas was calculated by determining the mass of the gas to be resupplied into the greenhouse dome, resulting in the following gas control algorithm:

$$Flow(gas,t) = \frac{Mass_{set}(gas) - Mass_{actual}(gas,t)}{\rho(gas)\Delta t} \tag{4-2}$$

where: $Flow(gas,t)$ = gas flow rate [m³/s]

$Mass_{set}(gas) = M(gas)\frac{Pp_{set}(gas)V_{dome}}{RT_{air}}$ = mass of gas required [kg]

$Mass_{actual}(gas,t) = M(gas)\frac{Pp_{actual}(gas,t)V_{dome}}{RT_{air}}$ = actual mass of gas [kg]

$M(gas)$ = Molecular mass of gas [kg/mol]

$Pp_{set}(gas)$ = partial pressure of gas at setpoint [Pa]

$Pp_{actual}(gas)$ = actual partial pressure of gas [Pa]

V_{dome} = volume of dome [m³]

R = universal gas constant [8.3144J/(mol K)]

T_{air} = air temperature [K]

$\rho(gas)$= gas density [kg/m³]

Δt = length of control cycle [s]

Total pressure of the greenhouse dome was maintained constant by controlling oxygen, carbon dioxide and nitrogen pressures separately as described above. Total pressure of the vacuum chamber was kept constant by controlling a solenoid valve that was connected to the vacuum pump. If the vacuum chamber pressure was above the setpoint, gas was pumped out. If it was below the setpoint the pump was stopped.

Figure 4-10 depicts the oxygen and carbon dioxide partial pressures during a test of the gas mixing control system that lasted 1 hour. Figure 4-11 shows the total pressures of the vacuum chamber and the greenhouse dome.

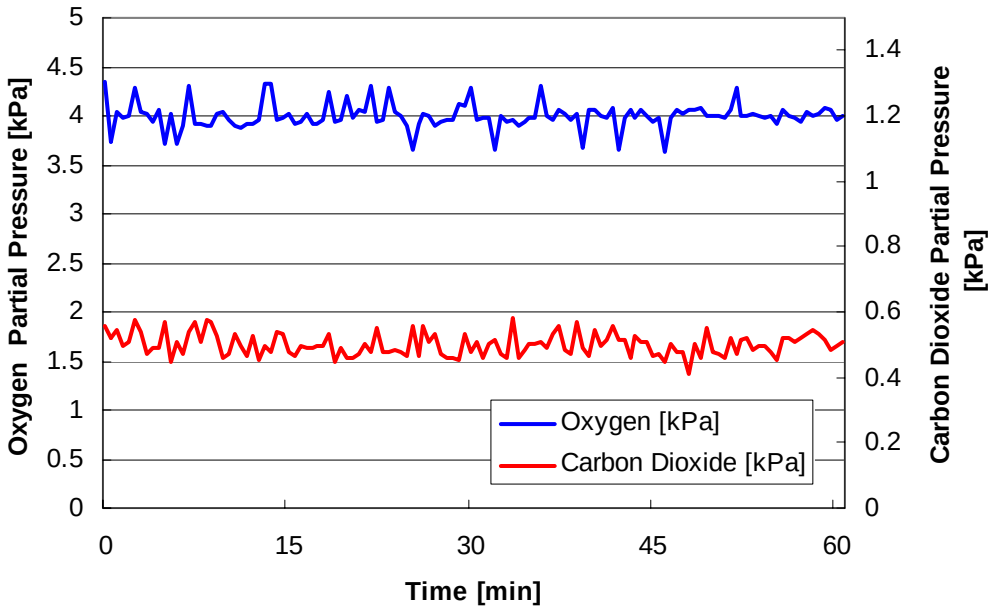

Figure 4-10. Gas mixing of dome greenhouse atmosphere without plants (oxygen set point at 4.0 kPa and carbon dioxide set point at 0.5 kPa).

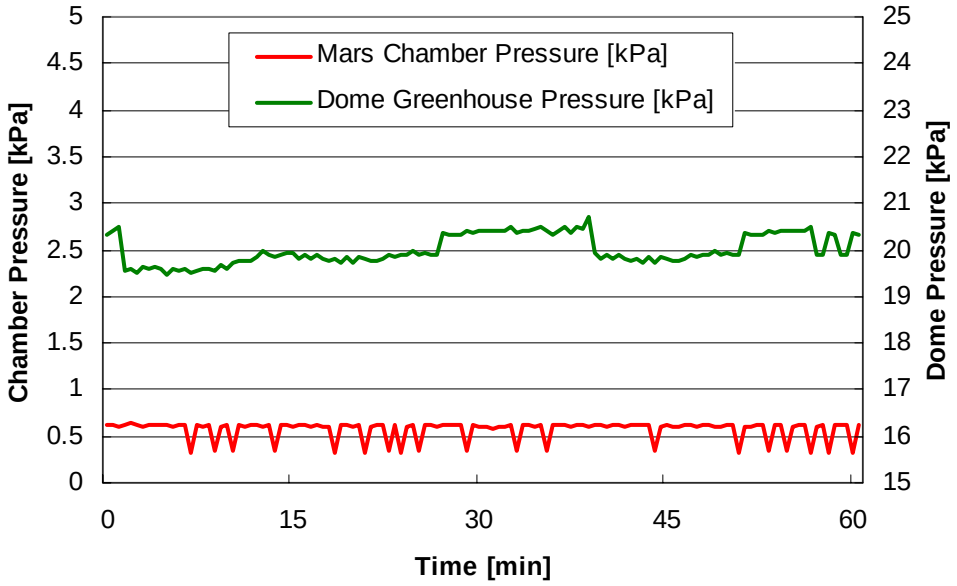

Figure 4-11. Pressure control of vacuum chamber (set point 0.6 kPa) and greenhouse dome (set points 20 kPa).

Air Temperature Control Algorithm

Maintaining the air temperature in a range where the plants are productive is essential in the cold Mars environment. Air temperature was kept constant by the heating coil that was installed in the center of the greenhouse dome at plant level. The heater was controlled by pulse width modulation with duty cycles of 0%-100%. At 100% the maximum power output was calculated to be 512.7 W:

$$P_{\max} = \frac{V^2}{R} = \frac{(110V)^2}{23.6\Omega} = 512.7W \qquad (4\text{-}3)$$

where: P_{max} = heating power [W]

V = voltage [V]

R = resistance [Ω]

To maintain the air temperature T_3 at a certain set point, the required power of the heating system was calculated by adding the required steady state power (determined in

the following section: see equations 4-5 & 4-6) to a proportional control term with a gain of 1/ $T3_{air,set}$:

$$P_{req}(t) = P_{ss}(T_{freezer}, T3_{air,set}, Light) + \frac{1}{T3_{air,set}}\left(T3_{air,set} - T(t)\right) \quad (4\text{-}4)$$

where: $P_{req}(t)$ = required heating power [W]

$P_{ss}(T_{freezer}, T3_{air,set}, Light)$ = steady state heating power [W]

$T3_{air,set}$ = air set point temperature [ºC]

$T3_{air}(t)$ = actual air temperature T_3 [ºC]

Figure 4-12 gives an example of how the temperature control algorithm regulated the air temperature. A constant air temperature of 20 ºC was maintained by varying the heating power. When the light was turned on the required heating power was much less than when the light was turned off.

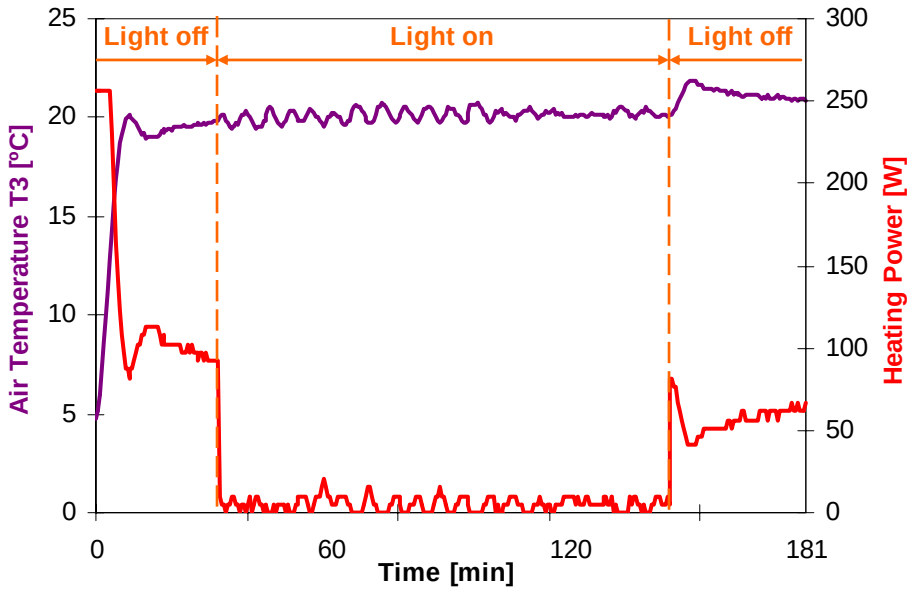

Figure 4-12. Air temperature control of greenhouse dome (set point at 20 ºC).

Heat and Mass Transfer Experiments without Plants

The first step of modeling the heat and mass transfer of this Mars greenhouse was to analyze the heat transfer without the plants. Figure 4-13 shows the location of the sensors for measuring the environmental parameters. The CO_2, O_2 and light sensors were installed at the plant level. Temperature was measured at seven locations

- T_1 at the aluminum dome base
- T_2 at the water collection slope
- T_3 is the air temperature at the plant level
- T_4 is the temperature of the exhaust air of the fan and heater.
- T_5 is the temperature of the exterior of the transparent greenhouse shell
- T_6 is the temperature of the vacuum chamber window
- T_7 is the temperature of the vacuum chamber wall

Relative humidity sensors were installed at the location of T_3 and T_4. Furthermore, total pressure was measured in the dome and in the vacuum chamber.

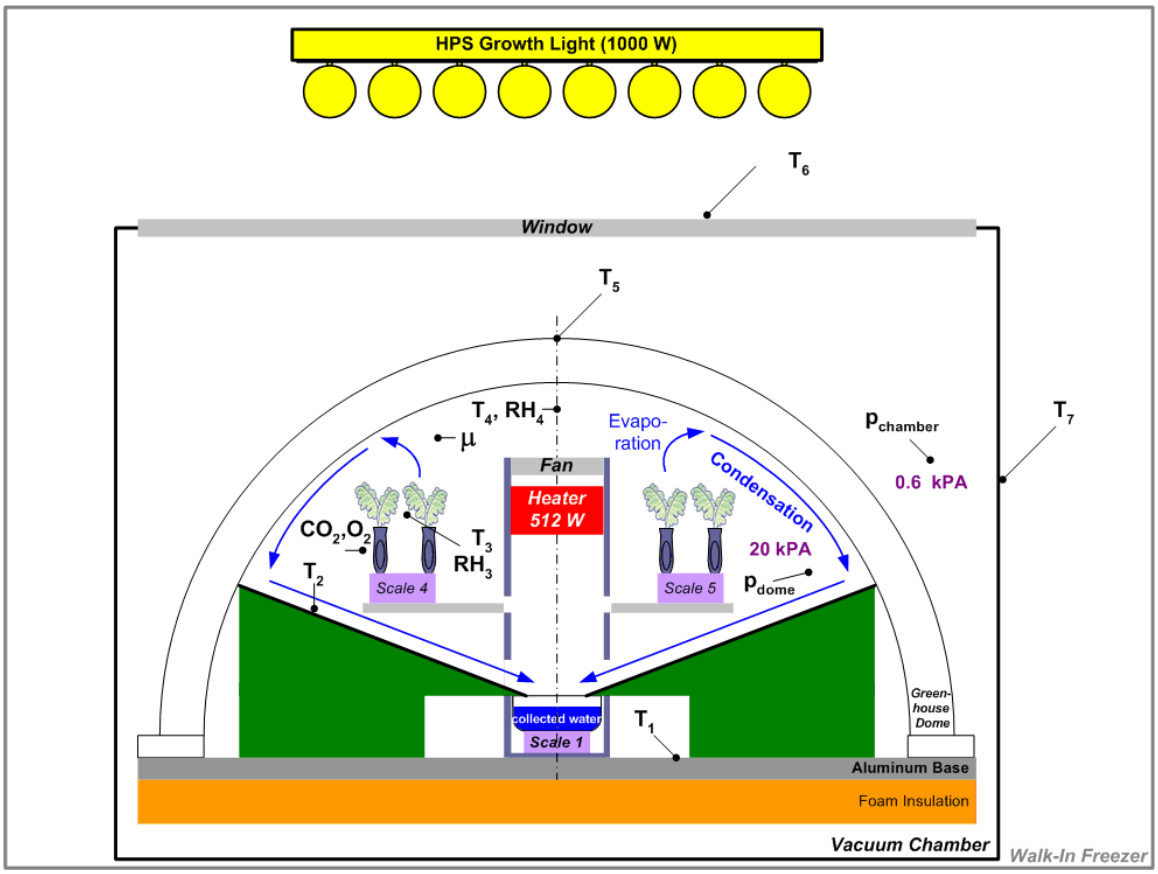

Figure 4-13. Sensor locations for heat and mass transfer experiments without plants.


A)

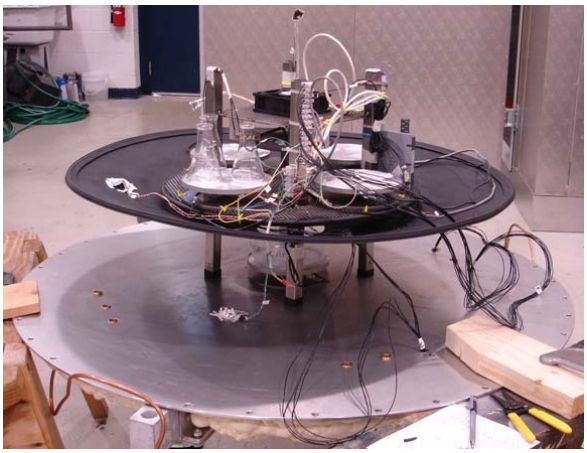
B)

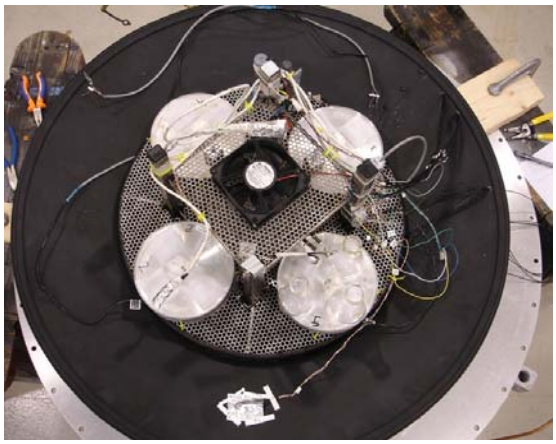
C)


D)

Figure 4-14. Preparation of the steady state experiments. A) Bottom of dome base with foam insulation. B) Side view of greenhouse dome with the sensors and scales installed. C) Top view of greenhouse dome without shell. D) Installation of greenhouse dome into the vacuum chamber.

An exact understanding of the temperature distribution at the different locations illustrated in Figure 4-13 was important to calculate the thermal resistances in Chapter 5. The greenhouse dome was subjected to a combination of different freezer temperatures, heating power levels and growth light states:

- Freezer temperatures at 0 ºC, -10 ºC and -20 ºC.
- Heating power levels at 0 W, 26 W, 51 W, 77 W and 103 W.
- Growth light switched on/off.

Useless combinations such as a heating power of 0W and the growth light switched off were left out, as well as combinations that resulted in very high dome temperatures

(e.g. 0 ºC freezer temperature, 103 W heating power and growth light switched on). Figure 4-15 depicts the trend of the seven different temperatures for a freezer temperature of 0 ºC, a heating power of 26 W and the growth light switched off. Temperature T_6 at the window and temperature T_7 at the chamber wall oscillated as the freezer temperature was controlled at 0 ºC within a band of +1 ºC and -1 ºC. The time required to achieve steady-state temperatures was always at least 10 to 12 hours. The steady state temperatures at the seven locations for the different combination of freezer temperatures, heating power levels and growth light state are given in table 4-2. Each experiment was conducted two times to minimize errors. Figures 4-16 to 4-20 depict the temperature distributions. It can be observed that the temperatures inside the dome increase linearly with the increased in heating power. The chamber window (T_6) and wall (T_7) temperatures increased only slightly with increasing heating power. On the other hand, T_6 and T_7 increased significantly when the growth light was turned on.

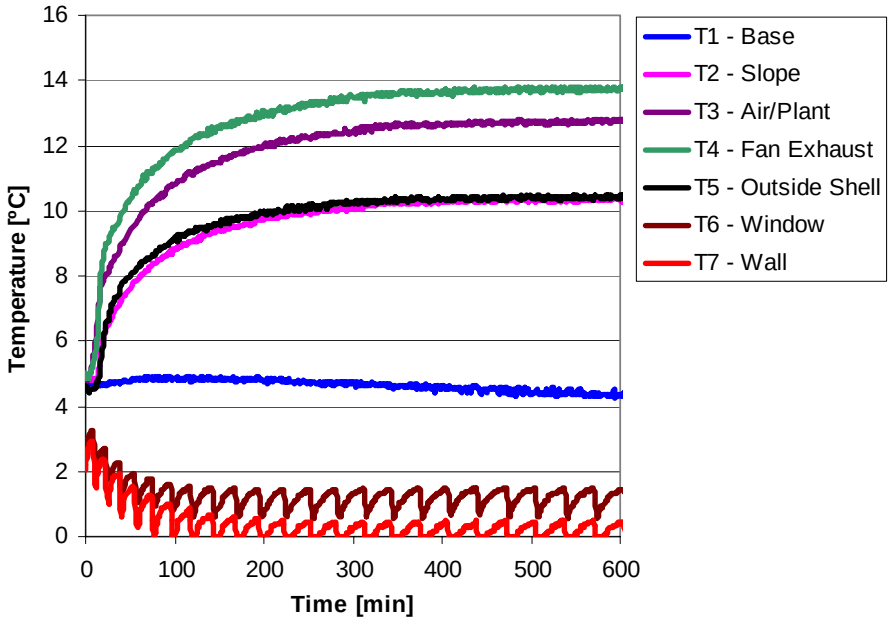

Figure 4-15. Temperature readings until steady state is achieved. (0 ºC freezer temperature, 26 W heating power and light switched off).

Table 4-2. Steady state temperature distribution under different freezer temperature, light and heating power conditions.

Freezer Temp. [ºC]	Lights (0=off, 1=on)	Heating Power [W]	Base T1 [ºC]	Slope T2 [ºC]	Air/ Plant T3 [ºC]	Fan Exhaust T4 [ºC]	Shell Outside T5 [ºC]	Window Outside T6 [ºC]	Wall Outside T7 [ºC]
0	**0**	**26**	4.34	10.35	12.74	13.72	10.43	0.90	0.01
0	**0**	**51**	5.96	15.29	19.17	20.75	15.68	1.83	0.34
0	**0**	**77**	6.98	18.93	24.06	26.11	19.69	2.28	0.49
0	**0**	**103**	8.56	24.09	30.25	32.60	24.49	2.39	0.11
-10	**0**	**26**	-3.44	2.68	5.29	6.38	2.81	-7.56	-9.63
-10	**0**	**51**	-3.06	6.61	10.76	12.40	7.17	-8.00	-9.94
-10	**0**	**77**	0.34	12.95	18.44	20.59	13.51	-7.00	-9.44
-10	**0**	**103**	2.84	17.73	24.01	26.61	17.96	-6.44	-9.38
-20	**0**	**51**	-10.81	-0.94	3.38	4.94	-0.03	-17.25	-19.13
-20	**0**	**77**	-10.31	3.44	9.06	11.12	4.29	-17.06	-19.31
-20	**0**	**103**	-7.19	9.32	15.51	17.96	9.60	-15.94	-18.88
-20	**0**	**128**	-4.13	14.39	21.34	24.32	14.14	-15.00	-18.63
-10	**1**	**0**	9.47	18.74	16.76	18.96	19.88	8.74	-6.22
-10	**1**	**26**	10.12	23.66	25.74	27.08	25.22	9.28	-6.74
-10	**1**	**51**	10.61	28.59	32.17	34.15	30.62	9.81	-6.66
-10	**1**	**77**	11.96	32.50	38.27	39.56	34.63	10.56	-6.31
-20	**1**	**0**	-5.06	6.13	5.60	6.09	7.73	-5.56	-15.38
-20	**1**	**26**	1.75	15.37	17.52	18.18	16.76	-5.25	-14.38
-20	**1**	**51**	5.09	19.88	23.39	24.48	20.88	-5.06	-14.13
-20	**1**	**77**	9.81	27.22	32.73	34.95	29.17	-3.08	-13.85
-20	**1**	**103**	11.63	31.73	38.98	41.22	33.68	-3.88	-13.20

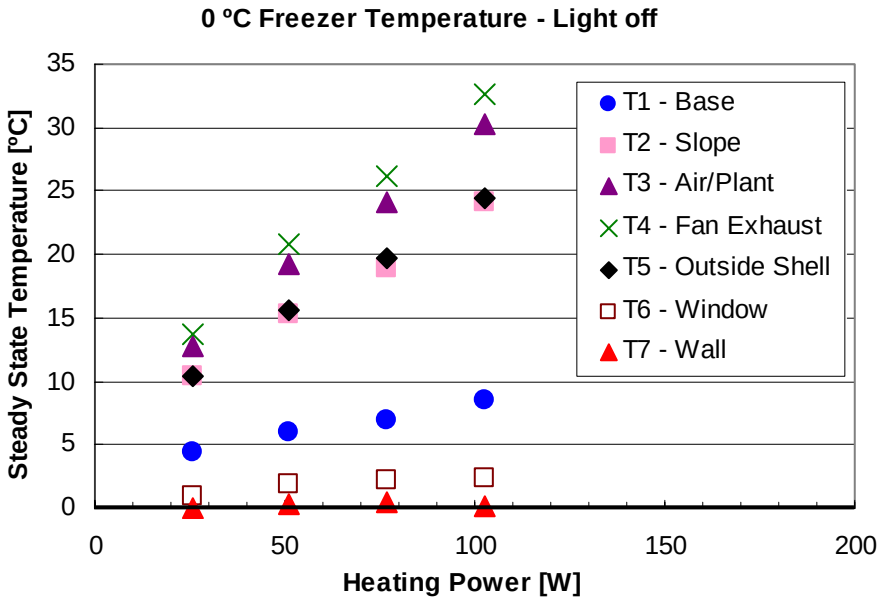

Figure 4-16. Steady state temperatures versus power of heater at seven different locations (T_1-T_7). Freezer temperature is 0 ºC and the growth light is switched off.

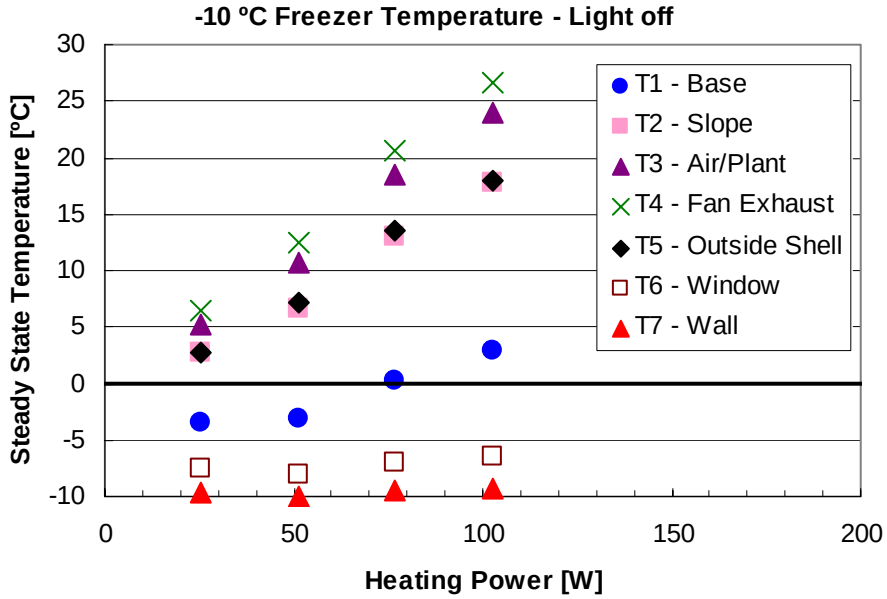

Figure 4-17. Steady state temperatures versus power of heater at seven different locations (T_1-T_7). Freezer temperature is -10 ºC and the growth light is switched off.

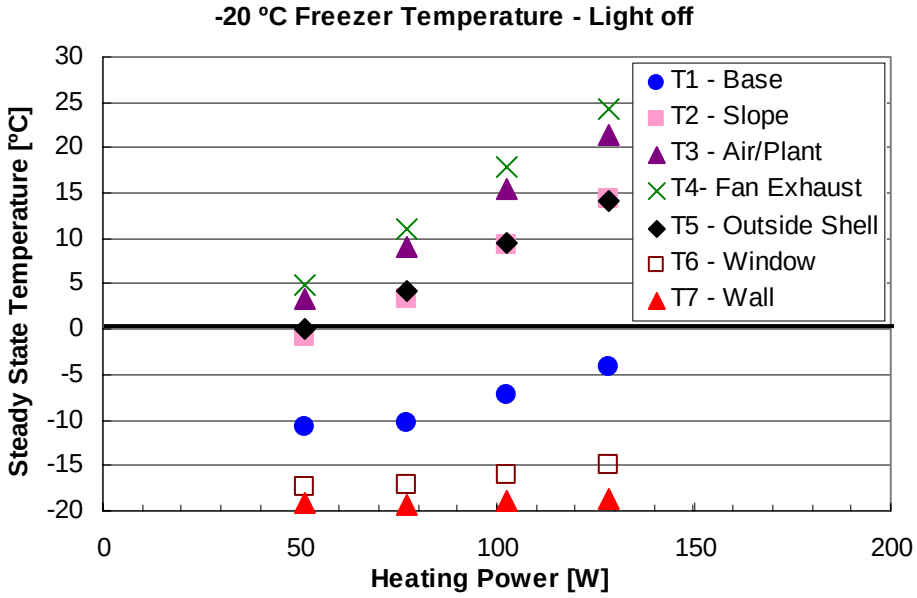

Figure 4-18. Steady state temperatures versus power of heater at seven different locations (T_1-T_7). Freezer temperature is -20 ºC and the growth light is switched off.

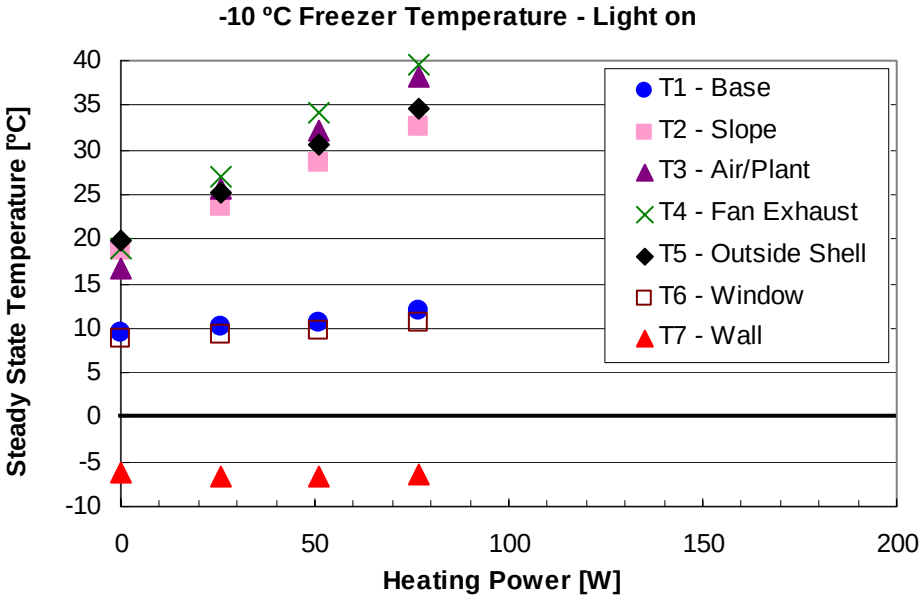

Figure 4-19. Steady state temperatures versus power of heater at seven different locations (T_1-T_7). Freezer temperature is -10 ºC and the growth light is switched on.

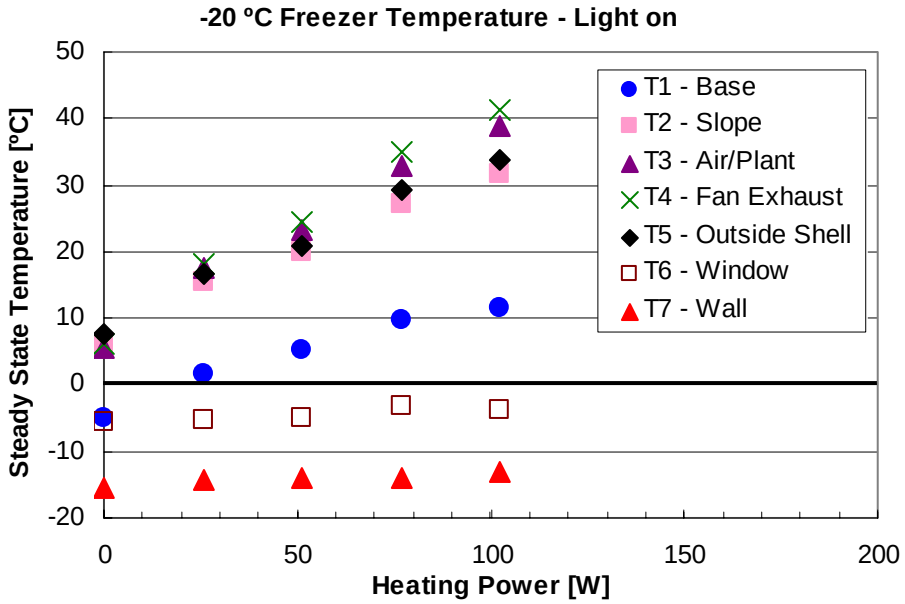

Figure 4-20. Steady state temperatures versus power of heater at seven different locations (T_1-T_7). Freezer temperature is -20 ºC and the growth light is switched on.

Figure 4-21 depicts the steady state air temperature T_3 of the greenhouse dome for different heating power and freezer temperatures. The steady state air temperature

increases linearly with increasing heater power. The linear equations for the freezer temperatures of 0 ºC, -10 ºC and -20 ºC are shown in Figure 4-21. According to the equations, the steady state air temperature is not equal to the freezer temperature when the heating system is switched off. This difference results from the waste heat that is introduced by running the fan continuously and the difference of freezer temperature and wall temperature of the vacuum chamber T_7 (see Table 4-2). Combining these three equations into one, the power of the heater required to heat the air to temperature T_3 with a freezer temperature of $T_{freezer}$ can be calculated as follows:

$$Pss = \frac{T_{3,air} - \{(0.831 \times T_{freezer}) + 7.741\}}{(-0.000598 \times T_{freezer}) + 0.23047} \tag{4-5}$$

where: Pss = power of heater [W]

$T_{3,air}$ = steady state temperature of air T_3 [ºC]

$T_{freezer}$ = temperature of freezer [ºC]

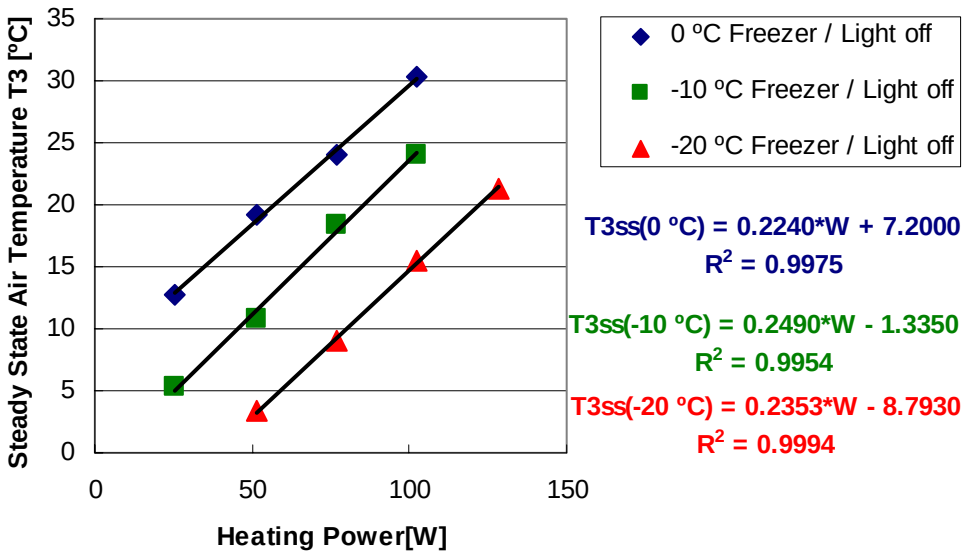

Figure 4-21. Steady state air temperatures (T_3) versus power of heater for freezer temperatures of 0 ºC, -10 ºC and -20 ºC (growth light switched off).

When the light is switched on, the power of the heater required to heat the air to temperature T_3 with a freezer temperature of $T_{freezer}$ can be calculated as following:

$$Pss = \frac{T_{3,air} - \{(0.951 \times T_{freezer}) + 26.27\}}{(-0.00526 \times T_{freezer}) + 0.2146} \quad (4\text{-}6)$$

Figure 4-22 depicts the heating power requirement depending on the freezer temperature for steady state air temperatures T_3 of 15 ºC, 20 ºC and 25 ºC. When the growth light was switched off and if the freezer temperature was -20 ºC, e.g., the required heater power was 95.5 W, 116.2 W and 136.8 W to achieve a steady state air temperature of 15 ºC, 20 ºC and 25 ºC respectively. If the growth light was switched on, the required heating power was reduced significantly. At a freezer temperature of -20 ºC and an air temperature of 20 ºC, the heating power was reduced by 79.8 W, with the light switched on.

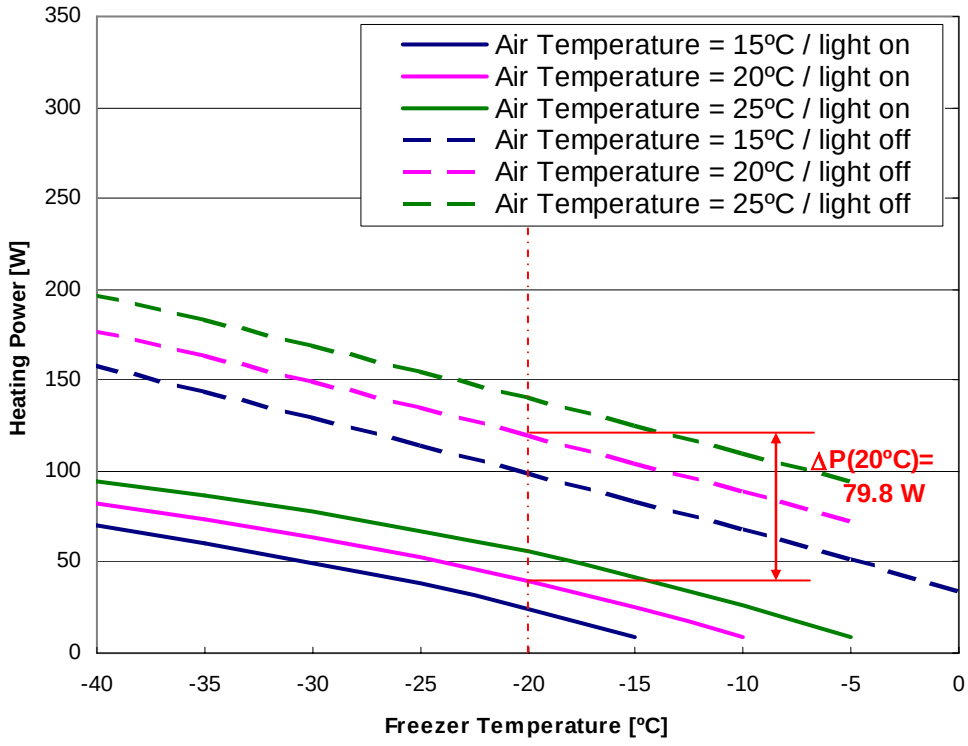

Figure 4-22. Freezer temperature versus power of heater for steady state air temperatures (T_3) of 15 ºC, 20 ºC and 25 ºC.

If the interior temperature of the greenhouse dome shell decreased below the dew point of the air temperature, condensation could occur. Figure 4-23 shows two photos of condensation on the inside of the greenhouse dome. High condensation occurred for low freezer temperatures (Photo B) as those low temperatures resulted in a lower greenhouse shell temperature. These photos also clearly show a stratification of temperature within the greenhouse dome. The top of the dome was warmed by radiation of the growth light and the air from the heating system that the fan blew across the inside shell. As the greenhouse shell was colder close to the water recollection funnel (black surface) condensation was more likely to occur there. The bottom of the greenhouse dome near the aluminum base showed less condensation, because the relative humidity was less in the lower part of the dome as the flasks were installed in the upper level. The curvature of the dome shell and the slope of the recollection funnel led to runoff of the water to the collection container located on scale 1 (see Figure 4-13). Under certain conditions, ice crystals had been observed on the aluminum base as temperatures may have dropped below 0ºC, even though the dome base was well insulated.

During the long-term experiments involving lettuce plants (see next section) water evaporated from the collection container and the relative humidity in the bottom part of the greenhouse increased. Condensate and frost formed on the lower part of the greenhouse shell and the dome base plate due to the low temperatures. This can be clearly observed in the two photos shown in Figure 7-1, which were taken after the vacuum chamber was opened at the end of the 7 day experiment.

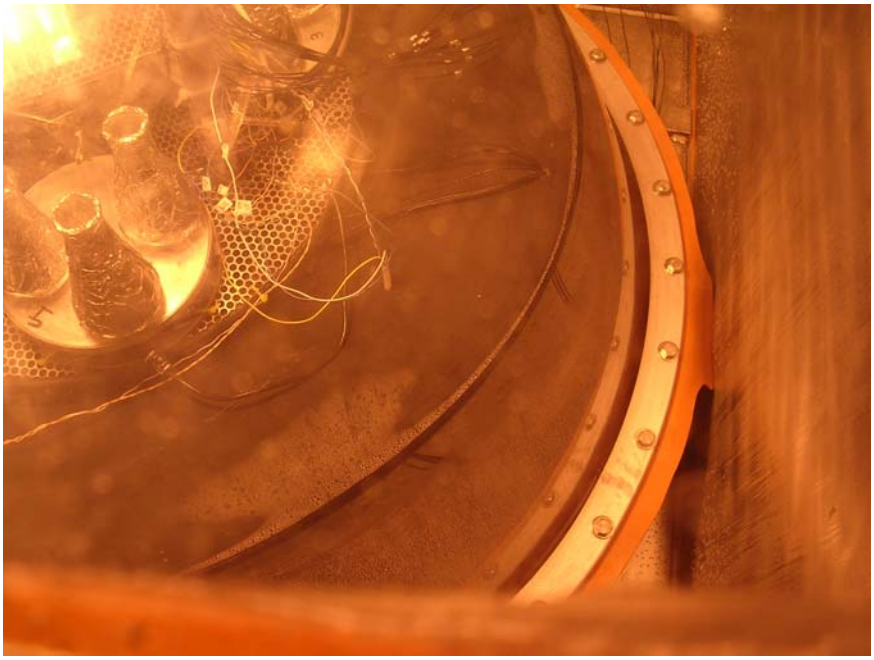
A)

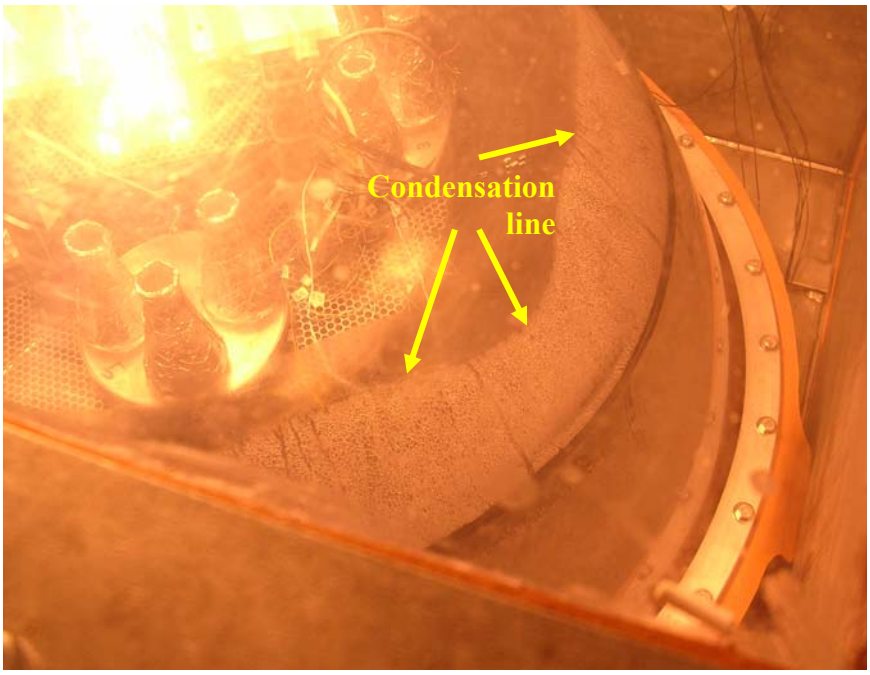

B)

Figure 4-23. Condensation inside of greenhouse shell with a greenhouse air temperature of 20 ºC. A) Freezer temperature at 0 ºC. B) Freezer temperature at -20 ºC.

Heat and Mass Transfer Experiments with Plants

Medium-term Plant Experiment involving Buttercrunch Lettuce

Selection criteria for the plants involved in the Mars greenhouse experiments were a short growth period, high evapo-transpiration rate, tolerance to cold temperatures, low

light requirements, suitability for hydroponic growth in 150 ml Ehrlenmeyer flasks and dome height constraints. Buttercrunch lettuce (*Lactuca Sativa* cv. Buttercrunch) was selected as lettuce is one of NASA's baseline crops (see Chapter 2) and it fulfills the criteria mentioned above. Six weeks old lettuce plants grown in soil under atmospheric conditions were transplanted into flasks filled with 50% water and 50% nutrient solution. The flasks were wrapped in aluminum foil to avoid growth of algae caused by direct radiation onto the nutrient solution. One hole of the stopper was cut open from the side and the plant was carefully inserted. Evaporation of the hydroponic solution was avoided by sealing the gap between the plant and the stopper with putty as shown in Figure 4-24. Eight flasks were placed into the greenhouse dome; two on each scale (see Figure 4-25).


A)

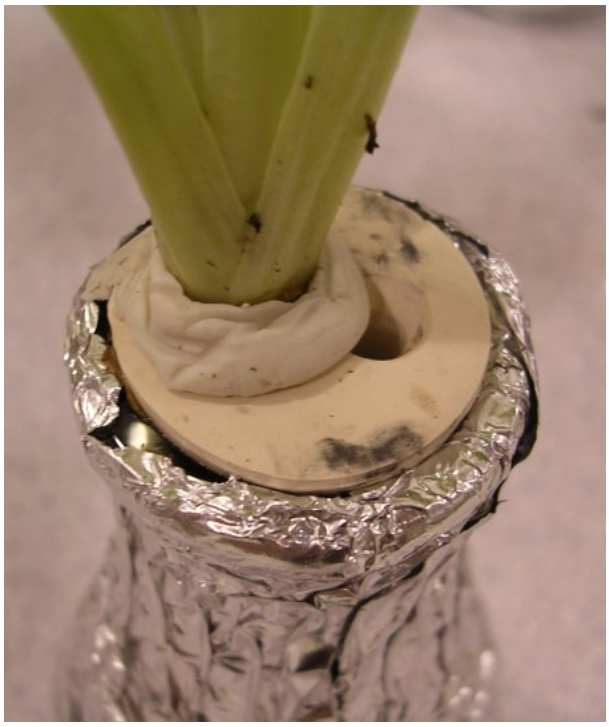
B)

Figure 4-24. Buttercrunch lettuce in Ehrlenmeyer flask. A) The average height of the shoot zone is 15 cm. B) Putty and a stopper prevent evaporation of the hydroponic solution as they separate the root from the shoot zone.

Figure 4-25. Installation of flasks containing the lettuce plants onto the scales.

The plants were exposed to a controlled environment inside the greenhouse dome for 36 hours. The environment conditions and their control methods are summarized in Table 4-3. The air temperature and the gas composition were tightly controlled by actuators. A total pressure of 25 kPa was selected as plants still were to be productive at this low pressure level. The partial pressure of oxygen was set to 4 kPa, resulting in an oxygen level of 16%, lower than on Earth because oxygen is a very precious resource during a space mission on Mars: it must be shipped from Earth as it is barely available in the Mars atmosphere and will be mainly used for human breathing. The partial pressure of carbon dioxide was set to a high level of 0.8 kPa, as carbon dioxide can easily be extracted from the Mars atmosphere. High levels of carbon dioxide are known to enhance plant growth.

The greenhouse humidity was passively controlled by the equilibrium between evaporation of the water from the plants and the open water surfaces versus the

condensation of water on the cold surfaces. The variation of the humidity in the time range of 5 to 10 hours after the experiment had been started can be observed in Figure 4-26. The light was switched on during the complete experiment and the radiation level was measured to be at a constant value of 684 µmol/(m²s) at plant level. Therefore, no condensation occurred on the greenhouse surface directly below the growth light.

Table 4-3. Buttercrunch lettuce environmental conditions and their control.

Parameter	Value	Controlled by
Greenhouse Dome Air/Plant Temperature	20 ºC	↑ heating coil ↓ freezer temperature
Greenhouse Dome Relative Humidity	variable	↑ plant evaporation (passive control) ↓ condensation on cold surface (passive control)
Greenhouse Dome Total Pressure	25 kPa	↑ N_2, O_2 and CO_2 mass flow controllers ↓ vacuum pump (& passively by leakage)
Greenhouse Dome Oxygen Partial Pressure	4 kPa	↑ O_2 mass flow controller ↓ vacuum pump (& passively by leakage)
Greenhouse Dome Carbon Dioxide Partial Pressure	0.8 kPa	↑ CO_2 mass flow controller ↓ vacuum pump (& passively by leakage)
Greenhouse Dome Radiation Level	684 µmol/(m²s)	↑ growth light on ↓ growth light off (& passively by condensation)
Vacuum Chamber Total Pressure	0.6 kPa	↑ leakage (passive control) ↓ vacuum pump
Freezer Temperature	-20 ºC (± 1ºC)	↑ thermostat on freezer ↓ thermostat on freezer

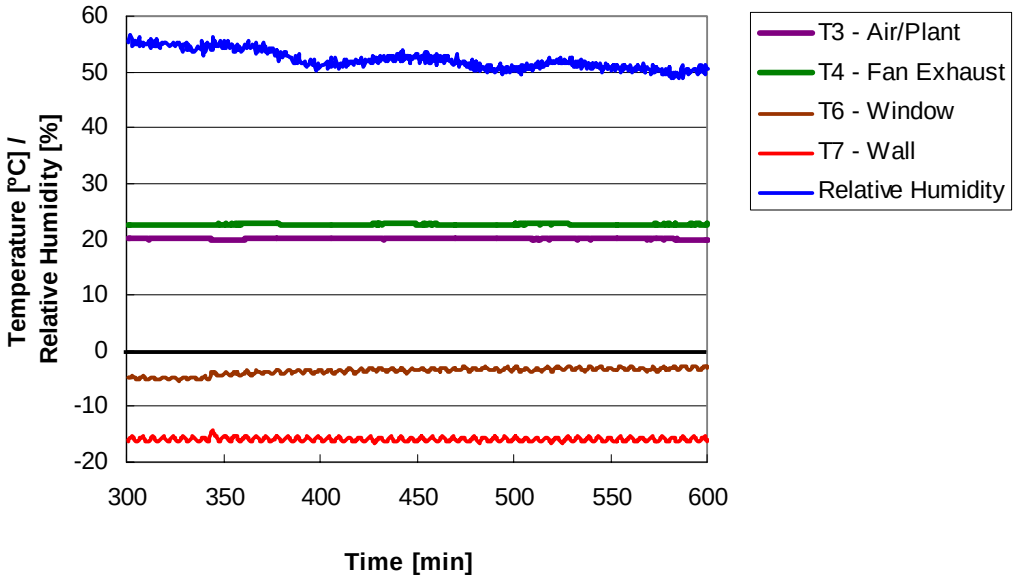

Figure 4-26. Constant temperature distribution and varying relative humidity during the buttercrunch lettuce experiment.

Figure 4-27 depicts the rates of plant evapo-transpiration from the scales 2-5. Scale 1 measured the water in the recollection container. It had been filled with 245 grams of water before the experiment in order to keep the humidity high at the beginning of the experiment. The change of the mass value of scale 1 is the difference between water evaporating from the open water surface and recollected water dripping into the container. A positive slope indicates more water was recollected than evaporated, a negative slope leads to the conclusion that more water was evaporated than re-collected. Surprisingly, in this experiment the slope of scale 1 had a negative value of –0.0661. Thus, the recollection system proved to be inefficient as less water was recollected than had evaporated. This resulted in higher humidities in the lower greenhouse part and therefore water condensation on the cold dome aluminum base. The plant evapo-transpiration can be calculated by dividing the water evaporation rate of the scale by the plant leaf area per scale.

In order to calculate the plant leaf area, the leaves were cut off the plants at the end of the experiment and the silhouettes were drawn on a white sheet of paper. The silhouettes were scanned together with a calibration square. The pictures were converted to black and white images and the silhouettes were filled with black ink. The pictures were read into matlab and an image processing code determined the ratio of white to black pixels. The resulting values of the plant leaf areas per scale are given in Table 4-4. Plant evapo-transpiration varied from 1.6 g/(min m²) to 2.87 g/(min m²). Evapo-transpiration rates for lettuce under atmospheric conditions are given as 1.23 g/(min m²) in NASA's Baseline Values and Assumptions Document (Hanford, 2004). Low pressure increases evaporation rates and therefore the evapo-transpiration values calculated in the

research described in this document seem reasonable. It should be noted that evapo-transpiration rates are further affected by other factors, including relative humidity, air temperature, leaf temperature, radiation level and lettuce cultivar, making it difficult to compare the values of different experiments.

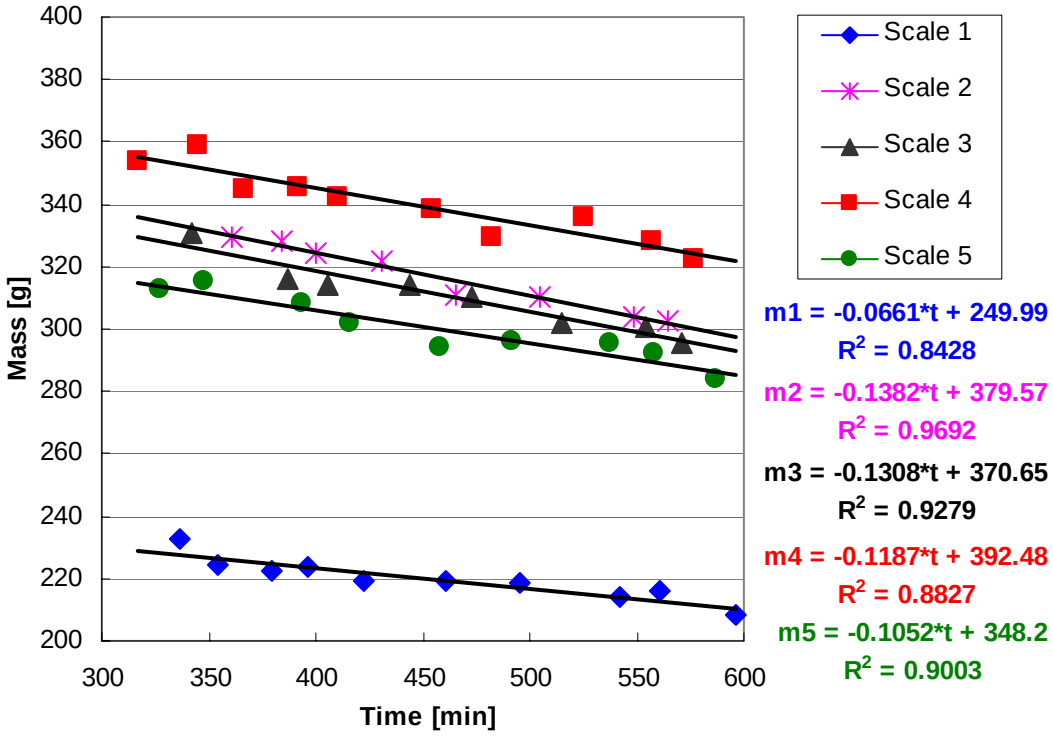

Figure 4-27. Plant evapo-transpiration rates of plants from 5 to 10 hours after the beginning of the experiment.

Table 4-4. Evaporation rates per scale with scales 2-5 containing two lettuce plants each.

	Scale 1	**Scale 2**	**Scale 3**	**Scale 4**	**Scale 5**
Evaporation/Time [g/min]	0.0661	0.1382	0.1308	0.1187	0.1052
Leaf Area Plant 1 [m²]	-	*0.042335*	*0.0234*	*0.039542*	*0.032599*
Leaf Area Plant 2 [m²]	-	*0.033219*	*0.02215*	*0.023296*	*0.033002*
Total Leaf Area [m²]		0.075554	0.045549	0.062838	0.065601
Evapo-transpiration Rate[g/min/m²]		**1.83**	**2.87**	**1.89**	**1.60**

At the end of the experiment, seven out of the eight plants appeared to be healthy and without visible damage. One plant started wilting after the water level inside the flask

decreased to a point where the roots could not reach the remaining water and nutrient solution (see Figure 4-28).

Figure 4-28. Lettuce plants after an exposure of 36 hours to the controlled Mars greenhouse environment. Healthy plant without any visible physical damage on the left side, wilted plant with roots that do not reach water and nutrient supply on the right side.

Long-term Plant Experiment involving Galactic Lettuce

For the long-term plant experiments Galactic lettuce plants (*Lactuca Sativa* cv. Galactic) were selected (see Figure 4-29). The plants were grown from seeds in the departmental environment-controlled growth chamber under atmospheric conditions with a day-night cycle of 12 hours. After four weeks, measuring an average height of 8 cm, the lettuce plants were transplanted into the flasks filled with the hydroponic nutrient solution. Similar to the previous experiment, eight plants were installed into the greenhouse dome, two per scale. Table 4-5 lists the environmental conditions the plants were exposed to and their control. All environmental parameters except of the total dome

pressure were kept the same as in the buttercrunch lettuce experiments. The greenhouse dome total pressure was lowered to 20 kPa.

Figure 4-29. Galactic lettuce plant for long-term experiments with an average height of 8 cm.

Table 4-5. Galactic lettuce environmental conditions and their control.

Parameter	Value	Controlled by
Greenhouse Dome Air/Plant Temperature	20 ºC	↑ heating coil ↓ freezer temperature
Greenhouse Dome Relative Humidity	variable	↑ plant evaporation (passive control) ↓ condensation on cold surfaces (passive control)
Greenhouse Dome Total Pressure	20 kPa	↑ N_2, O_2 and CO_2 mass flow controllers ↓ vacuum pump (& passively by leakage)
Greenhouse Dome Oxygen Partial Pressure	4 kPa	↑ O_2 mass flow controller ↓ vacuum pump (& passively by leakage)
Greenhouse Dome Carbon Dioxide Partial Pressure	0.8 kPa	↑ CO_2 mass flow controller ↓ vacuum pump (& passively by leakage)
Greenhouse Dome Radiation Level	0 or 684 µmol/(m²s)	↑ growth light on ↓ growth light off (& passively by condensation)
Vacuum Chamber Total Pressure	0.6 kPa	↑ leakage (passive control) ↓ vacuum pump
Freezer Temperature	-20 ºC (± 1ºC)	↑ thermostat on freezer ↓ thermostat on freezer

Figure 4-30 shows the locations of the sensors for the second set of plant experiments. Various temperature sensors were added or moved from their previous position: T_2 was moved from the recollection funnel to the inside of the greenhouse dome shell, T_5 was moved to the side of the exterior greenhouse shell, T_6 was fixed to the inside of the vacuum chamber wall, T_7 on the outside of the chamber wall at medium height, T_8 at the bottom of the chamber wall and T_9 measured the freezer air temperature.

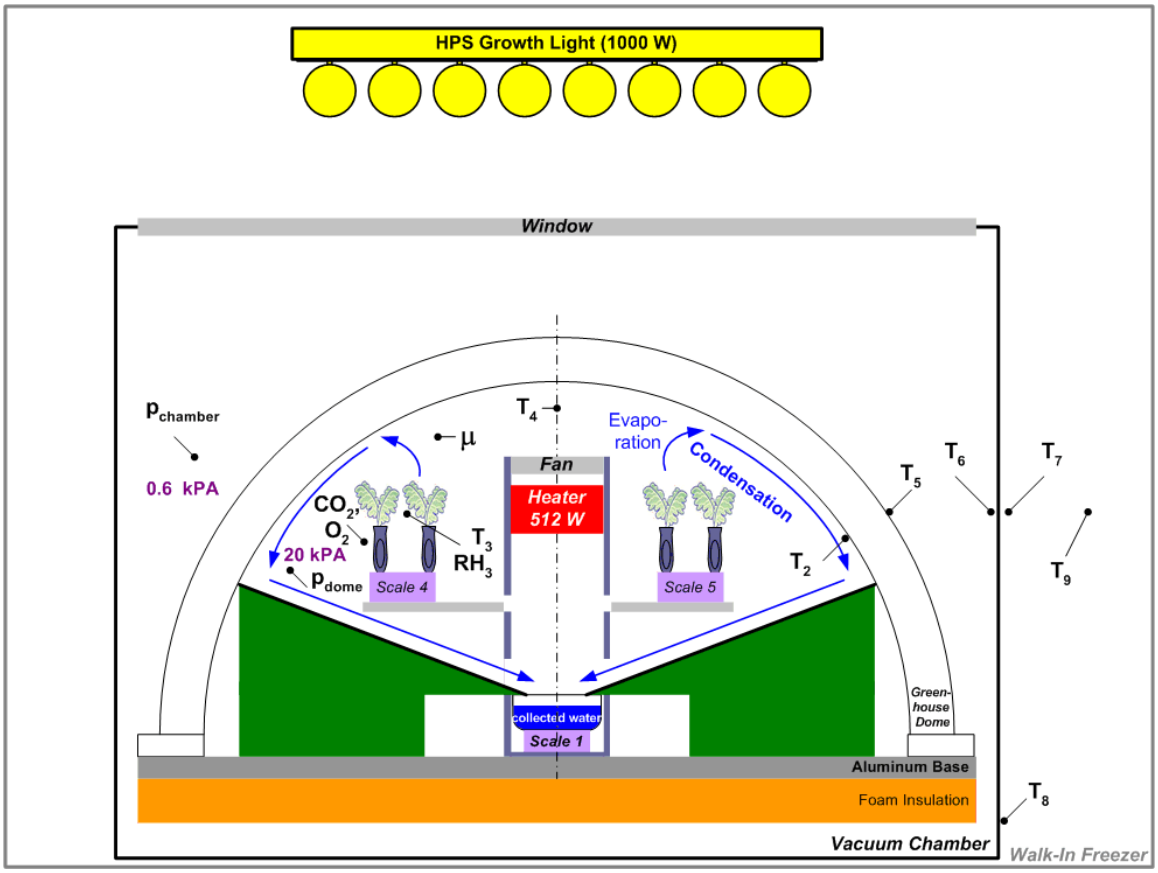

Figure 4-30. Sensor locations for the long-term experiments with galactic lettuce plants.

Plants were exposed to the low pressure controlled greenhouse environment for 7 days. Initially they were exposed to the growth light for 24 hours until steady state of all parameters was reached, the following days the day-night cycle was set to 12 hours. Figure 4-31 illustrates the temperature changes over time during the experiment. The air

temperature at plant level was controlled at 20 ºC, the freezer temperature was controlled at -20 ºC (± 1ºC). Figure 4-32 depicts the steady state temperatures during the day and night cycle, when the growth light was switched on/off, respectively. A heating power of 40 Watts was required to maintain an air temperature of 20 ºC at the plant level during the day cycle, a heater power of 119 Watts during the night cycle. The temperature of the fan exhaust was higher for the night cycle as more heating was required, all other temperatures were lower when the growth light was switched off compared to when the growth light was switched on.

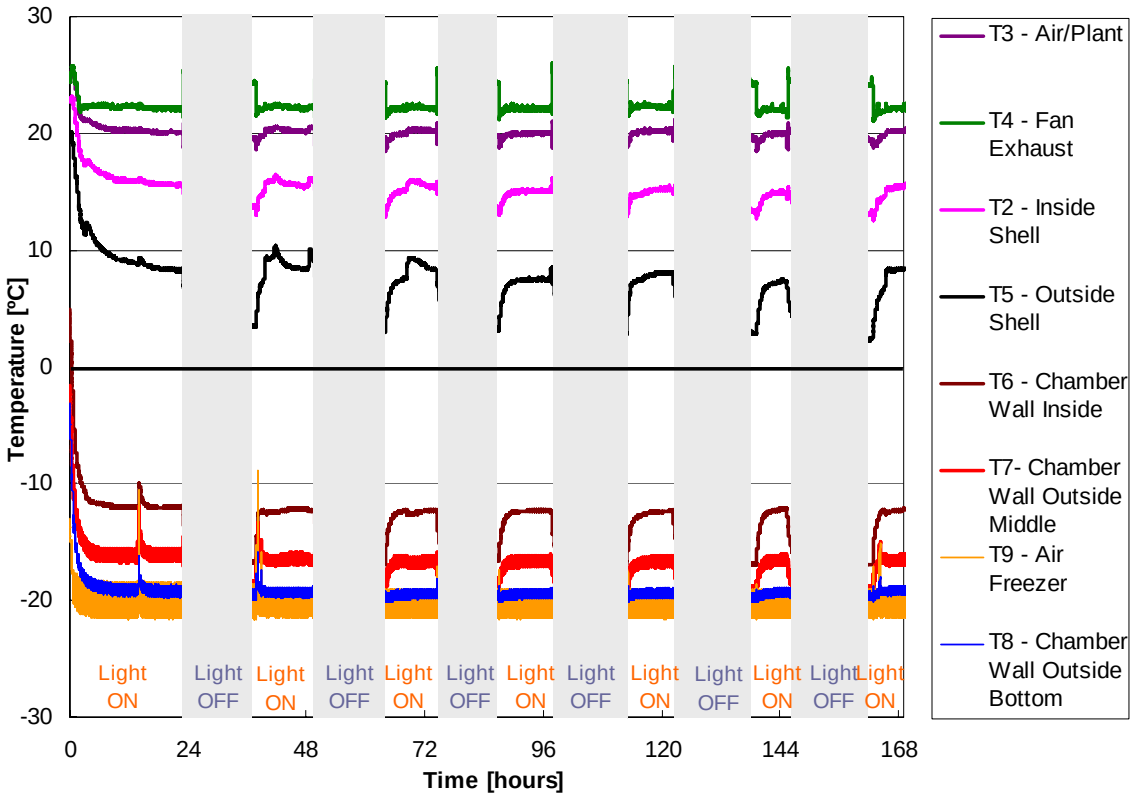

Figure 4-31. Temperature variations during the long-term galactic lettuce experiment.

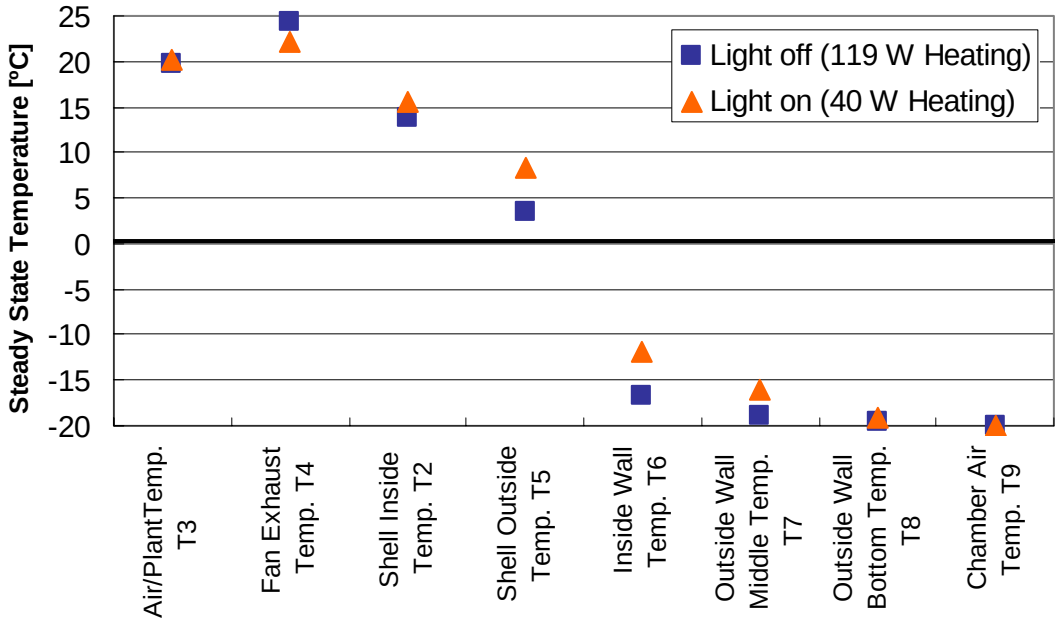

Figure 4-32. Comparison of steady state temperature distribution of the day cycle to the night cycle during the long-term plant experiments.

Figure 4-33 shows the variation of the relative humidity during the day and night cycle. Before the experiment started, when the greenhouse dome was closed but the freezer not switched on yet, the relative humidity rose to 70%. This high humidity was due to addition of water vapor to the atmosphere by plant evapo-transpiration and the lack of water vapor removal by condensation as the temperatures of the all surfaces of the greenhouse were at temperatures above 20 ºC and therefore above the dew-point. Relative humidity decreased to 35% during the first 24 hours when the growth light was switched on. During the following day-night cycles the relative humidity varied between a maximum of 35% when the growth light was switched on and a minimum of 28% when the growth light was switched off. Relative humidity was low during the night cycle as more condensation occurred due to the lower temperatures of the greenhouse surfaces.

Relative humidity was high during the day due to less condensation and more evapo-transpiration of the plants.

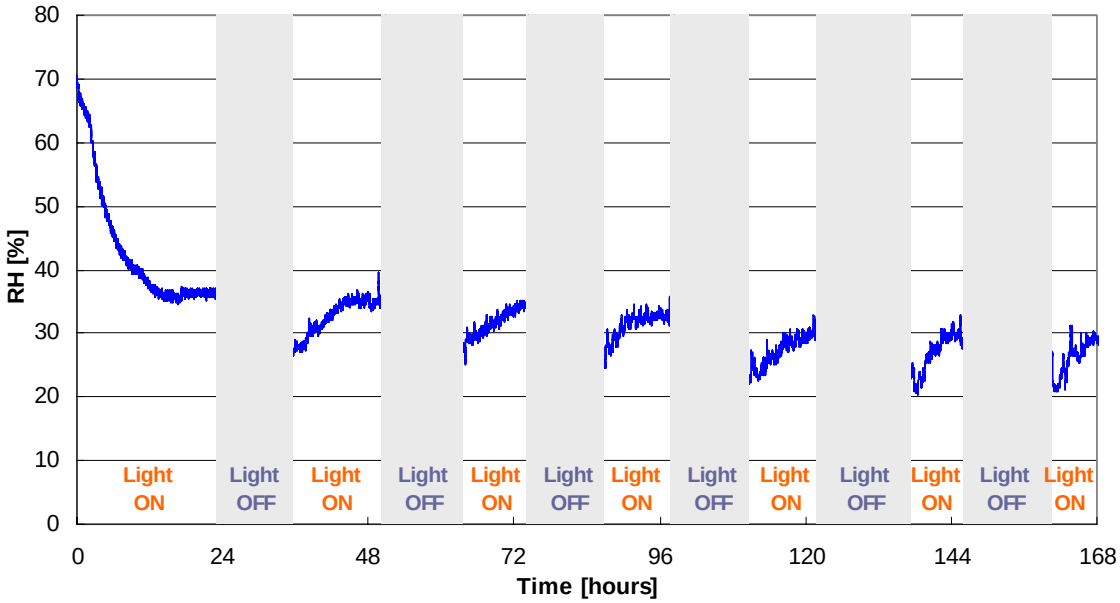

Figure 4-33. Relative humidity variation during the day and night cycle.

Figure 4-34 shows the effectiveness of the gas composition control, resulting in a constant gas composition even when all other environmental parameters were subject to great variations. Changes in temperature, relative humidity and radiation level did not affect the gas composition of 20 kPa total pressure, 4 kPa oxygen partial pressure and 0.8 kPa carbon dioxide partial pressure.

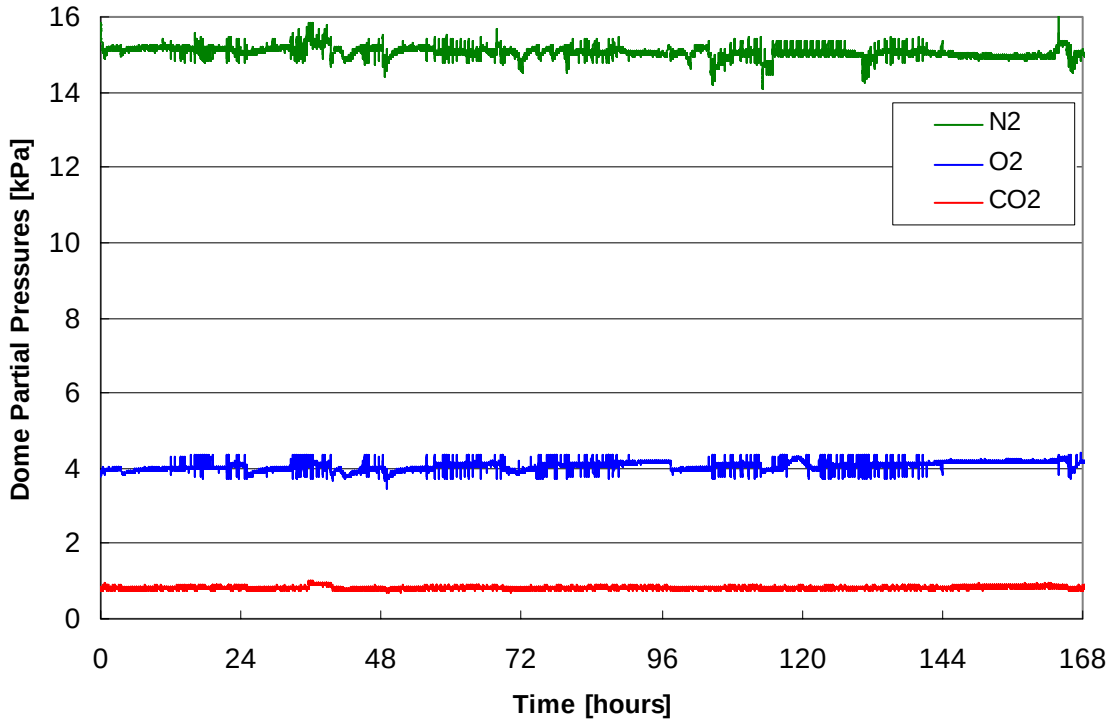

Figure 4-34. Gas composition control of the greenhouse atmosphere. Set points are 20 kPa for total pressure, 4 kPa for oxygen partial pressure and 0.8 kPa for carbon dioxide partial pressure.

Figure 4-35 shows the mass values of the scales that were measured from 5 to 10 hours after the galactic lettuce plant experiment had started. For this experiment only two out of the five scales were connected to the data acquisition system due to the limited amount of available channels because of the added temperature sensors. The evapo-transpiration rates of the plants were determined with the same leaf area calculation method described earlier in this Chapter. The evapo-transpiration rates were found to be 3.71 g/min/m² for scale 2 and 4.84 g/min/m² for scale 3. These evaporation rates are slightly higher than the ones in the Buttercrunch lettuce experiments. One possible reason is that the pressure was reduced from 25 kPa to 20 kPa, leading to an increase in mass diffusivity and therefore higher evaporation rates.

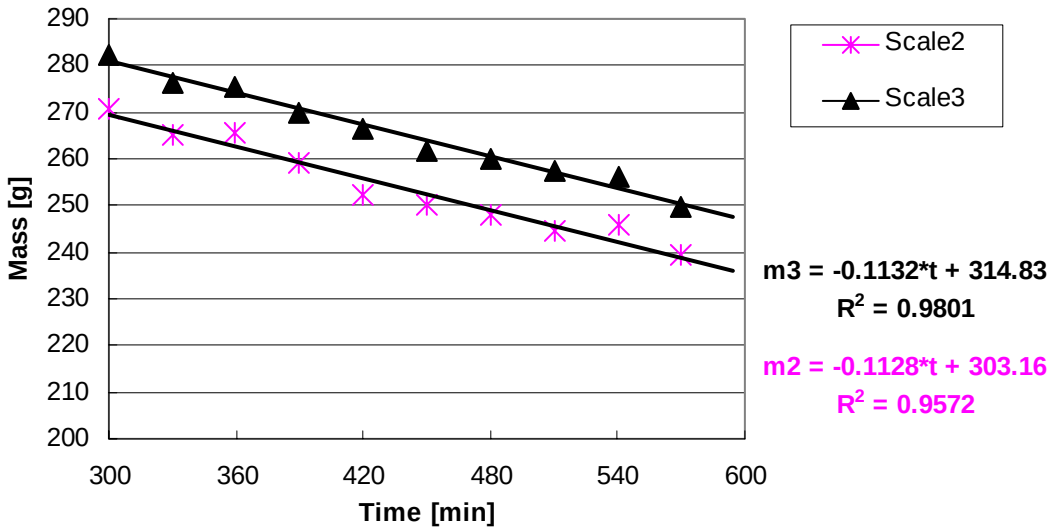

Figure 4-35. Water evaporation measured on scale 2 and 3 during the galactic lettuce plant experiment.

Figure 4-36 shows the galactic lettuce plants after they were exposed to the low pressure Mars greenhouse environment for 7 days. They showed only slight visible physical damage such as minor signs of water stress (see Figure 4-37 A and B).

Figure 4-36. Galactic lettuce plants after exposure of seven days to the low pressure Mars greenhouse environment.

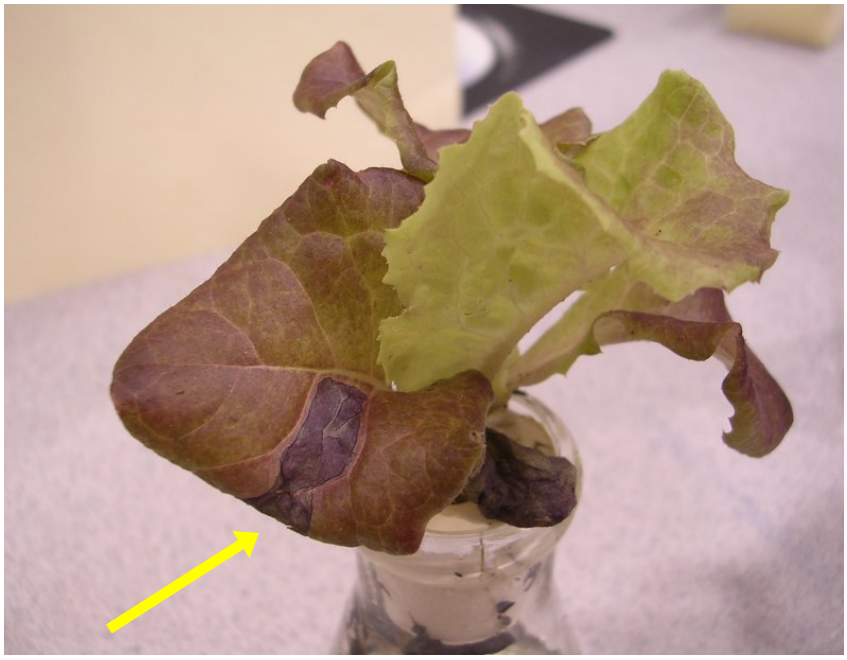
A)


B)

Figure 4-37. Visible damages of the plants. A) and B) Wilting/drying of the plant leaves.

CHAPTER 5
MATHEMATICAL MODEL DEVELOPMENT

Effect of Low Pressure on Heat and Mass Transfer

Operating the greenhouse dome at a reduced pressure in the low pressure Mars environment has a huge influence on the heat and mass transfer. Of the three heat transfer modes conduction, convection and radiation, convective heat transfer is the one that is most dependent on the total pressure. Regarding the mass transfer, evaporation rates have to be analyzed for pressure dependency. Furthermore, the effect of the low pressure on psychrometric relations should be studied, in order to be able to determine the state of the moist air.

Convection Heat Transfer

Convection is defined as heat transfer between a surface and a fluid moving over the surface. Convective heat transfer at low pressures is analyzed based on the equations given in Incropera and DeWitt (2002). The convection heat transfer depends on the convection coefficient and on the temperature difference of the moving fluid and the surface:

$$q'' = h(T_s - T_\infty) \tag{5-1}$$

where: q'' = heat flux [W/m²]

h = convection coefficient [W/(m^2 K)]

T_s = surface temperature [K]

T_∞ = fluid temperature [K]

If there is a temperature difference between the fluid stream and the surface a thermal boundary layer develops. The local heat flux may be obtained by applying Fourier's Law to the heat flux at the surface where y = 0. As there is no fluid motion at the surface, energy transfer occurs only by conduction:

$$q_s'' = -k_f \left.\frac{\partial T}{\partial y}\right|_{y=0} \tag{5-2}$$

Combining both equations leads to the following convection coefficient:

$$h = \frac{-k_f \left.\frac{\partial T}{\partial y}\right|_{y=0}}{T_s - T_\infty} \tag{5-3}$$

In order to find out if the boundary layer is laminar or turbulent the Reynolds number has to be calculated:

$$\mathrm{Re}_L = \frac{\rho u_\infty L}{\mu} \tag{5-4}$$

where: Re_L = Reynolds number [-]

ρ = density [kg/m³]

u_∞ = velocity [m/s]

μ = absolute viscosity [N s/m²]

L = characteristic length [m]

The critical Reynolds number for which transition from laminar to turbulent flow occurs is 5×10^5.

A parameter that provides a measure of the convection heat transfer is the dimensionless temperature gradient, the Nusselt Number:

$$Nu = \frac{hL}{k_f} = +\left.\frac{\partial T^*}{\partial y^*}\right|_{y^*=0} = f(x, \mathrm{Re}_L, \mathrm{Pr}) \tag{5-5}$$

where: $T^* = \frac{T - T_S}{T_\infty - T_S}$ = dimensionless temperature

$y^* = \frac{y}{L}$ = dimensionless variable

The average Nusselt number represents the average heat transfer independent of location:

$$\overline{Nu}_L = \frac{\bar{h}L}{k_f} = f(\mathrm{Re}_L, \mathrm{Pr}) \tag{5-6}$$

The Prandtl number is the ratio of the properties ν/α:

$$\mathrm{Pr} = \frac{\nu}{\alpha} = \frac{c_p \mu}{k_f} \tag{5-7}$$

where: ν = dynamic viscosity [m²/s]

α = thermal diffusivity [m²/s]

c_p = specific heat [kJ/(kg K)]

k_f = conduction coefficient [W/(m K)]

Laminar flow over a horizontal plate

For laminar flow, the Reynolds number has to be below the critical Reynolds number of 5×10^5:

$$\mathrm{Re}_{L,critical} = \frac{\rho u_\infty L}{\mu} = 5 \times 10^5 \tag{5-8}$$

For laminar flow the Nusselt number may be obtained from:

$$\overline{Nu}L = \frac{\bar{h}L}{k_f} = 0.664\,\mathrm{Re}_L^{1/2}\,\mathrm{Pr}^{1/3} \quad \mathrm{Pr} \geq 0.6 \tag{5-9}$$

Inserting Equations 5-4 and 5-7 into Equation 5-9, results into the following convection coefficient:

$$\overline{h_L} = 0.664 \frac{(\rho u_\infty)^{1/2}}{(\mu)^{1/6}} (c_p)^{1/3} \frac{(k_f)^{2/3}}{L^{1/2}} \quad \Pr \geq 0.6 \tag{5-10}$$

Therefore, convective heat transfer depends on the following parameters: High density, specific heat and thermal conductivity increase heat transfer. Low absolute viscosity increases heat transfer.

Specific heat as well as absolute viscosity are independent of density, i.e., pressure. They are only dependent on temperature. Thermal conductivity is also independent of the air pressure. Thus, the convection transfer coefficient decreases with the square root of density/pressure.

$$\overline{h_L} \sim (pressure)^{1/2} \quad \text{for } density \sim pressure \ (T = const) \tag{5-11}$$

Thus, the convection coefficient of a gas at a pressure of 20 kPa is 44.7 % of the convection coefficient of gas at a pressure of 100 kPa for laminar fluid flow with same velocity and temperature:

$$\overline{h_L}(20kPa) = \left(\frac{20}{100}\right)^{1/2} \times \overline{h_L}(100kPa) = 0.447\, \overline{h_L}(100kPa) \tag{5-12}$$

Turbulent flow over a horizontal plate

For turbulent flow, the Reynolds number has to be above the critical Reynolds number of 5×10^5. For turbulent flow the Nusselt number may be obtained from:

$$\overline{Nu}_L = \frac{\overline{h_L} L}{k_f} = 0.037\, \mathrm{Re}_L^{4/5}\, \mathrm{Pr}^{1/3} \tag{5-13}$$

Inserting the Reynolds and the Prandtl number into Equation 5-13:

$$\overline{h_L} = 0.037 \frac{(\rho \times u_\infty)^{4/5}}{(\mu)^{7/15}} (c_p)^{1/3} \frac{(k_f)^{2/3}}{L^{1/5}} \tag{5-14}$$

Thus, the convection transfer coefficient decreases with decreasing density, i.e. pressure. The convection coefficient of a gas at a pressure of 20 kPa is 27.6 % of the convection coefficient of a gas at 100 kPa for turbulent fluid flow with the same velocity and temperature:

$$\overline{h_L}(20kPa) = (20/100)^{4/5} \times \overline{h_L}(100kPa) = 0.276\,\overline{h_L}(100kPa) \tag{5-15}$$

Laminar free convection on a vertical plate

For laminar free convection on a vertical plate, the Nusselt number is defined as:

$$\overline{Nu}\,L = \frac{\overline{h_L}L}{k_f} = \frac{4}{3}\left(\frac{Gr_L}{4}\right)^{1/4} f(\mathrm{Pr}) \tag{5-16}$$

where: $f(\mathrm{Pr}) = \dfrac{0.75\,\mathrm{Pr}^{1/2}}{(0.0609 + 1.221\,\mathrm{Pr}^{1/2} + 1.238\,\mathrm{Pr})^{1/4}}$

The Grashof number is the ratio of the buoyancy to the viscous force:

$$Gr_L = \frac{g\beta(T_s - T_\infty)L^3}{\left(\dfrac{\mu}{\rho}\right)^2} \tag{5-17}$$

where: g = gravitational constant [m/s²]

$\beta = 1/T_\infty$ = coefficient of thermal expansion [1/K]

By inserting the Grashof number into Equation 4-16, the convection coefficient is:

$$\overline{h_L} = \frac{4}{3}\left(\frac{g\beta(T_s - T_\infty)L^3}{4\mu^2}\right)^{1/4} \rho^{1/2}\, f(\mathrm{Pr})\frac{k_f}{L} \tag{5-18}$$

Thus, the convection transfer coefficient decreases with decreasing density, i.e. pressure. The convection coefficient of a gas at a pressure of 0.6 kPa is 7.75 % of the convection coefficient of a gas at 100 kPa for laminar free vertical convection at the same temperature:

$$\overline{h_L}(0.6kPa) = (0.6/100)^{1/2} \times \overline{h_L}(100kPa) = 0.0775\,\overline{h_L}(100kPa) \tag{5-19}$$

It should be noted, that the convection coefficient also depends on gravity. Thus it would be further reduced by 61.3% on Mars, where the gravitational constant is only 3.69 m/s².

$$\overline{h_L}(3.69\text{m/s}^2) = (3.69/9.81)^{1/2} \times \overline{h_L}(9.81\text{m/s}^2) = 0.613\,\overline{h_L}(9.81\text{m/s}^2) \tag{5-20}$$

External free convection for a sphere

The following correlation is recommended for spheres exposed to external free convection flow:

$$\overline{Nu}_D = \frac{\overline{h_D} D}{k_f} = 2 + \frac{0.589 Ra_D{}^{1/4}}{[1 + (0.0469/\text{Pr})^{9/16}]^{4/9}} \quad Ra_D \le 10^{11} \quad \text{Pr} \ge 0.7 \tag{5-21}$$

The Rayleigh number is defined as:

$$Ra_D = Gr_D \,\text{Pr} = \frac{g\beta(T_s - T_\infty)D^3}{\left(\frac{\mu}{\rho}\right)^2} \frac{c_p \mu}{k_f} \tag{5-22}$$

Combining Equation 5-21 and Equation 5-22 leads to the following convection coefficient:

$$\overline{h_D} = \left(2 + \frac{0.589 \left(\frac{g\beta(T_s - T_\infty)D^3}{\mu^2} \frac{c_p \mu}{k_f} \right)^{1/4} \rho^{1/2}}{\left[1 + \left(0.0469/(\frac{c_p \mu}{k_f}) \right)^{9/16} \right]^{4/9}} \right) \frac{k_f}{D} \tag{5-23}$$

Therefore, the convection transfer coefficient decreases with decreasing density, i.e. pressure. As the pressure variable in Equation 5-23 is implicit, a direct ratio of the convection coefficient at standard pressure to the one at reduced pressure cannot be derived.

Mass Transfer by Evaporation

The diffusive flux depends on the mass diffusivity coefficient. Assuming ideal gas behavior, the kinetic theory of gases predicts that the mass diffusivity is indirectly proportional to the pressure at a constant temperature.

$$D_{AB} \sim \frac{T^{3/2}}{p} \tag{5-24}$$

where: D_{AB} = Mass diffusion coefficient [m²/s]

T = temperature [K]

p = pressure [kPa]

Thus, reducing the pressure to 20 kPa, would increase the mass diffusivity 5 times:

$$D_{AB}(20kPa) = (100/20) \times D_{AB}(100kPa) = 5 \times D_{AB}(100kPa) \tag{5-25}$$

Table 5-1 gives an overview of the effect of reduced pressure on the convective heat transfer coefficient and the mass diffusivity. Convection reduces considerably in the low pressure Mars greenhouse dome. In the vacuum chamber, convection is considered to be negligible, the major mode of heat transfer between the dome and the chamber is radiation. Mass diffusivity and therefore evaporation rates increase significantly at low pressures.

Table 5-1. Effect of reduced pressure on convective heat transfer coefficient and mass diffusion coefficient.

	Greenhouse Dome	**Vacuum Chamber**
CONVECTION	**h(20 kPa)/ h(100 kPa)**	**h(0.6 kPa)/ h(100 kPa)**
Forced Convection – Horizontal Plate	44.7% (laminar) 27.6% (turbulent)	
Free Convection – Vertical Plate		7.75% (Earth) 7.75% x 61.3% (Mars)
External Free Convection – Sphere		See Equation 5-23
DIFFUSION	**D(20 kPa)/ D(100 kPa)**	
Mass Diffusivity	500%	

Development of Low Pressure Psychrometrics for Non-Standard Atmospheres

While most publications address the psychrometric relationships of water vapor and air for open systems, sea level pressure and Earth's standard atmosphere composition (78.08% N_2, 20.98% O_2, 0.934% Ar, 0.0314% CO_2, etc), there is nothing in the theory for developing the relationships that restricts them to these systems (Shallcross, 1997; ASHRAE, 2001). In the literature, very few publications are dedicated to altitude effects on psychrometrics, as barometric pressure decreases with altitude (Haines, 1961; Hitchcock and Jacoby, 1980; Erickson and Garrett, 1981). Figure 5-1 shows the effect of reduced pressure on the saturation line of the psychrometric chart. However, psychrometric charts that correct for altitude assume that the gas composition is equal to Earth's. Compared to the Earth atmosphere, the atmosphere of the greenhouse differs significantly in terms of pressure and gas constituents. Furthermore, the greenhouse dome is a closed system, whereas the classic psychrometric relations were developed for open systems.

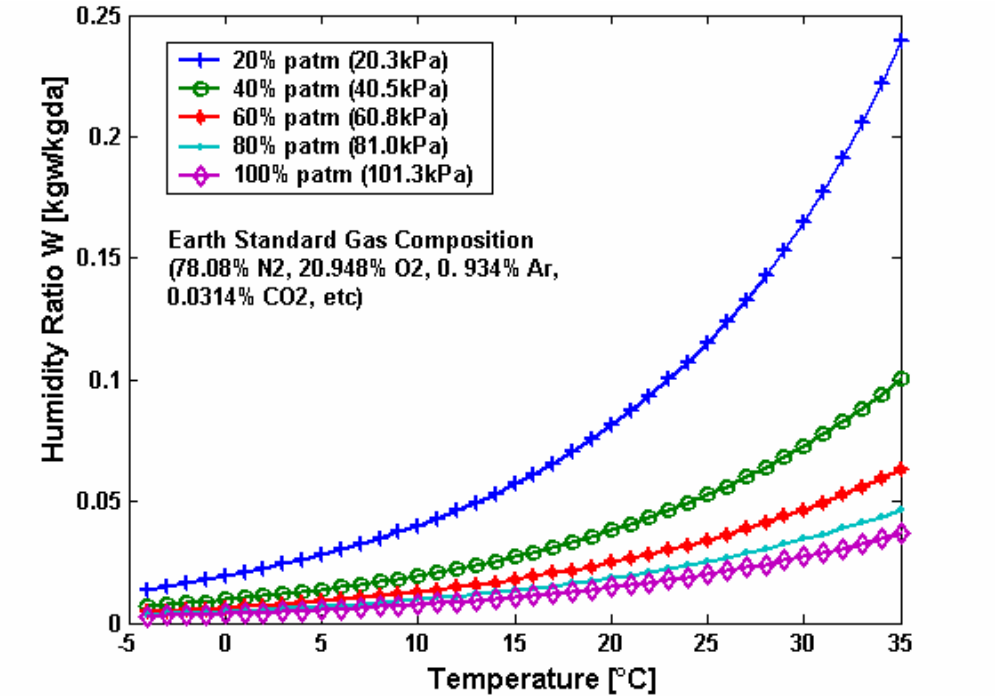

Figure 5-1. Effect of pressure on the saturation line of an open system with standard atmosphere composition

The psychrometric relations are based on the following fundamental laws of physics: ideal gas equation of state, conservation of energy, conservation of mass, Dalton's law of partial pressures and the Gibbs-Dalton law for energy, enthalpy and entropy (Gatley, 2002). If the total pressure of the system differs significantly from the sea level pressure of 101.3 kPa or the dry gas composition differs from the standard Earth atmosphere, the calculations can be modified to reflect this.

The psychrometric chart is a tool for determining the properties of the moist air and for visualizing the changes of these properties as a consequence of psychrometric processes. The-dry bulb temperature is shown on the abscissa of the chart and therefore the dry-bulb temperature isolines are vertical. The second psychrometric chart coordinate (the ordinate) is the humidity ratio, which is defined as the ratio of the mass of water vapor to the mass of the dry air in a moist air sample. Consequently, the humidity ratio isolines are horizontal. Generally, the properties isolines plotted on a psychrometric chart are: dry-bulb temperature isolines, humidity ratio isolines, adiabatic saturation temperature isolines, relative humidity isolines, water vapor saturation curve, enthalpy isolines and specific volume isolines (Gatley, 2002). The following section develops general psychrometric relations that can be used for closed low pressure systems and non-standard gas compositions.

Gas Theory

Equation of state

The classic psychrometric relationships are based on the assumption that moist air is a mixture of independent perfect gases (i.e. dry air and water vapor), and each gas is assumed to obey the perfect gas equation of state, where the compressibility factor equals one. If a low pressure environment is chosen, the perfect gas law applies even better,

since the virial coefficients play less role in low pressure gases as the interaction between molecules is less common. Therefore, the compressibility factor converges to 1 with decreasing pressure.

$$Z = \frac{pv}{RT} = 1 + (B'p) + (C'p^2) + (D'p^3) + ... \quad (5\text{-}26)$$

where: Z = compressibility (Z=1 for perfect gas)

p = pressure

B', C', D' = virial coefficients

Dry gas mixture

The dry gas mixture includes all gas components that remain gaseous and do not condense in the chosen temperature range. The molecular mass as well as the specific heat are important parameters for the development of the psychrometric relationships.

If the partial pressures of the dry gas components are known, the content by volume can be obtained:

$$\psi_{dry,i} = \frac{p_{dry,i}}{p_{dry}} \quad (5\text{-}27)$$

where: $\psi_{dry,i}$ = dry air content of gas component i by volume

$p_{dry,i}$ = partial pressure of gas component i

p_{dry} = total pressure of dry gas

Furthermore, the molecular mass of the dry gas mixture can be calculated:

$$m_{dry,i} = \psi_{dry,i} M_{dry,i} \quad (5\text{-}28)$$

$$m_{dry} = \sum \psi_{dry,i} M_{dry,i} \quad (5\text{-}29)$$

where: $m_{dry,i}$ = mass of gas component i

$M_{dry,i}$ = molecular mass of gas component i

m_{dry} = total mass of dry gas

By calculating the composition of the dry gas mix by mass, the specific heat of the dry gas mixture is obtained:

$$\zeta_{dry,i} = \frac{m_{dry,i}}{m_{dry,total}} \tag{5-30}$$

$$c_{p,dry,i} = \zeta_{dry,i} C_{p,dry,i} \tag{5-31}$$

$$c_{p,dry} = \sum \zeta_{dry,i} C_{p,dry,i} \tag{5-32}$$

where: $\zeta_{dry,i}$ = dry air content of gas component i by mass

$c_{p,dry,i}$ = specific heat of gas component i

$c_{p,dry}$ = specific heat of dry gas

The specific enthalpy of dry air is dependent on the temperature of the gas mix:

$$h_{dry} = c_{p,dry}\, t \tag{5-33}$$

where: h_{dry} = specific enthalpy of dry air

t = temperature of gas mix

Water vapor component

The molecular mass of water is 18.01528. The specific enthalpy of the saturated water vapor component is

$$h_g = (2501 + 1.805t) \tag{5-34}$$

where: h_g = specific enthalpy of water vapor

Construction of Modified Psychrometric Chart

Saturation line

The humidity ratio is defined as the ratio of the mass of water vapor to the mass of dry air contained in a sample. At saturation, air contains the maximum amount of water:

$$W_s = \frac{m_w}{m_{dry}} \frac{x_{ws}}{x_{dry}} = \frac{18.01528}{m_{dry}} \frac{p_{ws}(T)}{p_{dry}(T)} \tag{5-35}$$

where: W_s = humidity ratio at saturation

x_{ws} =mole fraction of water vapor in saturated moist air

x_{dry} = mole fraction of dry air in moist air

The total pressure of the moist air is the sum of the partial pressure of the dry air component and the water vapor.

$$p_{total} = p_{dry}(T) + p_w(T) \tag{5-36}$$

where: p_{total} = total pressure (barometric pressure)

p_w = partial pressure of water vapor

The classic psychrometric equations are for open systems where the partial pressure of the water vapor is small compared to the total pressure. The total pressure is assumed to be constant even when state change of water occurs, i.e. the partial pressure of dry air decreases when water vapor pressure increases and vice versa. In the case of a closed system, the partial pressure of the dry air component depends on the temperature and the initial conditions, as no dry gas leaves or enters the system boundaries and the volume is constant:

$$p_{dry}(T) = \frac{p_{dry}{}^{0}}{T^0} T \tag{5-37}$$

where: $p_{dry}{}^{0}$ = initial pressure of dry air component

T^0 = initial temperature of the gas mixture

Thus, increasing temperature and evaporation lead to an increasing total pressure, decreasing temperature and condensation to a decreasing total pressure.

The saturated water vapor pressure is a function of the dry-bulb temperature only: Saturation pressure over ice for the temperature range of –100 to 0° is given by

$$\ln p_{ws} = C_1 / T + C_2 + C_3 T + C_4 T^2 + C_5 T^3 + C_6 T^4 + C_7 \ln T \tag{5-38}$$

where: C_1 = -5.6745359E+03

C_2 = 6.9325247E+00

C_3 = - 9.6778430E-03

C_4 = 6.2215701E-07

C_5 = 2.0747825E-09

C_6 = -9.4840240E-13

C_7 = 4.1635019E+00

Saturation pressure over liquid water for the temperature range of 0 to 200° is given by

$$\ln p_{ws} = C_8 / T + C_9 + C_{10} T + C_{11} T^2 + C_{12} T^3 + C_{13} \ln T \tag{5-39}$$

where: C_8 = -5.8002206E+03

C_9 = 1.3914993E+00

C_{10} =- 4.8640239E-02

C_{11} = 4.1764768E-05

C_{12} = -1.4452093E-08

C_{13} = 6.5459673E+00

In both Equations:

ln = natural logarithm

p_{ws} = saturation pressure [Pa]

T = absolute temperature [K]

Humidity isolines

The relative humidity is the ratio of the mole fraction of water vapor in a given moist air sample to the mole fraction in an air sample saturated at the same temperature and pressure:

$$\phi = \left. \frac{x_w}{x_{ws}} \right|_{t,p} = \left. \frac{p_w}{p_{ws}} \right|_{t,p} \tag{5-40}$$

where: ϕ = relative humidity

The relative humidity isolines are constructed for a given relative humidity and varying dry-bulb temperatures:

$$W = \frac{m_w}{m_{dry}} \frac{x_w}{x_{dry}} = \frac{m_w}{m_{dry}} \frac{\phi\, p_{ws}(T)}{p_{dry}} \tag{5-41}$$

The degree of saturation equals to the relative humidity for closed systems:

$$\mu = \left. \frac{W}{W_s} \right|_{t,\,p} = \left. \frac{p_w}{p_{ws}} \right|_{t,\,p} = \phi \tag{5-42}$$

where: μ = degree of saturation

Specific enthalpy isolines

The specific enthalpy is the sum of the dry gas specific enthalpy plus the specific enthalpy of the water vapor:

$$h = h_{dry} + W h_g = c_{p,dry}\, t + W(2501 + 1.805\, t) \tag{5-43}$$

The lines of constant enthalpy are constructed for a given enthalpy and varying dry bulb temperatures:

$$W = \frac{h - (c_{p,dry}\, t)}{2501 + 1.805 t} \tag{5-44}$$

Specific volume isolines

The specific volume of a gas mixture is defined as the volume of the mixture per unit dry gas:

$$v = \frac{V}{m_{dry}} \tag{5-45}$$

where: v = specific volume of moist air in terms of unit mass of dry air

V = total volume

The gas volume as well as the mass of the dry air of a closed system are constant. Therefore, the specific volume is also constant:

$$v = \frac{RT}{m_{dry} p_{dry}} = \frac{RT^0}{m_{dry} p_{dry}^0} = const. \tag{5-46}$$

Vapor pressure isolines

The humidity ratio is related to the water vapor pressure and the partial pressure of the dry air as follows:

$$W = \frac{m_w}{m_{dry}} \frac{p_w}{p_{dry}} \tag{5-47}$$

Adiabatic saturation temperature isolines

The wet-bulb temperature is considered to be the temperature measured by a thermometer with the outside surface kept wet. As moist gas passes the thermometer, some of the liquid evaporates causing the temperature of the wet-bulb thermometer to drop. As wet-bulb temperature is dependent on the gas velocity in respect to the thermometer and the radiative heat transfer, it is not possible to predict the wet-bulb temperature precisely. Consequently, adiabatic saturation temperature is considered in this document. Adiabatic saturation temperature t_{ad} is defined as the temperature at which water, by evaporating into moist air at a given dry-bulb temperature and absolute humidity can bring the air to saturation adiabatically at the same temperature t_{ad} (Shallcross, 1997). However, for the air-water system of this document the curves of adiabatic saturation temperature and wet-bulb temperature coincide. The adiabatic saturation temperature is related to the humidity ratio by the following correlation:

$$W = \frac{(2501 - 2.381 t_{ad}) W_{wet} - c_{p,dry}(t - t_{ad})}{2501 + 1.805 t - 4.186 t_{ad}} \tag{5-48}$$

where: t_{ad} = adiabatic saturation temperature

Dew-point temperature isolines

The dew-point temperature is related to the humidity ratio by the following equation:

$$W_s = \frac{m_W}{m_{dry}} \frac{p_{ws}(T_{dew})}{p_{dry}} \tag{5-49}$$

where: T_{dew} = dew-point temperature

Table 5-2 lists the psychrometric parameters of the greenhouse dome atmosphere with the selected composition for the plant experiments. Figure 5-2 shows the psychrometric chart for the greenhouse dome atmosphere. It can be utilized to determine the dew-point temperature at which condensation starts to occur on the greenhouse shell. One important difference from the classical psychrometric chart is that the dew-point temperature isolines are not horizontal, as the pressure of the dry air changes with temperature in a closed system.

Table 5-2. Psychrometric parameters of a low pressure atmosphere (76% N_2, 20% O_2, 4% CO_2) with initial conditions of 20 kPa dry air at 20°C and a constant specific volume of 0.004138m³/kg.

T_{dry} [°C]	Humidity Φ	p_{Ws} [Pa]	p_W [Pa]	p_t [Pa]	w [kg/kg$_{da}$]	t_{dew} [ºC]	μ	h [kJ/kgda]	t_{ad} [ºC]
5	100%	872.49	872.49	19849	0.0281	5.02	1	75.6	5.00
10	100%	1228.00	1228.00	20546	0.0389	10.03	1	108.0	10.00
15	100%	1705.45	1705.45	21364	0.0531	15.03	1	149.2	15.00
20	100%	2338.80	2338.80	22339	0.0715	20.01	1	201.5	20.00
25	100%	3169.22	3169.22	23510	0.0953	25.00	1	267.7	25.00
30	100%	4246.03	4246.03	24928	0.1256	29.98	1	350.9	30.00
5	90%	872.49	785.24	19762	0.0253	3.51	0.9	68.5	3.79
10	90%	1228.00	1105.20	20423	0.0350	8.47	0.9	98.2	8.68
15	90%	1705.45	1534.90	21194	0.0478	13.40	0.9	135.8	13.58
20	90%	2338.80	2104.92	22105	0.0644	18.33	0.9	183.4	18.48
25	90%	3169.22	2852.29	23193	0.0858	23.25	0.9	243.4	23.39
30	90%	4246.03	3821.43	24504	0.1130	28.17	0.9	318.8	28.30
5	80%	872.49	697.99	19675	0.0225	1.83	0.8	61.5	2.48
10	80%	1228.00	982.40	20300	0.0311	6.74	0.8	88.4	7.27
15	80%	1705.45	1364.36	21023	0.0425	11.61	0.8	122.3	12.04
20	80%	2338.80	1871.04	21871	0.0572	16.47	0.8	165.2	16.83
25	80%	3169.22	2535.37	22876	0.0762	21.32	0.8	219.2	21.64
30	80%	4246.03	3396.82	24079	0.1005	26.16	0.8	286.7	26.45

Table 5-2 continued

T_{dry} [°C]	Humidity Φ	p_{Ws} [Pa]	p_W [Pa]	p_t [Pa]	w [kg/kg$_{da}$]	t_{dew} [°C]	μ	h [kJ/kgda]	t_{ad} [°C]
5	70%	872.49	610.74	19587	0.0197	-0.04	0.7	54.4	1.09
10	70%	1228.00	859.60	20177	0.0272	4.80	0.7	78.6	5.71
15	70%	1705.45	1193.81	20853	0.0371	9.61	0.7	108.9	10.37
20	70%	2338.80	1637.16	21637	0.0501	14.40	0.7	147.1	15.03
25	70%	3169.22	2218.45	22560	0.0667	19.17	0.7	194.9	19.71
30	70%	4246.03	2972.22	23654	0.0879	23.93	0.7	254.7	24.42
5	60%	872.49	523.49	19500	0.0169	-2.18	0.6	47.4	-0.42
10	60%	1228.00	736.80	20055	0.0233	2.60	0.6	68.8	4.04
15	60%	1705.45	1023.27	20682	0.0318	7.33	0.6	95.5	8.53
20	60%	2338.80	1403.28	21403	0.0429	12.04	0.6	128.9	13.05
25	60%	3169.22	1901.53	22243	0.0572	16.72	0.6	170.6	17.59
30	60%	4246.03	2547.62	23230	0.0754	21.40	0.6	222.6	22.16
5	50%	872.49	436.24	19413	0.0141	-4.67	0.5	40.3	-2.05
10	50%	1228.00	614.00	19932	0.0194	0.03	0.5	59.0	2.20
15	50%	1705.45	852.72	20512	0.0265	4.69	0.5	82.1	6.50
20	50%	2338.80	1169.40	21169	0.0358	9.30	0.5	110.8	10.84
25	50%	3169.22	1584.61	21926	0.0477	13.89	0.5	146.4	15.21
30	50%	4246.03	2123.02	22805	0.0628	18.47	0.5	190.5	19.61
5	40%	872.49	348.99	19326	0.0112	-7.67	0.4	33.2	-3.83
10	40%	1228.00	491.20	19809	0.0156	-3.05	0.4	49.2	0.17
15	40%	1705.45	682.18	20341	0.0212	1.51	0.4	68.7	4.23
20	40%	2338.80	935.52	20936	0.0286	6.03	0.4	92.6	8.33
25	40%	3169.22	1267.69	21609	0.0381	10.51	0.4	122.1	12.48
30	40%	4246.03	1698.41	22381	0.0502	14.96	0.4	158.4	16.67
5	30%	872.49	261.75	19238	0.0084	-11.48	0.3	26.2	-5.79
10	30%	1228.00	368.40	19686	0.0117	-6.95	0.3	39.4	-2.09
15	30%	1705.45	511.63	20171	0.0159	-2.49	0.3	55.3	1.65
20	30%	2338.80	701.64	20702	0.0215	1.91	0.3	74.5	5.45
25	30%	3169.22	950.76	21292	0.0286	6.26	0.3	97.8	9.31
30	30%	4246.03	1273.81	21956	0.0377	10.58	0.3	126.3	13.22
5	20%	872.49	174.50	19151	0.0056	-16.75	0.2	19.1	-7.97
10	20%	1228.00	245.60	19563	0.0078	-12.32	0.2	29.6	-4.66
15	20%	1705.45	341.09	20000	0.0106	-7.98	0.2	41.9	-1.32
20	20%	2338.80	467.76	20468	0.0143	-3.72	0.2	56.3	2.06
24	20%	2985.13	597.03	20870	0.0180	-0.36	0.2	69.9	4.81
30	20%	4246.03	849.21	21531	0.0251	4.63	0.2	94.2	9.01
5	10%	872.49	87.25	19064	0.0028	-25.59	0.1	12.1	-10.40
10	10%	1228.00	122.80	19441	0.0039	-21.25	0.1	19.8	-7.61
15	10%	1705.45	170.54	19829	0.0053	-17.04	0.1	28.4	-4.84
20	10%	2338.80	233.88	20234	0.0072	-12.95	0.1	38.2	-2.06
25	10%	3169.22	316.92	20658	0.0095	-8.96	0.1	49.3	0.75
30	10%	4246.03	424.60	21107	0.0126	-5.03	0.1	62.1	3.61

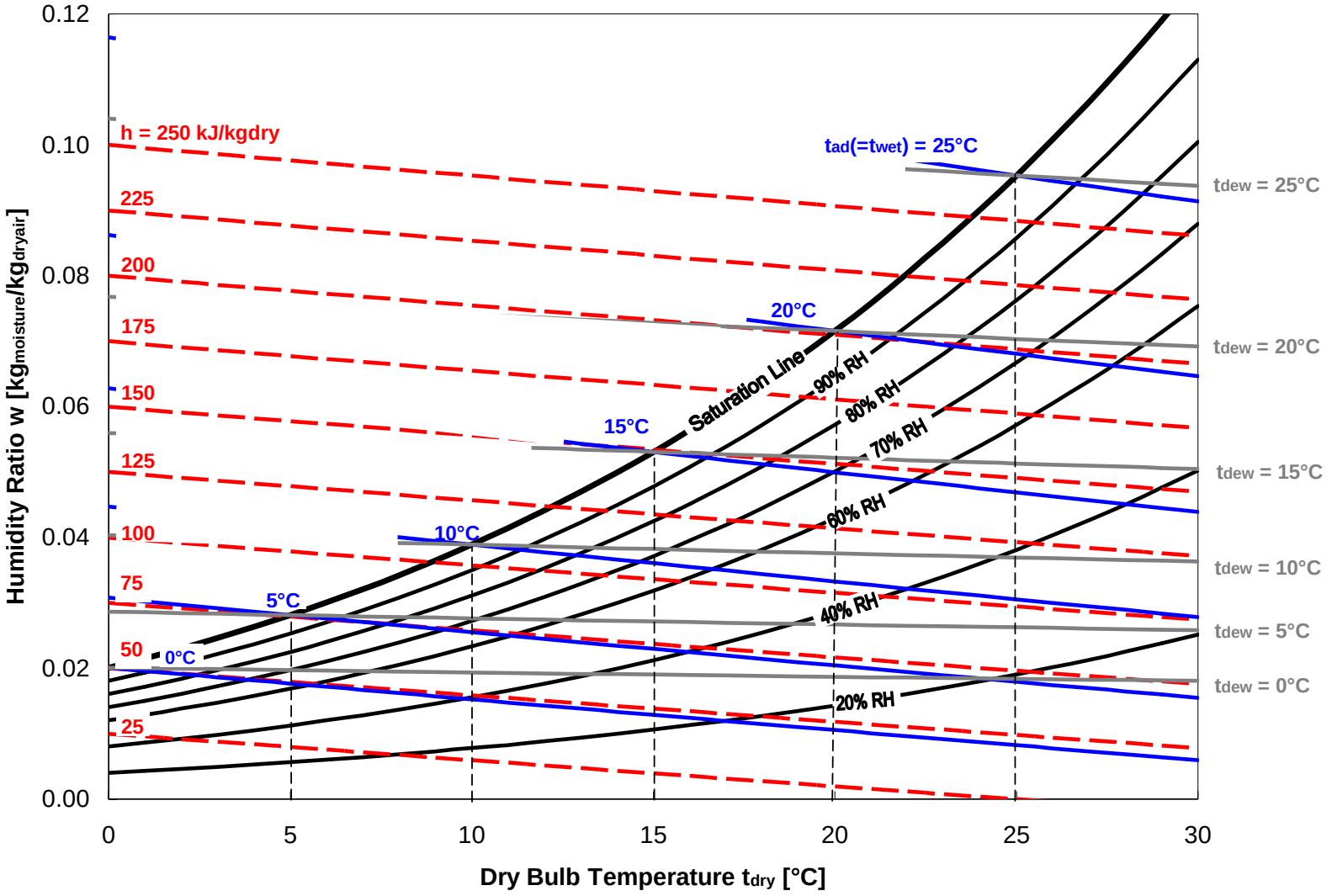

Figure 5-2. Psychrometric chart of low pressure atmosphere (76% N_2, 20% O_2, 4% CO_2) with initial conditions of 20 kPa dry air at 20°C and a constant specific volume of 0.004138m³/kg.

One–dimensional Steady State Heat Transfer Model of the Greenhouse Dome

Overall Thermal Resistance Model

A one-dimensional steady state analysis was selected as heat transfer model. The heat inside of the greenhouse produced by the absorbed growth light radiation and the heating system is transferred to the outside in the following steps. First convection heat transfer takes place between the air and the greenhouse inner shell, then heat is transferred through the greenhouse dome by conduction. Heat transfer between the greenhouse surface and the inner chamber wall occurs mainly due to radiation. Natural convection of the outside dome and the interior chamber walls is negligible as the convection coefficient is reduced significantly by the low pressure of 0.6 kPa (see Table 5-1). The effect of low pressure on convective heat transfer has been discussed extensively at the beginning of this Chapter. Heat transfer through the vacuum chamber occurs by conduction. Finally, heat is removed from the vacuum chamber wall by convection. At the same time, heat is also transferred out of the greenhouse through the dome base. Thick foam insulation had been installed under the base to minimize the heat loss through the floor.

The equivalent thermal circuit concept is a useful tool for the development of a one-dimensional steady state heat transfer model. The thermal resistance is defined as the ratio of the temperature difference (the driving potential) to the corresponding heat transfer rate. Figure 5-3 depicts the modes of heat transfer and states the equivalent thermal resistance circuit.

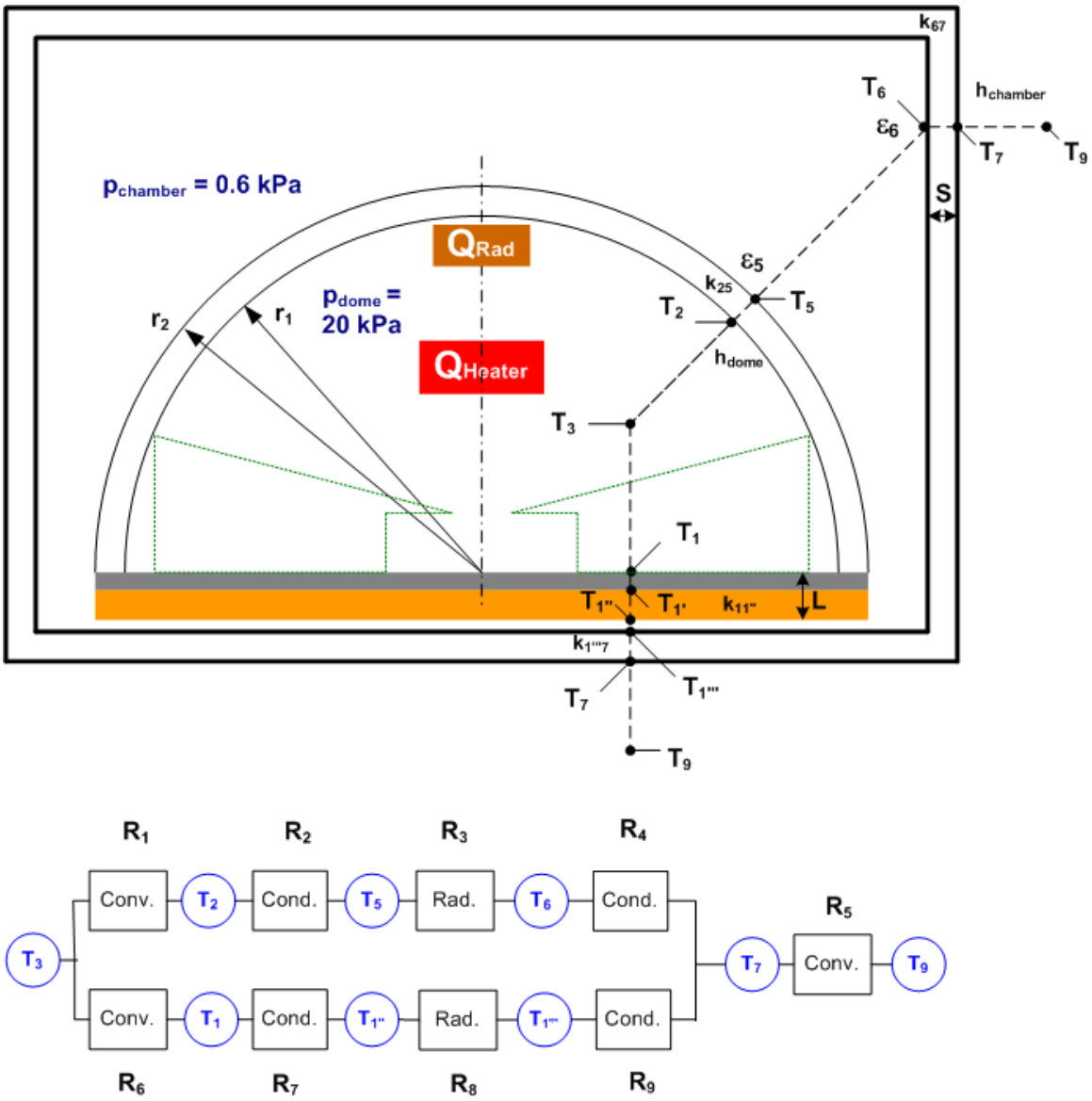

Figure 5-3. Heat transfer of greenhouse dome and thermal resistance circuit.

Individual Thermal Resistances and Thermal Coefficients

The total heat flux out of the greenhouse dome is the sum of the absorbed light plus the heat added by the heating coil. The heat flux is the ratio of the temperature difference to the total resistance:

$$Q_{total} = Q_{Heater} + Q_{Light} = \frac{T_3 - T_9}{R_{total}} \tag{5-50}$$

In analog to the electric circuit the total resistance is determined by the series-parallel configuration of the individual resistances:

$$R_{total} = \frac{1}{\frac{1}{R_1 + R_2 + R_3 + R_4} + \frac{1}{R_6 + R_7 + R_8 + R_9}} + R_5 \tag{5-51}$$

The conduction resistance R_7 is very large compared to the other resistances as the dome base is very well insulated. Thus, the total resistance reduces to:

$$R_{total} = R_1 + R_2 + R_3 + R_4 + R_5 \tag{5-52}$$

where: $R_1 = \frac{T_3 - T_2}{Q_{total}} = \frac{1}{h_1 2\pi r_1^{\,2}}$ = Convection heat transfer

$$R_2 = \frac{T_2 - T_5}{Q_{total}} = \frac{1}{2\pi k_{25}}\left(\frac{1}{r_1} - \frac{1}{r_2}\right) = \text{Conduction heat transfer}$$

$$R_3 = \frac{T_5 - T_6}{Q_{total}} = \frac{1}{\frac{\sigma_s (T_5 + T_6)(T_5^{\,2} + T_6^{\,2}) 2\pi r_2^{\,2}}{\frac{1}{\varepsilon_5} + \left(\frac{1 - \varepsilon_6}{\varepsilon_6}\right)\left(\frac{2\pi r_2^{\,2}}{A_{Chamber}}\right)}} = \text{Radiation heat transfer}$$

$$R_4 = \frac{T_6 - T_7}{Q_{total}} = \frac{S}{k_{67} A_{Chamber}} = \text{Conduction heat transfer}$$

$$R_5 = \frac{T_7 - T_9}{Q_{total}} = \frac{1}{h_7 A_{Chamber}} = \text{Convection heat transfer}$$

r_1 = inner dome radius [m]

r_2 = outer dome radius [m]

h_1 = convection coefficient dome inside [W m^{-2} K^{-1}]

k_{25} = conduction coefficient dome [W m^{-1} K^{-1}]

σ_s = Stefan-Boltzmann constant [5.670 * 10^{-8} W m^{-2} K^{-4}]

ε_s = emissivity of greenhouse dome outside [-]

ε_6 = emissivity of chamber inside [-]

S = thickness of chamber [m]

k_{67} = conduction coefficient chamber [W m^{-1} K^{-1}]

$A_{chamber}$ = Area of chamber [m^2]

h_7 = convection coefficient chamber outside [W m^{-2} K^{-1}]

The thermal resistances and coefficients, defined above, can be solved straight-forward by inserting the steady state temperatures data of the Galactic lettuce experiment and the dimensions of the dome and chamber. Table 5-3 lists the temperature data at the selected locations. Table 5-4 gives an overview of the calculated thermal resistances and heat transfer coefficients. It can be observed that the data are different for the case when the light is switched on, compared to the light being switched off. This results from the temperature differences for both cases. The temperatures of the surfaces are higher when the light is switched on, because part of the radiation is absorbed by the dome shell and chamber wall.

The radiation coefficients ε_5 and ε_6 depend on each other and the equation cannot be solved without knowing one of them (see Figures 5-4 and 5-5). As the polycarbonate dome is very transparent a high emissivity of 0.9 was chosen, resulting in an emissivity value of the chamber of 0.55 for the light turned off and 0.48, when the light is turned on.

Table 5-3. Steady state temperature data of the long-term experiment involving Galactic lettuce plants.

Freezer Temp. [ºC]	Light	Heating Power [W]	Air T3 [ºC]	Fan T4 [ºC]	Shell Inside T2 [ºC]	Shell Outside T5 [ºC]	Inside Wall T6 [ºC]	Outside Wall Middle T7 [ºC]	Outside Wall Bottom T8 [ºC]	Chamber Air T9 [ºC]
-20	off	119	19.68	24.42	13.81	3.47	-16.73	-18.83	-19.51	-20.01
-20	on	40	20.12	22.16	15.61	8.35	-11.99	-16.04	-19.16	-19.96

Table 5-4. Thermal resistances and coefficients based on the data obtained of the long-term experiment involving Galactic lettuce plants.

	Unit	Light off	Light on
R1 - Convection	K/W	0.0494	0.0379
h1 - Convection	W/(Km²)	11.3306	14.7518
R2 - Conduction	K/W	0.0869	0.0610
k25 - Conduction	W/(Km)	0.0404	0.0576
R3 - Radiation	K/W	0.1697	0.1709
ε5 - Radiation	-	0.90	0.90
ε6 - Radiation	-	0.55	0.48
R4 - Conduction	K/W	0.0176	0.0340
k67 - Conduction	W/(Km)	0.1139	0.0591
R5 -Convection	K/W	0.0099	0.0329
h7 - Convection	W/(Km²)	16.7858	5.0598
R-total	K/W	**0.3336**	**0.3368**

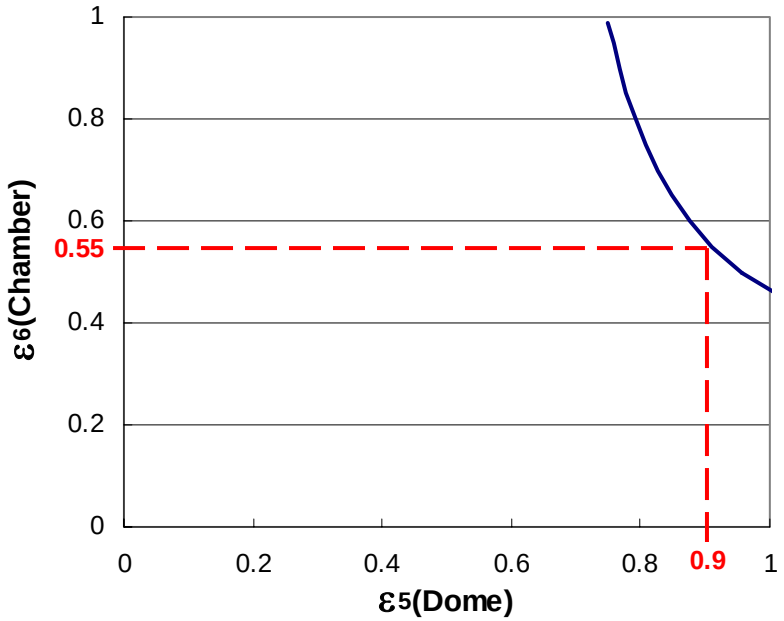

Figure 5-4. Emissivities of the polycarbonate dome and the stainless steel chamber (light off).

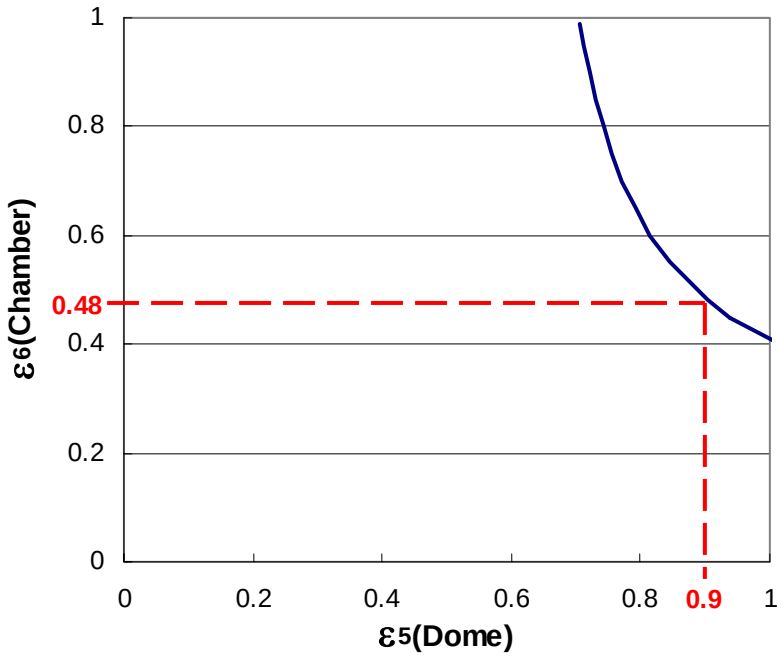

Figure 5-5. Emissivities of the polycarbonate dome and the stainless steel chamber (light on).

The thermal coefficients of Table 5-4 and the dimensions of the dome and the chamber are entered into a simulation module programmed in LabView. As the radiation resistance varies with the temperature of the dome and the chamber, a direct determination of the steady-state temperatures is not possible. A loop recalculates the temperatures beginning from the initial conditions until steady state is reached. Table 5-5 lists the simulated temperatures at the selected locations.

Table 5-5. Simulated temperatures based on the thermal resistance model.

Freezer Temp. [ºC]	Lights (0=off, 1=on)	Heating Power [W]	Air/ Plant T3 [ºC]	Shell Inside T2 [ºC]	Shell Outside T5 [ºC]	Inside Wall T6 [ºC]	Outside Wall T7 [ºC]	Chamber Air T9 [ºC]
0	**0**	**26**	8.28	7.00	4.74	0.72	0.26	0.00
0	**0**	**51**	16.03	13.51	9.08	1.41	0.51	0.00
0	**0**	**77**	23.89	20.09	13.40	2.12	0.76	0.00
0	**0**	**103**	31.57	26.48	17.54	2.84	1.02	0.00
-10	**0**	**26**	-1.26	-2.54	-4.80	-9.28	-9.74	-10.00
-10	**0**	**51**	6.88	4.36	-0.07	-8.59	-9.49	-10.00
-10	**0**	**77**	15.10	11.30	4.61	-7.88	-9.24	-10.00
-10	**0**	**103**	23.10	18.02	9.07	-7.16	-8.98	-10.00
-20	**0**	**51**	-2.15	-4.67	-9.10	-18.59	-19.49	-20.00
-20	**0**	**77**	6.48	2.67	-4.02	-17.88	-19.24	-20.00
-20	**0**	**103**	14.83	9.75	0.80	-17.16	-18.98	-20.00
-20	**0**	**128**	22.64	16.32	5.21	-16.47	-18.73	-20.00
-10	**1**	**0**	16.14	13.14	8.33	-4.71	-7.40	-10.00
-10	**1**	**26**	24.08	20.10	13.70	-2.97	-6.54	-10.00
-10	**1**	**51**	31.47	26.54	18.62	-1.30	-5.72	-10.00
-10	**1**	**77**	38.93	33.01	23.51	0.44	-4.86	-10.00
-20	**1**	**0**	7.55	4.55	-0.26	-14.71	-17.40	-20.00
-20	**1**	**26**	15.82	11.84	-5.44	-12.97	-16.54	-20.00
-20	**1**	**51**	23.49	18.56	10.64	-11.30	-15.72	-20.00
-20	**1**	**77**	31.21	25.29	15.79	-9.56	-14.86	-20.00
-20	**1**	**103**	38.69	31.79	20.69	-7.82	-14.01	-20.00

Table 5-6 compares the temperature values obtained through the simulation to the temperatures measured during the initial heat transfer experiments. The model works well for high heating power. Furthermore, the errors are smaller when the light is turned on compared to the light being turned off. The main contribution to the difference between the measured and simulated values is the assumption that the heat transfer is only occurring in one direction. Thus, the vertical temperature distribution of the greenhouse air and therefore the greenhouse shell is not accounted for.

Table 5-6. Comparison of measured and simulated temperature values.

Freezer Temp. [ºC]	Lights (0=off, 1=on)	Heating Power [W]	Measured Air/Plant Temp. T_3 [ºC]	Simulated Air/Plant Temp. T_3 [ºC]	Error Temp ΔT_3 [K]	Measured Wall Temp. T_7 [ºC]	Simulated Wall Temp. T_7 [ºC]	Error Temp ΔT_7 [K]
0	**0**	**26**	12.74	**8.28**	4.46	0.01	**0.26**	-0.25
0	**0**	**51**	19.17	**16.03**	3.14	0.34	**0.51**	-0.17
0	**0**	**77**	24.06	**23.89**	0.17	0.49	**0.76**	-0.27
0	**0**	**103**	30.25	**31.57**	-1.32	0.11	**1.02**	-0.91
-10	**0**	**26**	5.29	**-1.26**	6.55	-9.63	**-9.74**	0.11
-10	**0**	**51**	10.76	**6.88**	3.88	-9.94	**-9.49**	-0.45
-10	**0**	**77**	18.44	**15.10**	3.34	-9.44	**-9.24**	-0.20
-10	**0**	**103**	24.01	**23.10**	0.91	-9.38	**-8.98**	-0.40
-20	**0**	**51**	3.38	**-2.15**	5.53	-19.13	**-19.49**	0.36
-20	**0**	**77**	9.06	**6.48**	2.58	-19.31	**-19.24**	-0.07
-20	**0**	**103**	15.51	**14.83**	0.68	-18.88	**-18.98**	0.10
-20	**0**	**128**	21.34	**22.64**	-1.30	-18.63	**-18.73**	0.10
-10	**1**	**0**	16.76	**16.14**	0.62	-6.22	**-7.40**	1.18
-10	**1**	**26**	25.74	**24.08**	1.66	-6.74	**-6.54**	-0.20
-10	**1**	**51**	32.17	**31.47**	0.70	-6.66	**-5.72**	-0.94
-10	**1**	**77**	38.27	**38.93**	-0.66	-6.31	**-4.86**	-1.45
-20	**1**	**0**	5.60	**7.55**	-1.95	-15.38	**-17.40**	2.02
-20	**1**	**26**	17.52	**15.82**	1.70	-14.38	**-16.54**	2.16
-20	**1**	**51**	23.39	**23.49**	-0.10	-14.13	**-15.72**	1.59
-20	**1**	**77**	32.73	**31.21**	1.52	-13.85	**-14.86**	1.01
-20	**1**	**103**	38.98	**38.69**	0.29	-13.20	**-14.01**	0.81

Total Thermal Resistance

Figures 5-6 and 5-7 depict the heating power versus the temperature difference between the dome air and the freezer based on the initial heat and mass transfer experiments without plants. The slope of the regression line is the value of the thermal resistance. The absorbed radiation of the growth light contributes to approximately 76-83 Watts of the total heat flux according to the linear regression equations in Figure 5-7. The total thermal resistance is higher for lower air temperatures and higher when the light is switched on.

The total thermal resistance for the simulation model (based on the Galactic lettuce experiment data) was determined to be 0.3336 K/W when the light is switched off and

0.3368 K/W when the light is being turned on. Those data points fit well into the total resistance range determined in Figures 5-6 and 5-7.

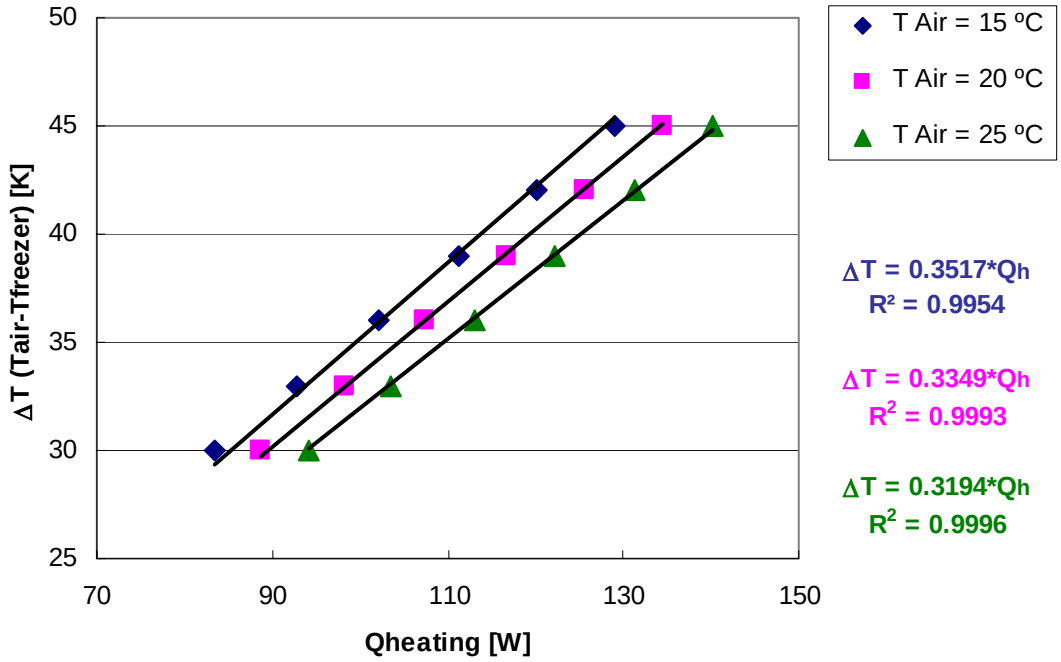

Figure 5-6. Required heating power versus temperature difference of the dome air to the freezer. Slope of linear regression is the total thermal resistance (light off).

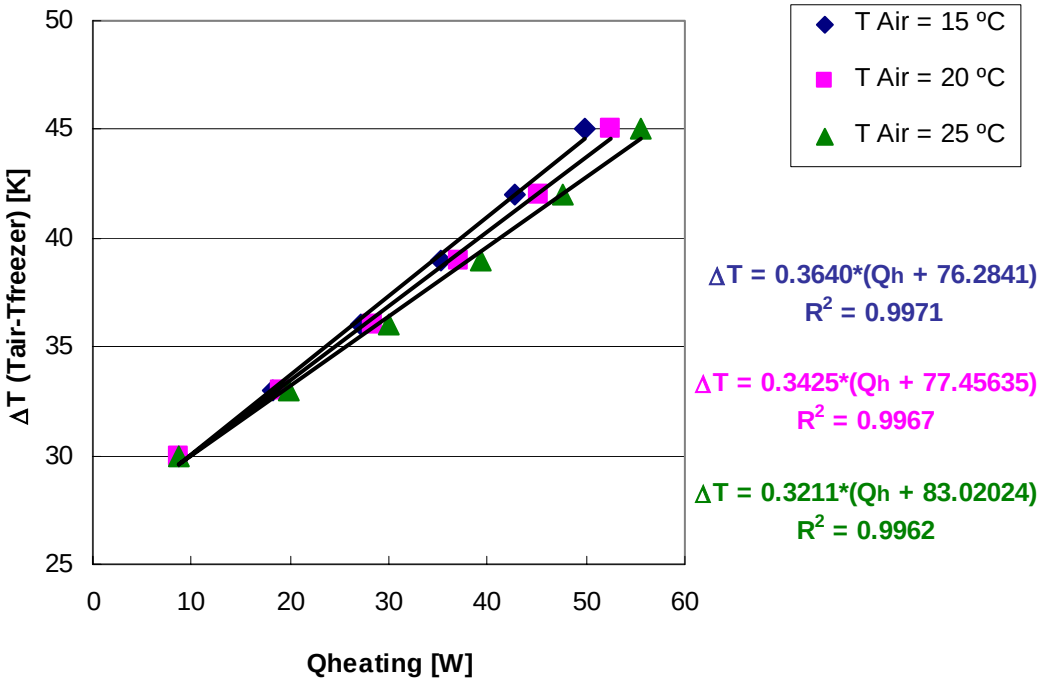

Figure 5-7. Required heating power versus temperature difference of the dome air to the freezer. Slope of linear regression is the total thermal resistance (light on).

Comparison of Radiation and Convection in the Chamber at Mars Pressure

One assumption of the thermal resistance model was that inside the vacuum chamber, at a low pressure of 0.6 kPa, convection is much smaller than radiation and therefore convection was neglected. By comparing the heat flux through radiation to the heat flux through convection, it can be verified if the assumption was correct.

In order to calculate the convective heat loss of the dome sphere and the chamber wall, the flow condition has to be analyzed first, by determining the Rayleigh number (see Equation 5-22). The Rayleigh number is below the critical Rayleigh number for convection of the dome as well as for the chamber, therefore the flow is laminar in both cases. The convection coefficient of the dome is calculated with Equation 5-23 and the coefficient of the chamber wall with Equation 5-18. The convection heat loss is 3.9 W for the dome and 12.2 W for the chamber wall. Compared to the radiation heat loss of 119 W, the convection heat loss is only 3.3% for the dome and 10.3% for the chamber wall. Thus, the assumption that convective heat transfer can be neglected is correct, if the radiation heat loss is relatively high. If the power of the heating system decreases and the difference between the chamber wall and dome temperatures is much smaller, convective heat loss plays a bigger role. This is the major reason, why in Table 5-6 the difference of the simulated and the measured values increases for low heating power. Table 5-7 lists the calculated values for the comparison of the convective heat transfer inside of the vacuum chamber to the radiation heat transfer.

Table 5-7. Comparison of convection heat transfer to radiation heat transfer in the chamber at a pressure of 0.6 kPa.

	Shell Outside T_5 [ºC]	Air Chamber T_∞ [ºC]	Inside Wall T_6 [ºC]				
Light on	8.35	-5.995	-11.99				
Light off	3.47	-8.365	-16.73				
			Convection Dome				
	Ra	**Ra_{crit}**	**Flow**	**h_{conv}**	**Q_{conv}**	**Q_{rad}**	**Q_{conv}/Q_{rad}**
Light on	6.30E+04	10^{11}	laminar	0.2072	3.8577	119	**3.25%**
Light off	6.37E+04	10^{11}	laminar	0.2077	3.8393	119	**3.26%**
			Convection Chamber Wall				
	Ra	**Ra_{crit}**	**Flow**	**h_{conv}**	**Q_{conv}**	**Q_{rad}**	**Q_{conv}/Q_{rad}**
Light on	5.06E+04	10^{9}	laminar	0.1897	12.1868	119	**10.28%**
Light off	5.15E+04	10^{9}	laminar	0.1905	12.1578	119	**10.31%**

Transient Heat Transfer Model for Greenhouse Temperature Simulation

For the transient heat transfer model, the overall system is split up into the greenhouse atmosphere, the greenhouse dome, the vacuum chamber and the greenhouse base plate. Four differential equations (5-53 to 5-56) are set up based on the energy balance of the four sub-systems. The change of the internal energy is equal to the sum of the heat fluxes into and out of the system due to energy conservation.

$$(c_p \rho V)_{atm} \frac{T_3^{n+1} - T_3^{n}}{\Delta t} = Q_{rad} + Q_h - [h_1 A_{dome}(T_3^{n} - T_{25}^{n}) + h_1 A_{base}(T_3^{n} - T_1^{n})] \quad (5\text{-}53)$$

where: T_3^{n+1} = temperature of greenhouse atmosphere at next time step [K]

T_3^{n} = temperature of greenhouse atmosphere at current time step [K]

Δt = time step [s]

$c_{p,atm}$ = specific heat of greenhouse atmosphere [J/kg K]

ρ_{atm} = density of greenhouse atmosphere at 20 kPa [kg/m³]

V_{atm} = volume of greenhouse atmosphere [m³]

Q_{rad} = heat gain from radiation [W]

Q_h = heat gain from heating system [W]

$$(c_p \rho V)_{dome} \frac{T_{25}^{n+1} - T_{25}^{n}}{\Delta t} = h_1 A_{dome} (T_3^{n} - T_{25}^{n}) - h_{rad} A_{rad} (T_{25}^{n} - T_{67}^{n}) \quad (5\text{-}54)$$

where: T_{25}^{n+1} = temperature of dome shell at next time step [K]

T_{25}^{n} = temperature of dome shell at current time step [K]

$c_{p,dome}$ = specific heat of polycarbonate dome shell [J/kg K]

ρ_{dome} = density of polycarbonate dome shell [kg/m³]

V_{dome} = volume of polycarbonate dome shell [m³]

$$(c_p \rho V)_{chamber} \frac{T_{67}^{n+1} - T_{67}^{n}}{\Delta t} = h_{rad} A_{rad} (T_{25}^{n} - T_{67}^{n}) - h_7 A_{chamber} (T_{67}^{n} - T_{freeezer}^{n}) \quad (5\text{-}55)$$

where: T_{67}^{n+1} = temperature of vacuum chamber at next time step [K]

T_{67}^{n} = temperature of vacuum chamber at current time step [K]

$c_{p,chamber}$ = specific heat of stainless steel vacuum chamber [J/kg K]

$\rho_{chamber}$ = density of stainless steel vacuum chamber [kg/m³]

$V_{chamber}$ = volume of stainless steel vacuum chamber [m³]

$$(c_p \rho V)_{base} \frac{T_1^{n+1} - T_1^{n}}{\Delta t} = h_1 A_{base} (T_3^{n} - T_1^{n}) \quad (5\text{-}56)$$

where: T_1^{n+1} = temperature of base at next time step [K]

T_1^{n} = temperature of base at current time step [K]

$c_{p,base}$ = specific heat of aluminum dome base [J/kg K]

ρ_{base} = density of aluminum dome base [kg/m³]

V_{base} = volume of aluminum dome base [m³]

The equations above are based on the assumption that the conduction resistance of the dome, the vacuum chamber and the base plate are very small and therefore the inside and outside temperatures are lumped into one equivalent temperature, T_{25}, T_{67} and T_1 respectively. Furthermore, the dome base plate is considered to be perfectly insulated as it was assumed for the steady state heat transfer model.

The four differential equations contain the four unknown temperature variables T_3^{n+1}, T_{25}^{n+1}, $T_{67}^{n+1}$and T_1^{n+1}. With the initial conditions of the four temperature variables, the system can be solved. Figure 5-8, Figure 5-9 and Figure 5-10 compare the simulation data to the experimental data for three different heating power conditions.

In all three cases the temperature rise of the simulation is much slower than in the experiment, i.e. it takes longer for the air and dome temperature to reach steady state. Consequently, the thermal inertia is higher for the simulation compared to the experimental data. Furthermore, it can be observed that the air temperature experiences a sudden rise at the beginning of the simulation as the difference between the energy gain by heating and the energy loss by convection is relatively high. The steady-state temperatures of the simulation are lower than the steady-state temperatures of the experiment. The same phenomenon was also seen in the thermal resistance model results.

The transient heat transfer model is a good first approach to simulate the transient temperature variations of the experiment. In combination with the psychrometric model, the state of the greenhouse air can be assessed and occurrence of condensation can be predicted. Figure 5-11 shows the LabView Front Panel for the overall model. A condensation warning appears if the greenhouse shell temperature is below the dew point temperature.

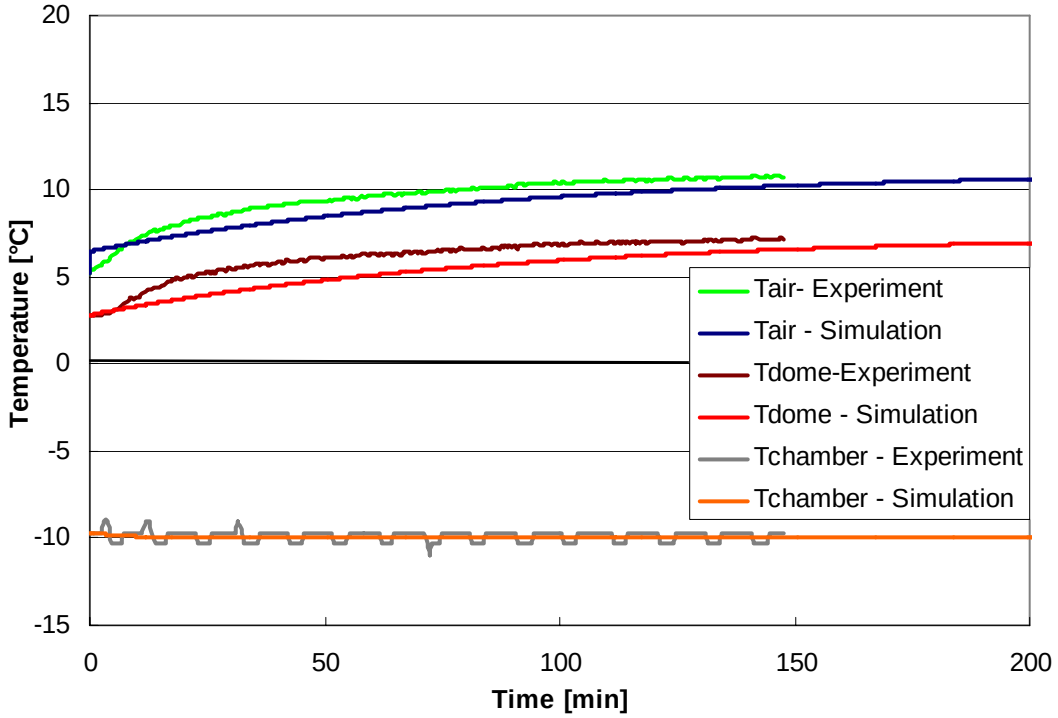

Figure 5-8. Simulation of greenhouse atmosphere, dome and vacuum chamber temperatures (light off, 51W heating power, -10° C freezer temperature).

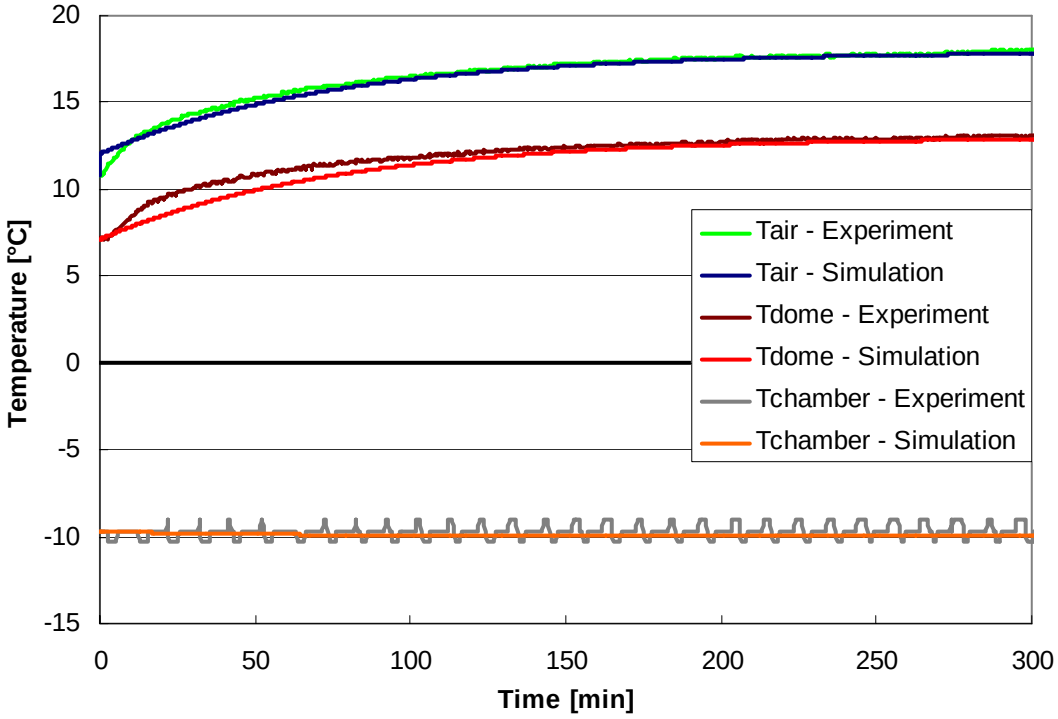

Figure 5-9. Simulation of greenhouse atmosphere, dome and vacuum chamber temperatures (light off, 77 W heating power, -10° C freezer temperature).

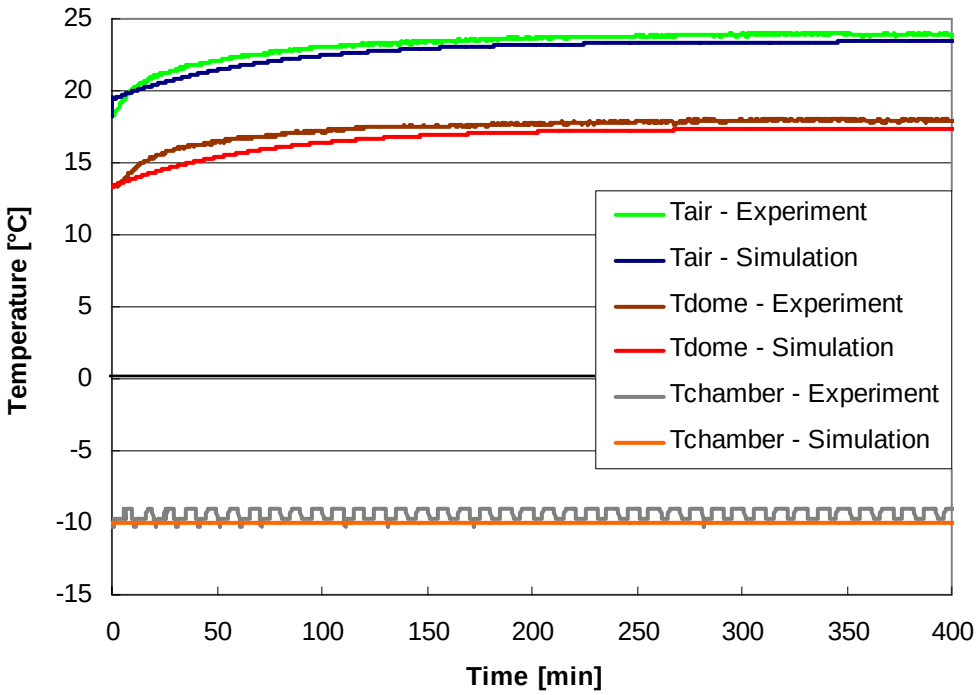

Figure 5-10. Simulation of greenhouse atmosphere, dome and vacuum chamber temperatures (light off, 103 W heating power, -10° C freezer temperature).

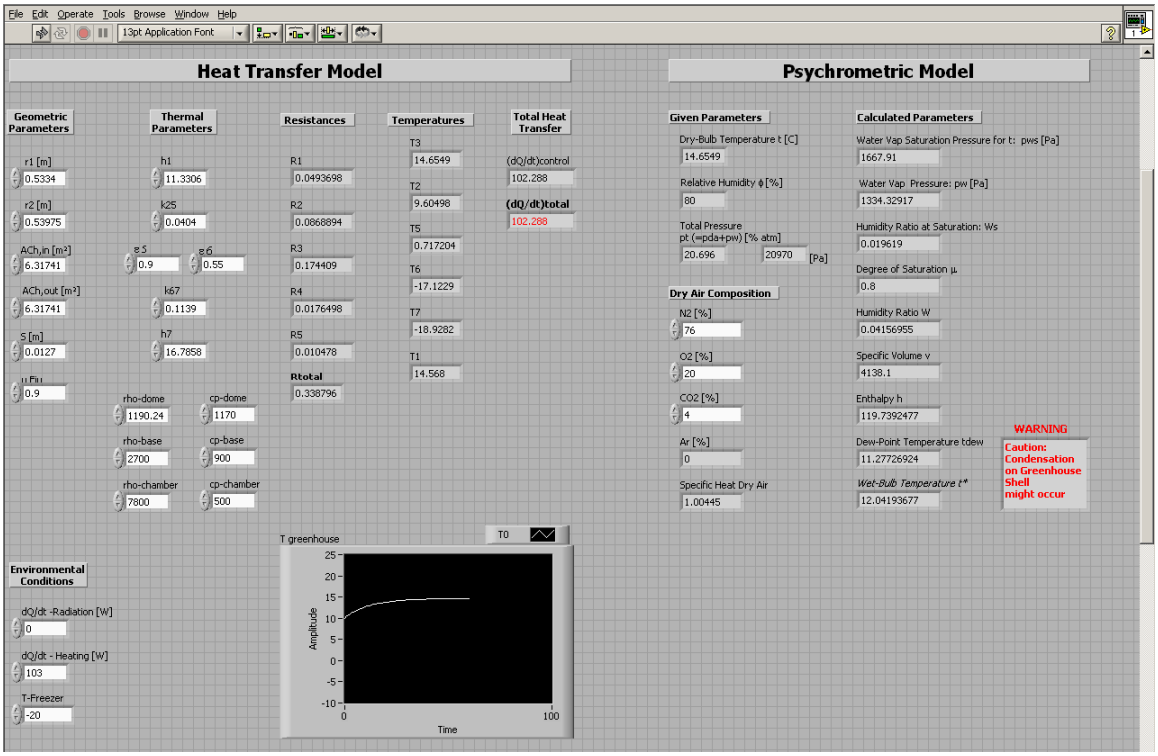

Figure 5-11. LabView front panel of overall model for simulation.

CHAPTER 6
RESULTS AND CONCLUSION

An understanding of the heat and mass transfer of a Mars greenhouse is essential to develop the environmental control system. The environmental control system is responsible for keeping the atmosphere parameters in a range where plant growth is productive.

In this research, a Mars chamber was developed simulating the environment on Mars. A small scale Mars greenhouse was exposed to the simulated Mars environment. Tests included experiments on the heat and mass transfer without and with plants. The data obtained through the thermal experiments without plants were used to refine the gas composition and temperature control algorithm. Furthermore, the temperature distribution data within the greenhouse and the chamber were utilized in the model development.

Two sets of plant experiments were successfully conducted. The mid-term experiment involved eight buttercrunch lettuce plants that were exposed to the low pressure Mars greenhouse environment for 36 hours. Temperature, pressure and atmosphere composition of the greenhouse and the simulated Mars environment were controlled. Evapo-transpiration, relative humidity and light levels were measured continuously. One plant started to wilt as the water supply ceased. The long-term experiments involved Galactic lettuce plants that were exposed to the low pressure Mars greenhouse environment for 7 days. After one day of continuous exposure to the growth light, a day-night cycle of 12 hours was implemented. The temperature of the greenhouse shell decreased significantly during the night cycle, resulting in the formation of

condensation and frost, especially in the lower colder part of the greenhouse. Relative humidity also decreased during the night cycle as more water condensed than evaporated. The plants showed no significant visible damage after seven days, only minor wilting was observed as the water supply was depleted.

Data from the experiments were analyzed to develop a thermal resistance model that can be used to predict steady-state greenhouse temperatures for various Mars environment conditions. The analytical data of the model fitted well with the experimental data for low freezer temperatures, i.e., high temperature differences between the Mars environment and the greenhouse temperature, as the thermal resistance model was based on the assumption that at low pressures convection is insignificant compared to radiation heat transfer. The transient heat transfer model was utilized to simulate the transient temperature variations of the equipment over time.

Low pressure psychrometric relations were developed for closed systems at various gas compositions other than the standard atmosphere. The psychrometric model can be used to predict the state of the moist air. Knowledge of the psychrometric parameters is especially important for the prediction of the occurrence of condensation.

CHAPTER 7
FUTURE WORK

The results of this study show that there is a vertical temperature and humidity stratification of the greenhouse dome atmosphere. The installation of a heater on the cold greenhouse aluminum base and improved insulation would lead to a more uniform atmosphere, preventing the build-up of condensate and ice in the lower part of the greenhouse (see Figure 7-1).

If a passive humidity control system is selected, the water should condense on the greenhouse shell above the gravity-driven recollection funnel. At the same time, condensate should not collect above the plant level as it would interfere with the radiation required for plant growth. Another option of condensing the water out of the atmosphere would be to pipe air out of the greenhouse to a heat exchanger with the Mars environment and to feed back the water and the dried air separately into the dome. Temperature of the condensation surface should be monitored carefully as the temperature should be below the dew point but above the freezing point. Gravity driven water collection systems should be applied where possible as they work in the low-gravity Mars environment and avoid the installation of pumps.

The duration of the experiments was limited by the decreasing water supply to the plants. An efficient water recycling system, that collects the condensate and feeds it back to the plants would minimize the required resupply of water from the outside and increase the length of the experiment.

Future research should also include full growth cycles of the plants from seeds to maturity as small plants are much more vulnerable to environmental changes. A simulated day-night cycle with gradual intensity increase of the growth light could be implemented, as it would replicate the Mars environment more accurately.

A)

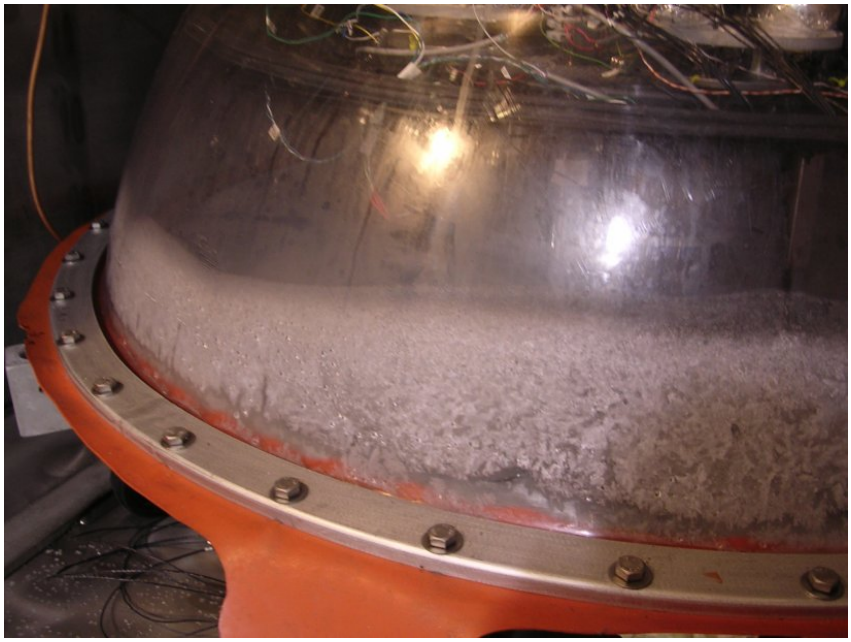

B)

Figure 7-1. Ice building up on the bottom part of the greenhouse shell. A) Overview. B) Detailed view of the ice-crystals.

APPENDIX A
STRUCTURAL ANALYSIS OF DOME SHELL, BASE PLATE AND CYLINDRICAL CALIBRATION CHAMBER

Structural Analysis of the Spherical Greenhouse Dome

Most Mars greenhouse experiments utilize enclosures that are under compression, because they incorporate standard atmosphere on the outside and low pressure inside of the vessel. In this case, a structural analysis should be performed to avoid a stability failure under compression. Whereas, the greenhouse dome (operated at 20-25 kPa pressure) in this project is placed in a vacuum chamber operated at the low Mars pressure of 0.6 kPa. Therefore, the structural analysis should be performed for a semi-sphere under tension:

The yield stress of the hemisphere is defined as:

$$\sigma_{\max} = \frac{P_{crit} r}{t} \tag{A-1}$$

where: P_{crit} = critical pressure [3.67 psi = 0.25 atm.]

r = radius of sphere [21 in (0.53 m)]

t = wall thickness [0.25 in (0.635 cm)]

The yield stress of the sphere of 308.28 psi (2126 kPa) is well below the maximum yield stress of 1000 psi (6895 kPa). Therefore, the safety factor is 3.24.

Assuming a safety factor of 1.5 leads to the conclusion, that the greenhouse dome should not be operated at a pressure difference of more than 7.9 psi or 0.5 atm.

Structural Analysis of Base Plate for Greenhouse Dome

A ¼ inch aluminum plate serves as the base of the greenhouse dome. It is re-enforced with aluminum tubes welded to the bottom of the plate. Figure A-1 shows the bottom view of the dome base plate.

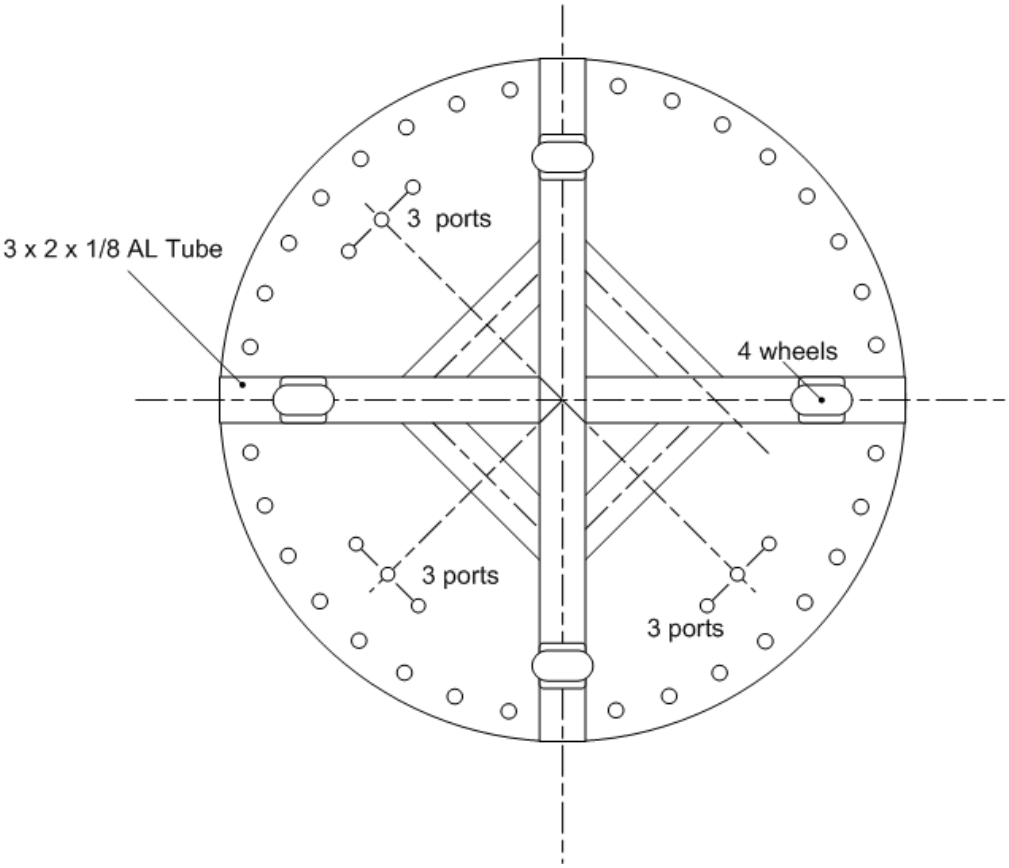

Figure A-1. Bottom view of greenhouse dome base.

For the structural analysis the dome base is split up into four uniformly circular sectors with 90 degree angles (see Figure A-2). First the structural analysis is performed of a plate with the main two bracings considered as beams. A second analysis also takes the additional square bracing into account. The structural analyses of this section are based upon the equations found in American Aluminum Association (1981).

Structural Analysis of the Base Plate without Additional Bracings

The first analysis assumes a triangular load over the full beam depicted in Figure A-2.

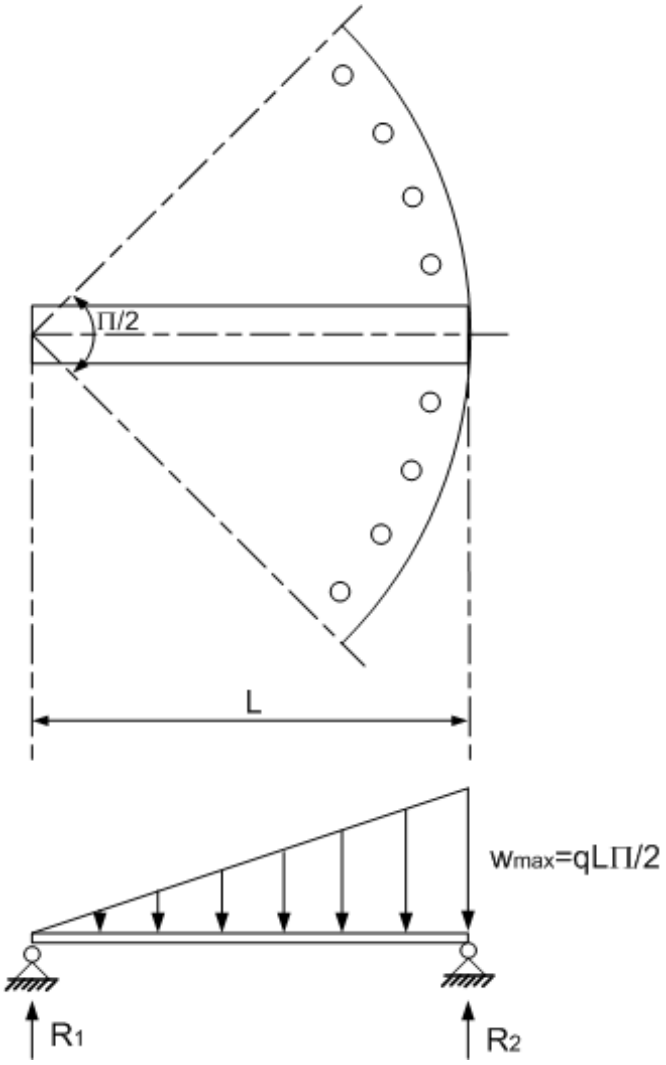

Figure A-2. Triangular load over full beam.

The total load on the sector, i.e., beam, is the area of the triangle and can be calculated by multiplying the pressure difference by the wedge area:

$$W = \frac{w_{\max} L}{2} = \frac{qL^2 \pi}{4} \tag{A-2}$$

where: W = total load [lb]

w_{max} = maximum distributed loading [lb/in]

L = length of beam [m]

q = pressure differential [psi]

Therefore, the maximum loading of the beam is:

$$w_{\max} = \frac{qL\pi}{2} \tag{A-3}$$

The reactions R_1 and R_2 at the supports are:

$$R_1 = \frac{wL}{6} \tag{A-4}$$

$$R_2 = \frac{wL}{3} \tag{A-5}$$

The bending moment varies with the location x on the beam:

$$M(x) = \frac{Wx}{3L^2}(L^2 - x^2) = \frac{w_{\max} x(L^2 - x^2)}{6L} \qquad 0 \le x \le L \tag{A-6}$$

The maximum bending moment is encountered at 0.55774 L:

$$M_{\max}(x = 0.5774L) = 0.1283WL = 0.1283\frac{qL^3\pi}{4} \tag{A-7}$$

The deflection varies with the location x on the beam:

$$def(x) = \frac{Wx}{180EIL^2}(3x^2 - 10L^2x^2 + 7L^4) \qquad 0 \le x \le L \tag{A-8}$$

The maximum deflection is encountered at 0.5193 L:

$$def_{\max}(x = 0.5193L) = 0.01304\frac{WL^3}{EI} = 0.01304\frac{qL^5\pi}{4EI} \tag{A-9}$$

Structural Analysis of the Base Plate with Additional Bracings

The second structural analysis also considers the additional bracing in the form of a square. Similar to the first analysis the plate is split up into four sectors and the main bracing is considered as a beam (see Figure A-3).

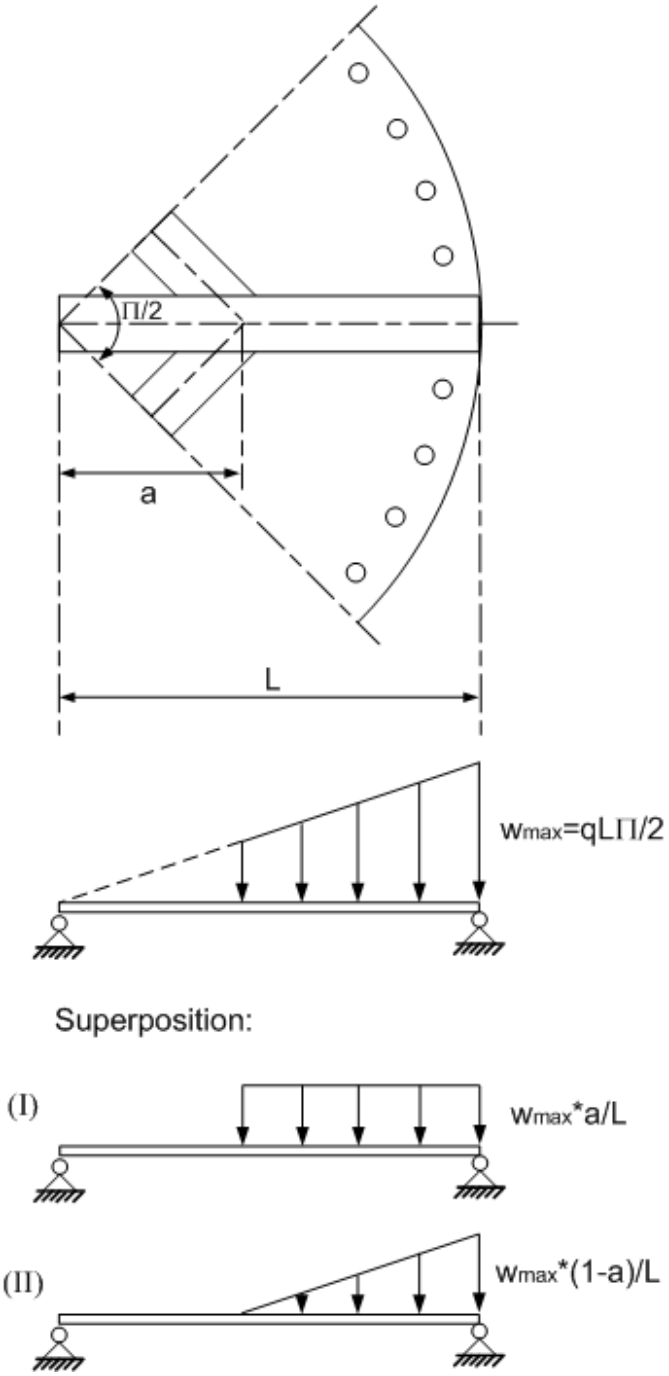

Figure A-3. Trapezoidal load over part of the beam.

The load inside of the additional bracing (for x < a) is taken by the interior bracings, therefore only the distributed load outside the additional bracing (for x>a) is considered. This leads to a trapezoidal load distribution as shown in Figure A-3.

In this case also Equation A-2 applies, leading to a maximum load of the beam, similarly to the triangular load distribution (see Equation A-3):

$$w_{\max} = \frac{qL\pi}{2} \tag{A-10}$$

The trapezoidal load on the beam can be calculated by super positioning a uniform load (see Figure A-4) and a triangular load (see Figure A-5) for x>a.

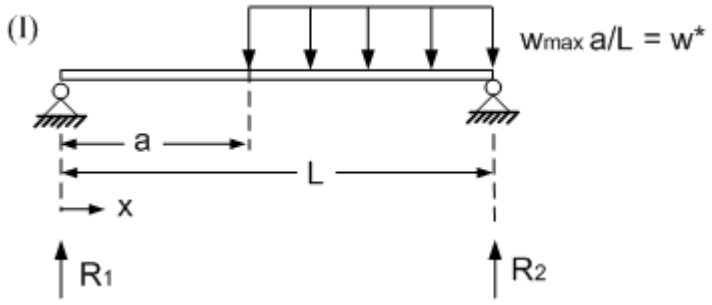

Figure A-4. First part of superposition: uniform load for x>a.

The uniform load w* is related to the maximum trapezoidal load w_{max} (defined in Equation A-10) as follows:

$$w^* = \frac{a}{L} w_{\max} \tag{A-11}$$

The reactions R_1 and R_2 at the supports are:

$$R_1 = \frac{(L-a)^2 w^*}{2L} \tag{A-12}$$

$$R_2 = \frac{(L^2 - a^2) w^*}{2L} \tag{A-13}$$

The bending moment M_1 for x<a is:

$$M_1(x) = R_1 x \qquad 0 \le x \le a \qquad \text{(A-14)}$$

$$M_1(x) = \frac{(L-a)^2 a}{2L^2} w_{\max} x = \frac{(L-a)^2 aq\pi}{4L} x \qquad 0 \le x \le a \qquad \text{(A-15)}$$

The bending moment M_2 for x>a is:

$$M_2(x) = R_2(x-L) - \frac{(L-x)^2}{2} w^* \qquad a \le x \le L \qquad \text{(A-16)}$$

$$M_2(x) = [\frac{(L^2-a^2)(L-x)}{2L} - \frac{(L-x)^2}{2}] \frac{a}{L} w_{\max} \qquad a \le x \le L \qquad \text{(A-17)}$$

$$M_2(x) = [\frac{(L^2-a^2)(L-x)}{L} - (L-x)^2] \frac{aq\pi}{4} \qquad a \le x \le L \qquad \text{(A-18)}$$

The second part of the superposition is a triangular load on the beam for x>a as shown in Figure A-5.

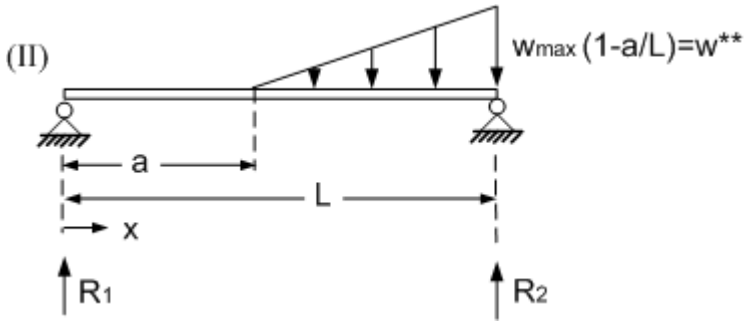

Figure A-5. Second part of superposition: triangular load for x>a.

The maximum triangular load w** is related to the maximum load of the trapezoid w_{max} (defined in Equation A-10) as follows:

$$w^{**} = \left(1 - \frac{a}{L}\right) w_{\max} \qquad \text{(A-19)}$$

The reactions R_1 and R_2 at the supports are:

$$R_1 = \frac{(L-a)^2 w^{**}}{6L} \tag{A-20}$$

$$R_2 = \frac{(L-a)w^{**}}{2} - \frac{(L-a)^2 w^{**}}{6L} = \frac{(L-a)w^{**}}{6L}(2L+a) \tag{A-21}$$

The bending moment M_1 for x<a is:

$$M_1(x) = R_1 x \qquad 0 \le x \le a \tag{A-22}$$

$$M_1(x) = \frac{(L-a)^2 w^{**}}{6L} x = \frac{(L-a)^2}{6L}\left(1-\frac{a}{L}\right) w_{\max} x \qquad 0 \le x \le a \tag{A-23}$$

$$M_1(x) = \frac{(L-a)^2 q\pi}{12}\left(1-\frac{a}{L}\right) x \qquad 0 \le x \le a \tag{A-24}$$

The bending moment M_2 for x>a is:

$$M_2(x) = R_2(L-x) - \frac{(L-x)}{2(L-a)} w^{**}(L+x-2a)\left[(L-x)\frac{2w^{**}+(\frac{x-a}{L-a})w^{**}}{3(w^{**}+(\frac{x-a}{L-a})w^{**})}\right]$$

$$a \le x \le L \tag{A-25}$$

$$M_2(x) = w^{**}\left\{\frac{(L-a)}{6L}(2L+a)(L-x) - \frac{(L-x)}{2(L-a)}\left[(L-x)\frac{2L+x-3a}{3}\right]\right\}$$

$$a \le x \le L \tag{A-26}$$

$$M_2(x) = w^{**}\left\{\frac{(L-a)(L-x)(2L+a)}{6L} - \frac{(L-x)^2}{2(L-a)}\frac{2L+x-3a}{3}\right\} \qquad a \le x \le L \tag{A-27}$$

$$M_2(x) = \frac{q\pi}{12}\left\{\frac{(L-a)^2(L-x)(2L+a)}{L} - (L-x)^2(2L+x-3a)\right\} \quad a \le x \le L \tag{A-28}$$

The bending moments M_1 and M_2 of the trapezoidal load are calculated by superposition, i.e. summing up the bending moments of the uniform and of the triangular load:

$$M_1(x) = \frac{(L-a)^2 aq\pi}{4L}x + \frac{(L-a)^2 q\pi}{12}\left(1-\frac{a}{L}\right)x \qquad 0 \le x \le a \qquad \text{(A-29)}$$

$$M_1(x) = \frac{(L-a)^2 (L+2a) q\pi}{12L}x \qquad 0 \le x \le a \qquad \text{(A-30)}$$

$$M_2(x) = (L-x)\frac{q\pi}{12}\left\{[\frac{(L^2-a^2)}{L}-(L-x)]3a + \left[\frac{(L-a)^2(2L+a)}{L}-(L-x)(2L+x-3a)\right]\right\}$$
$$a \le x \le L \qquad \text{(A-31)}$$

Figure A-6 shows the bending moments of the beam under a load in form of a trapezoid. The bending moments are decreasing for increasing distance a of the bracing from the center of the plate.

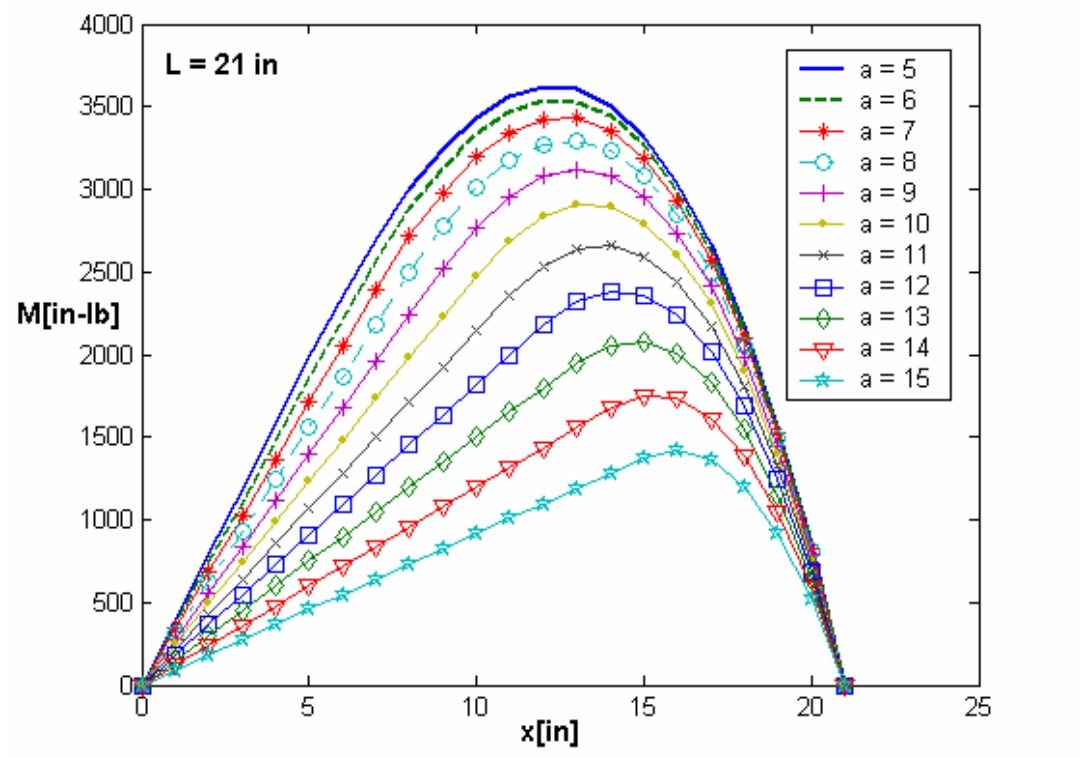

Figure A-6. Bending moments of beam for trapezoidal load varies with the distance a of the additional bracing.

The section modulus S_{beam} of a 3 x 2 x 1/8 aluminum bar is 0.978 in^3 (16.03 cm^3) and the moment of inertia I_x about the x-axis is 1.467 in^4 (61.06 cm^4) (American Aluminum Association, 1981). The total moment of inertia of the beam and the plate is calculated as follows:

$$I_{total} = I_{plate} + A_{Plate} d_{plate}^{\ 2} + I_{beam} + A_{beam} d_{beam}^{\ 2} \tag{A-32}$$

where: I_{total} = total inertia [3.23 in^4 (134.44 cm^4)]

I_{plate} = inertia of plate section [$\frac{6 \times 0.25^3}{12} = 0.00781\ in^4$ (0.3251 cm^4)]

A_{plate} = area of plate section [1.5 in^2 (9.68 cm^2)]

d_{plate}=distance to plate centroid[$\frac{A_{tube} \times 1.5 + A_{plate} \times 3.125}{A_{tube} + A_{plate}} - 1.25 = 0.91\ in$ (2.3cm)]

I_{beam} = inertia of beam [1.467 in^4 (61.06 cm^4)]

A_{beam} = area of plate section [1.1875 in^2 (7.66 cm^2)]

d_{beam} = distance to beam centroid [0.47 in (1.19 cm)]

With the moment of inertia, the section modulus S_{total} of the plate and the beam is defined as:

$$S_{total} = \frac{I_{total}}{c} \tag{A-33}$$

where: S_{total} = section modulus of plate and beam[1.34 in^3]

c = distance centroid to base [$\frac{A_{tube} \times 1.5 + A_{plate} \times 3.125}{A_{tube} + A_{plate}} = 2.41 in$ (6.12 cm)]

The stress is defined as ratio of the bending moment M to the section modulus S:

$$\sigma = \frac{M}{S} \tag{A-34}$$

The maximum stress for tension and compression is 16000 psi (110316 kPa). Applying a safety factor of 1.65, results in a maximum stress of 9700 psi (33879 kPa). The maximum stress allowed near a welding is 6500 psi (44816 kPa) (American Aluminum Association, 1981). Table A-1 lists the properties of the stress analysis for the base plate without and with the additional bracings (at a = 7 in (17.8 cm). Calculations are done for the beam and for the combination of the beam and the plate. The calculated stress for the plate without the additional bracings is higher then for the plate with the bracings. In all cases the stress was below 4000 psi (27579 kPa), i.e. below the maximum allowed stress of 6500 psi (44816 kPa) near weldings.

Table A-1. Structural analysis of base plate without and with additional bracings.

Base plate without bracings (load in form of triangle over full beam)

L [in]	q [psi]	E [psi]	M_{max} [in-lb]	I [in^4]	S [in^3]	def [in]	σ [psi]
21	4	1.05E+07	3732.8	1.47	0.978	1.08E-02	3816.77
21	4	1.05E+07	3732.8	3.23	1.34	4.94E-03	2783.39

Base plate with bracings (load in form of a trapezoid over part of the beam)

L [in]	a [in]	q [psi]	E [psi]	M_{max} [in-lb]	I [in^4]	S [in^3]	def [in]	σ [psi]
21	7	4	1.05E+07	3429	1.47	0.978	-	3506.13
21	7	4	1.05E+07	3429	3.23	1.34	-	2556.86

Structural Analysis of Cylinder used as Sensor Calibration Chamber

The stability behavior of cylindrical shells loaded by external pressure varies with length, shell thickness and wall curvature. Their behavior ranges from that of a pure long cylinder to behavior approaching that of flat plates for short cylinders (Galambos, 1998).

Maximum Allowable Pressure

Calculation of the maximum allowable pressure is the first step to determine structural failure of a cylinder including axial buckling and wall material yielding. In

order to evaluate the maximum allowable pressure, the cylinder has to be classified into one of the three following categories: short, intermediate or long cylinder.

Short cylinder behavior

The criterion for a cylinder to be classified as a short cylinder is:

$$1.1\Big/\sqrt{\left(\frac{D}{t}\right)} < \left(\frac{L}{D}\right) < 5.5\Big/\sqrt{\left(\frac{D}{t}\right)} \tag{A-35}$$

where: L = length of cylinder [12 in (30.5 cm)]

D = diameter of cylinder [8 in (20.32 cm)]

t = wall thickness [0.25 in (0.635 cm)]

As the length to diameter ratio is 1.5, the cylinder cannot be classified as a short cylinder, defined by a length to radius ratio between 0.2 and 1.0.

Intermediate cylinder behavior

The criterion for a cylinder to be classified as an intermediate cylinder is:

$$5.5\Big/\sqrt{\left(\frac{D}{t}\right)} < \left(\frac{L}{D}\right) < 0.55\sqrt{\left(\frac{D}{t}\right)} \tag{A-36}$$

As the length to diameter ratio is 1.5, the cylinder can be classified as an intermediate cylinder, defined by a length to radius ratio between 1.0 and 3.1.

At the same time, the parameter θ should be between 10 and 32 (=D/t) for an intermediate cylinder. θ is calculated at 15.4 by utilizing the following equation:

$$\theta = 1.818\left(\frac{L}{D}\right)\sqrt{\left(\frac{D}{t}\right)} \tag{A-37}$$

The critical external pressure of an intermediate cylinder is defined as:

$$P_{crit} = \frac{2.6E}{\left[\left(\frac{L}{D}\right)\left(\frac{D}{t}\right)^{2.5}\right]} \tag{A-38}$$

Therefore, the critical pressure equals 134.7 psi (equivalent to 9.2 atmospheres). Utilizing a safety factor of 1.5 leads to the conclusion, that the external pressure should not exceed 89.9 psi (equivalent to 6.4 atmospheres).

Long cylinder behavior

The criterion for a cylinder to be classified as a long cylinder is:

$$\left(\frac{L}{D}\right) > 2.1\sqrt{\left(\frac{D}{t}\right)} \tag{A-39}$$

As the length to diameter ratio is 1.5, the cylinder cannot be classified as a long cylinder, defined by a length to radius ratio above 11.9.

Axial Buckling

After the cylinder has been classified as an intermediate cylinder and the critical external pressure was determined to be 134.4 psi (927 kPa), the cylinder should be checked for axial buckling. A safety factor of at least 10 should be applied.

The wall stress should be calculated at the critical pressure:

$$\sigma_{axial} = \frac{P_{crit} D}{4t} \tag{A-40}$$

The critical wall stress is defined as:

$$\sigma_{crit.} = 1.21\frac{Et}{D} \tag{A-41}$$

where: E = modulus of elasticity of wall material [450000 psi (3102641 kPa)]

The ratio of the critical wall stress (17015.6 psi (117318 kPa)) to the actual wall stress (1077.2 psi (7427 kPa) at critical pressure) equals 15.8 fulfilling our design criterion of a safety factor of 10.

Wall Yielding

The cylinder should be checked for wall yielding at the critical external pressure calculated at 124.4 psi (858 kPa). A safety factor of at least 1.6 is required

For an intermediate cylinder the circumferential stress is defined by:

$$\sigma_{circumferential.} = \frac{P_{crit} D}{4t} \tag{A-42}$$

The ratio of the critical circumferential stress (2154.5 psi (14855 kPa)) to the actual wall stress (1077.2 psi (7427 kPa) at critical pressure) is determined to be 2.0 fulfilling our design criterion of a safety factor of 2 for wall yielding.

APPENDIX B
SENSOR CALIBRATION

Pressure

The two pressure sensors (ASCX15AN, Sensym ICT) were calibrated against a portable precision pressure gauge (Digiquartz 760 Series, Paroscientific Inc.). Both sensors were calibrated by linear regression analysis. Sensor #1 was calibrated for a range from 0 kPa to 75 kPa, as it was used in the greenhouse dome. Sensor #2 was calibrated for a range from 0 kPa to 28 kPa, as it was used in the vacuum chamber:

$$Pr1[kPa] = 22.7546*Vout-5.1814 \quad \text{(B-1)}$$

$$Pr2[kPa] = 22.7386*Vout -5.8444 \quad \text{(B-2)}$$

Pressure sensor calibration data is shown in Figures B-1 and B-2.

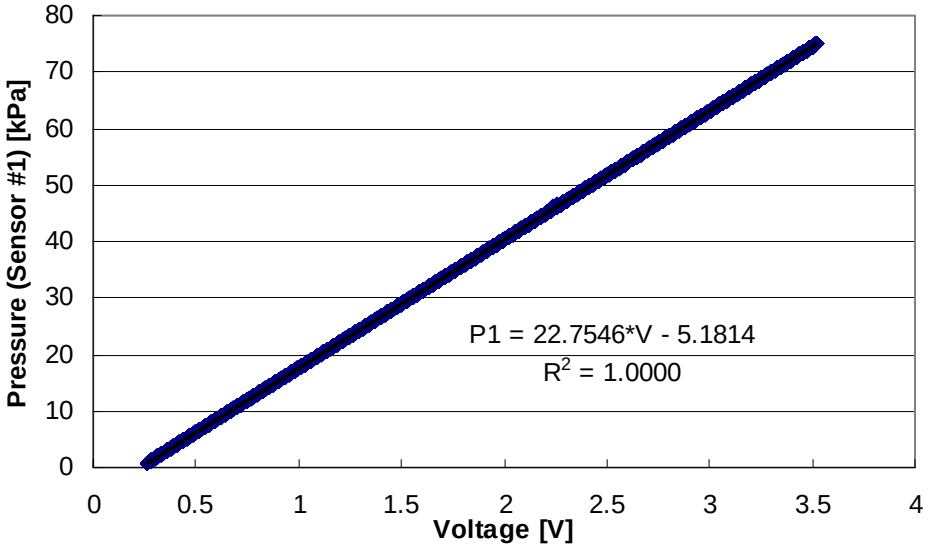

Figure B-1. Pressure sensor #1 calibration.

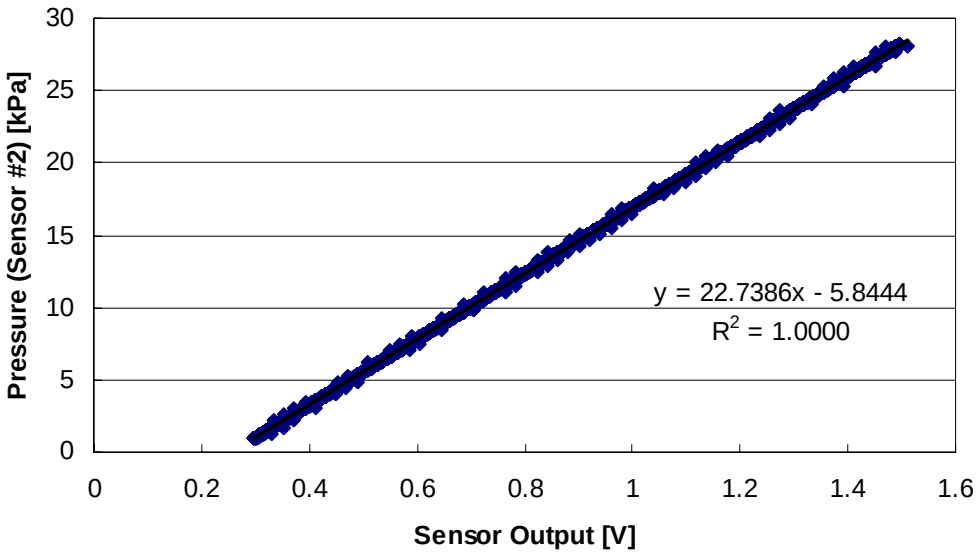

Figure B-2. Pressure sensor #2 calibration.

Temperature

The digital temperature sensors (DS18B20, Dallas Semiconductor) were exposed to a variety of pressure and gas composition combinations. The sensor readings were not affected by pressure or gas mixture.

Relative Humidity

Relative humidity (RH) measurement is affected by pressure and gas composition changes. However, the capacitance RH sensors output differed by less than 3% when compared to the hygrometer standard (HMP 237, Vaisala) as described in Chapter 4 of this dissertation. Therefore, the factory calibration was used for the four RH sensors:

$$RH1[\%]=(Vout-0.894)/0.0315 \quad \text{(B-3)}$$

$$RH2[\%]=(Vout-0.875)/0.0313 \quad \text{(B-4)}$$

$$RH3[\%]=(Vout-0.894)/0.0315 \quad \text{(B-5)}$$

$$RH4[\%]=(Vout-0.855)/0.0319 \quad \text{(B-6)}$$

Carbon Dioxide Concentration

The carbon dioxide sensor (GMP 221, Vaisala) was calibrated under different gas composition and pressures with the method described in Mu (2005):

$$CO2\ [\%] = Slope(P)*Vout + Intercept(P) \quad \text{(B-7)}$$

where: $Slope(P) = 0.0267*P^2 - 1.9901*P + 41.991$

$Intercept(P) = -0.0031*P^2 + 0.2598*P - 7.179$

In contrast to Mu (2005), a parabolic regression fit was chosen for the slope and intercept equations, because the error was significantly less compared to a linear regression.

Figures B-3 and B-4 depict the calibration of the carbon dioxide sensor.

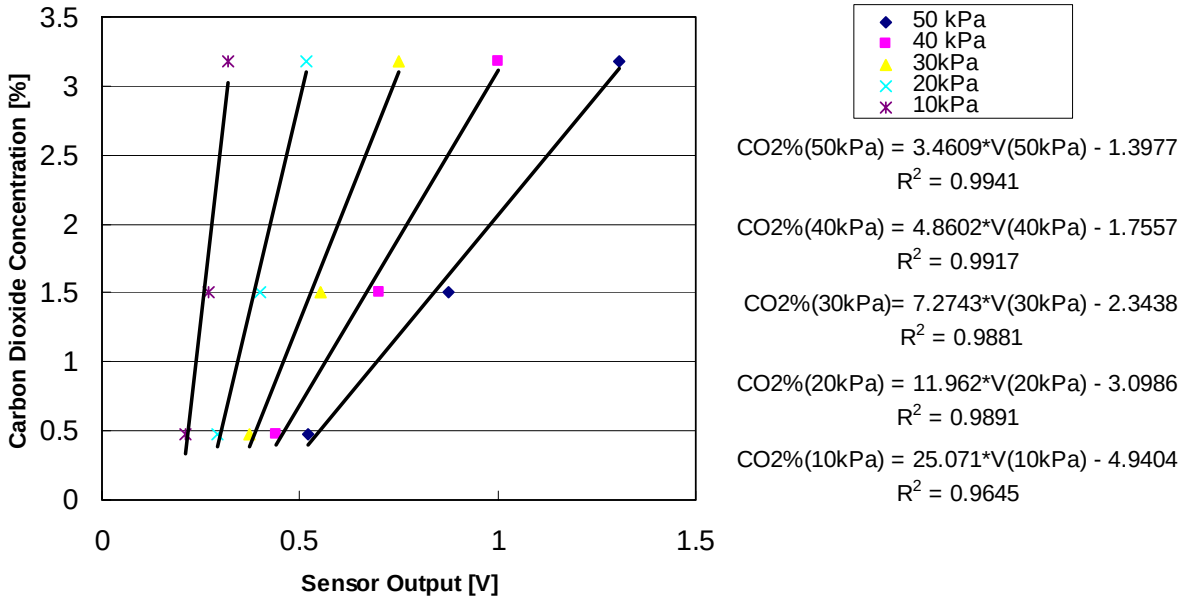

Figure B-3. Carbon dioxide sensor calibration.

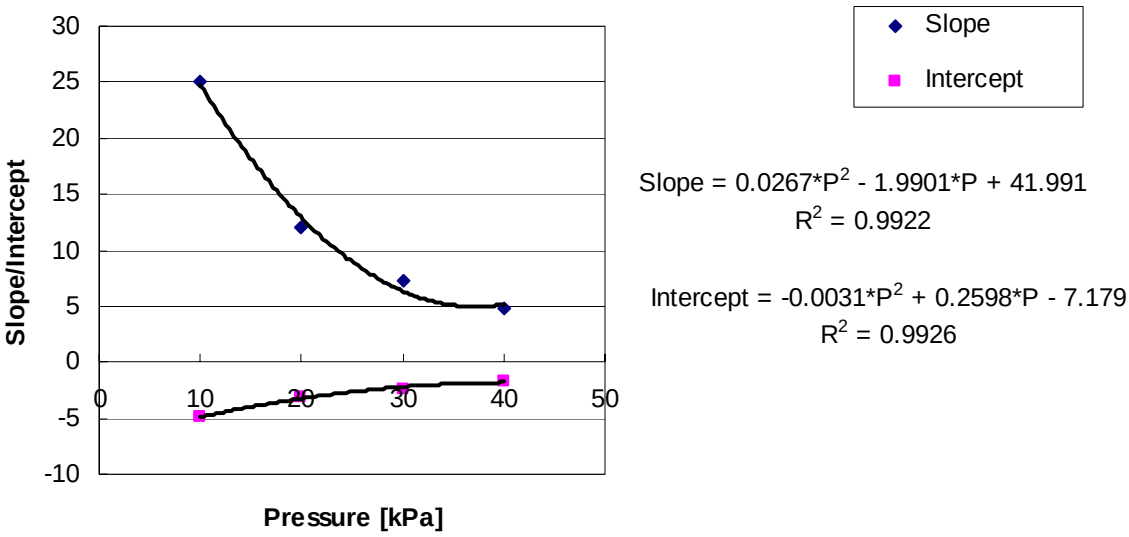

Figure B-4. Carbon dioxide sensor calibration.

Oxygen Concentration

The two oxygen sensors (Max250, Maxtec) ware calibrated under different gas composition and pressures with the same method as the carbon dioxide sensor (Mu, 2005):

$$O2\ [\%] = Slope(P)*mVout + Intercept(P) \quad \text{(B-8)}$$

where: $Slope1(P) = 0.023*P^2 - 1.6411*P + 33.25$

$Intercept1(P) = -0.0069*P2 + 0.5047*P - 8.1629$

$Slope2(P) = 0.0479*P2 - 3.4467*P + 70.061$

$Intercept2(P) = -0.0315*P2 + 2.300*P - 45.376$

A parabolic regression fit was chosen for the slope and intercept equations, because the error was significantly less compared to a linear regression. Figures B-5 and B-6 depict the calibration of the oxygen sensor #1; Figures B-7 and B-8 depict the calibration of the oxygen sensor #2.

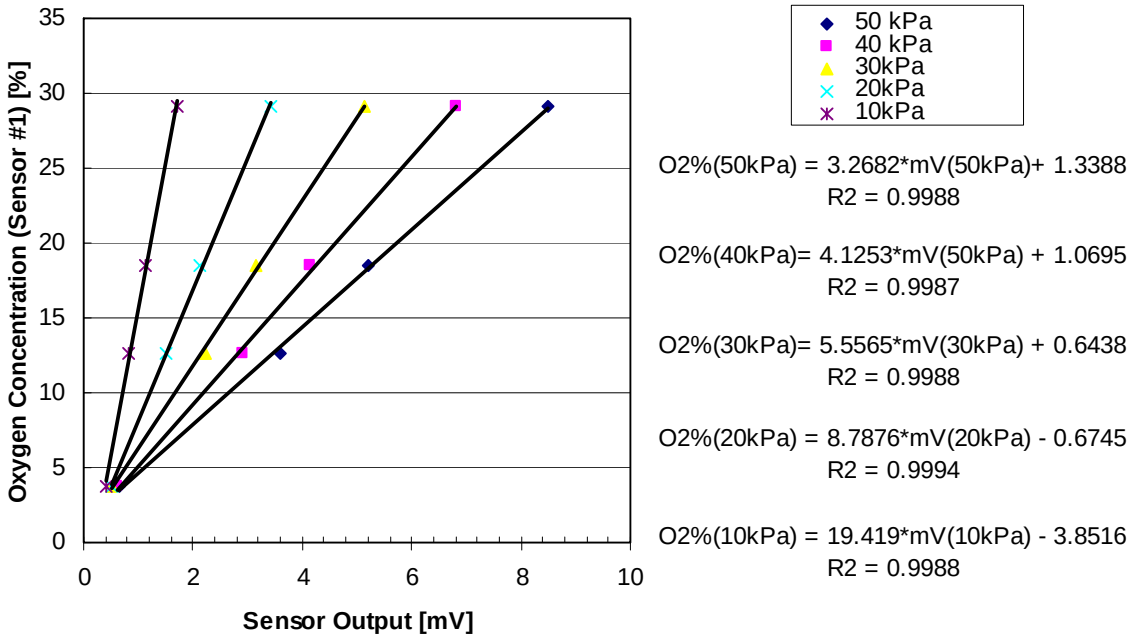

Figure B-5. Oxygen sensor #1 calibration.

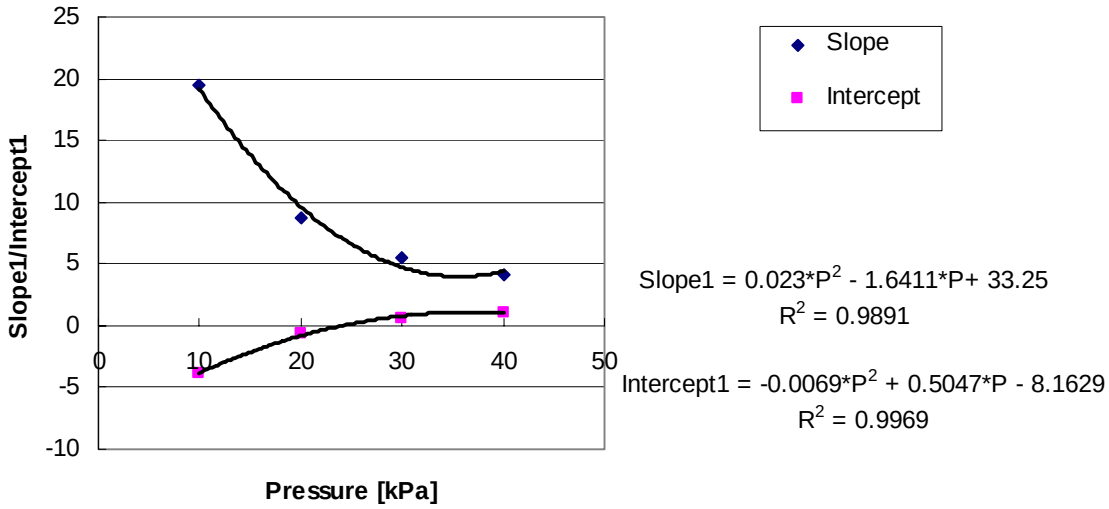

Figure B-6. Oxygen sensor #1 calibration.

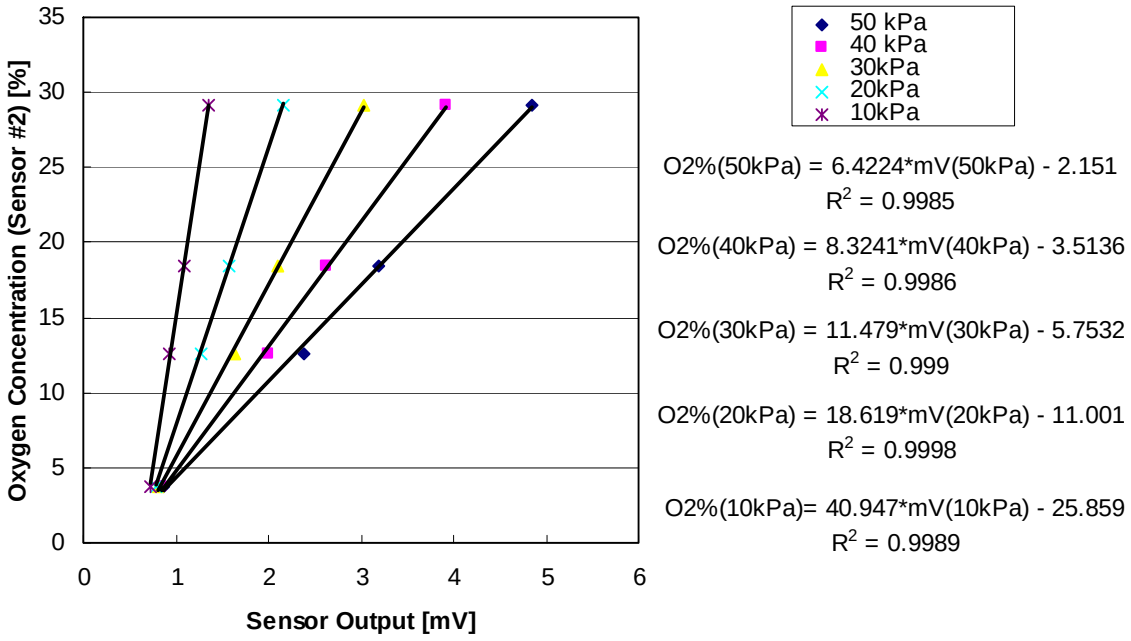

Figure B-7. Oxygen sensor #2 calibration.

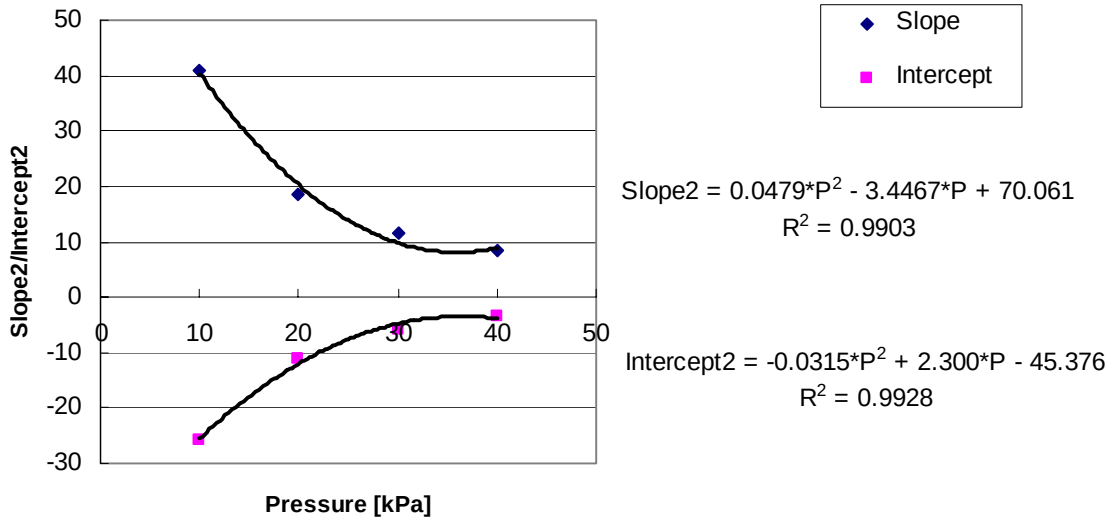

Figure B-8. Oxygen sensor #2 calibration.

Load Cells

The load cells of the scales were calibrated against standard weights by linear regression analysis:

$$massScale1\ [g] = 188.84 * mVout1 - 682.7 \quad \text{(B-9)}$$

$$massScale2\ [g] = 207.64 * mVout2 - 1259 \quad \text{(B-10)}$$

$$massScale3\ [g] = 189.9 * mVout3 - 624.67 \quad \text{(B-11)}$$

$$massScale4\ [g] = 119.11 * mVout4 - 1222.6 \quad \text{(B-12)}$$

$$massScale5\ [g] = 215.86 * mVout5 - 670.27 \quad \text{(B-13)}$$

The load cell calibration is shown in Figure B-9.

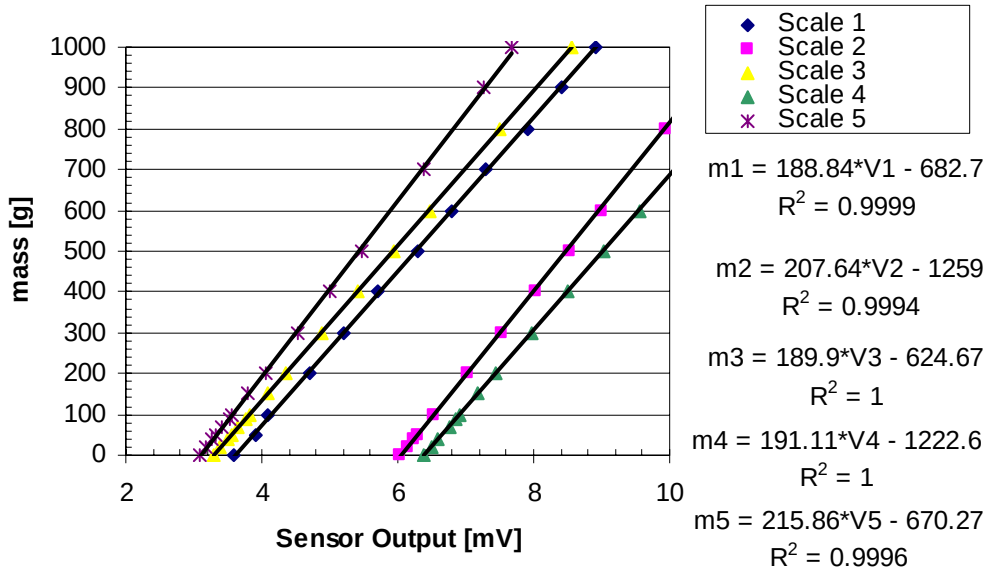

Figure B-9. Load cell calibration.

Radiation

The light sensor (LI-190SA, LI-Cor Inc.) was exposed to a variety of pressure and gas composition combinations. The sensor readings were not affected by pressure or gas mixture. Therefore, the factory calibration was used:

$$Rad[\mu mol/(m^2 s)] = mVout * 1000 / 4.83 \quad \text{(B-14)}$$

Amplification of Low Voltage Sensors

The sensors with an output in the milivolt range, such as the oxygen sensor, the light sensor and the scales had to be amplified in order be read correctly. Signal amplification was achieved by utilizing Burr-Brown's Low Power Instrumentation Amplifier. The amplification was set to 106.38 (50kΩ/470 Ω). The amplification circuit is shown in Figure B-10.

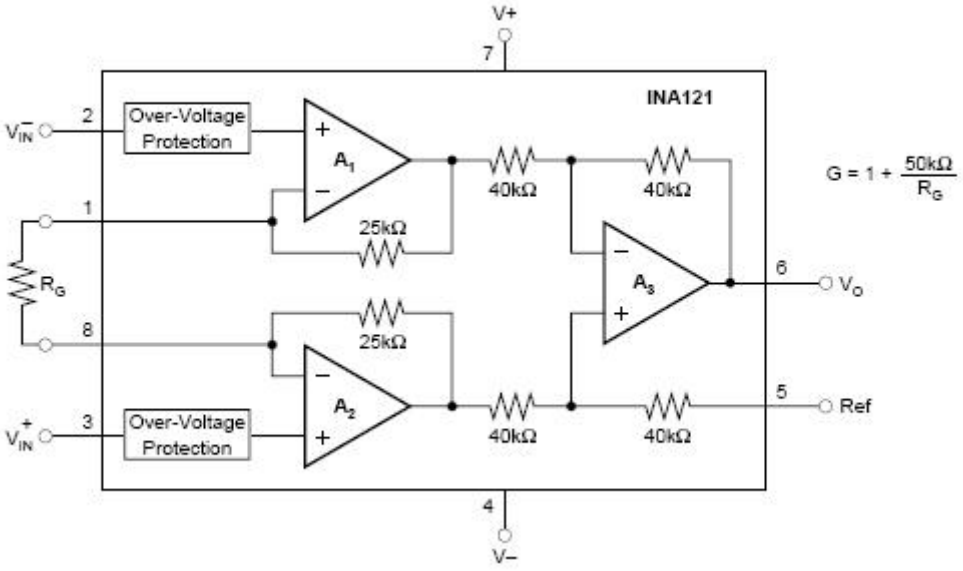

Figure B-10. Amplifier circuit.

LIST OF REFERENCES

Albright, L. D.; Gates, R.D.; Arvanitis, K.G. and Drysdale, A. E. 2001. Plants on Earth and in Space. *IEEE Control Systems Magazine* 21(5): 28-41.

American Aluminum Association. 1981. *Engineering data for aluminum structures.* Construction Manual Series. Section 3. Washington, DC.

Andre, M. and Massimino, D. 1992. Growth of plants at reduced pressures. Experiments in wheat: technological advantages and constraints. *Advances in Space Research* 12(5): 97-106.

Andre, M. and Richaud, C. 1986. Can plants grow in quasi-vacuum? In: *CELSS 1985 Workshop.* Ames Research Center. NASA Publication TM 88215: 395-404.

American Society of Heating, Refrigeration and Air-Conditioning Engineers (ASHRAE). 2001. *Handbook: Fundamentals*. SI Edition. Atlanta, GA: ASHRAE.

Boardman, N.K. 1977. Comparative photosynthesis of sun and shade plants. *Annual Reviews of Plant Physiology* 28: 355-377.

Brown, D. and Lacey, R.E. 2002. A distributed control system for low pressure plant growth chambers. *2002 ASAE Annual International Meeting*. Paper No 02-3078. American Society of Agricultural Engineers. Chicago, IL.

Bucklin, R.A.; Fowler, P.A.; Rygalov, V.Y.; Wheeler, R.M.; Mu, Y.; Hublitz, I. and Wilkerson, E.G. 2004. Greenhouse design for the Mars environment: Development of a prototype, deployable dome. *Acta Horticulturae* 659: 127-134.

Carr, M. H. 1981. *The surface of Mars.* Yale University Press. New Haven, CT.

Clawson, J. M.; Hoehn, A.; Stodiek, L. S. and Todd, P. 1999. AG-Pod - The integration of existing technologies for efficient, affordable space flight agriculture. *29th International Conference of Environmental Systems.* SAE Technical Paper Series, 1999-01-2176. Denver, CO.

Corey, K. A.; Barta, D. J.; Edeen, M.A. and Henninger, D. L. 1997a. Atmospheric leakage and method for measurement of gas exchange rates of a crop stand at reduced pressure. *Advances in Space Research* 20(10): 1861-1867.

Corey, K. A.; Barta, D. J. and Henninger, D. L. 1997b. Photosynthesis and respiration of a wheat stand at reduced atmospheric pressure and reduced oxygen. *Advances in Space Research* 20(10): 1869-1877.

Corey, K. A.; Barta, J.D. and Wheeler, R. M. 2002. Toward Martian agriculture: Responses of plants to hypobaria. *Life Support & Biosphere Science* 8: 103-114.

Corey, K. A.; Bates, M.E. and Adams. S.L. 1996. Carbon dioxide exchange of lettuce plants under hypobaric conditions. *Advances in Space Research* 18 (4/5): 265-272.

Daunicht, H. J. and Brinkjans, H. J. 1996. Plant responses to reduced air pressure: Advanced techniques and results. *Advances in Space Research* 18 (4/5): 273-281.

Downs, R.J. and Hellmers, H.1975. *Environment and the experimental control of plant growth.* Academic Press Inc. Ltd. London, UK.

Duffield, B. E. 2003. *Advanced life support requirements document.* JSC-38571, Revision C, National Aeronautics and Space Administration, Lyndon B. Johnson Space Center. Houston, TX.

Eckart, P. 1996. *Spaceflight life support and biospherics.* Space Technology Library, Microcosm Press. Torrance, CA.

Erickson, L.R. and Garrett, R.E. 1981. Atmospheric pressure effect on vapor pressure deficit and potential moisture loss for horticultural commodities. *Transactions of the ASAE* 24: 252-254.

Ferl, R.J.; Schuerger, A.C.; Paul, A.-L.; Gurley, W.B.; Corey, K and Bucklin, R.A. 2002. Plant adaptation to low atmospheric pressures: potential molecular responses. *Life Support and Biosphere Science* 8: 93-101.

Fowler, P.A.; Bucklin, R.A.; Wheeler, R.M. and Rygalov, V.Y. 2002. Monitoring and control for artificial climate design. *International Conference on Environmental Systems.* Paper 02ICES-2286. Society of Automotive Engineers. San Antonio, TX.

Galambos, T.V. 1998. *Guide to stability criteria for metal structures*. 5th Edition. John Wiley and Sons. New York, NY.

Gatley, D. P. 2002. *Understanding psychrometrics.* American Society of Heating, Refrigeration and Air-Conditioning Engineers (ASHRAE). Atlanta, GA.

Gertner, B. 1999. *Mars greenhouse study: Natural vs. artificial lighting.* Lockheed Martin Space Mission Systems & Services Science, Engineering, Analysis, and Test. HDID-2G42-1167. Houston, TX.

Goto, E.; Arai, Y. and Omasa, K. 2002. Growth and development of higher plants under hypobaric conditions. *International Conference on Environmental Systems.* Tech Paper No. 2002-01-2439. Society of Automotive Engineers. San Antonio, TX.

Goto, E.; Ohta, H.; Iwabuchi, K. and Takakura, T. 1996. Measurement of net photosynthetic and transpiration rates of spinach and maize plants under hypobaric condition. *Journal of Agricultural Meteorology* 52(2): 117-123.

Haines, R. W. 1961. How to construct high-altitude psychrometric charts. *Heating, Piping, and Air Conditioning* 33(10): 144.

Hanford, A.J. 2004. *Advanced life support baseline values and assumptions document.* NASA Technical Memorandum 208941.

He, C.; Davies, F.T.; Lacey, R.E.; Drew, M.C. and Brown, D.L. 2003. Effect of hypobaric conditions on ethylene evolution and growth of lettuce and wheat. *Plant Physiology* 160: 1341-1350.

Hitchcock, A. and Jacoby, G.C. 1980. Measurement of relative humidity in museums at high altitude. *Studies in Conservation* 25: 78-86.

Hublitz, I. 2000. *Engineering concepts for inflatable Mars surface greenhouses.* MS thesis. Division of Astronautics, Technische Universität München, Germany.

Incropera, F.P. and DeWitt, D.P. 2002. *Fundamentals of heat and mass transfer.* 5th Edition. John Wiley and Sons. New York, NY.

Iwabuchi, K.; Goto, E. and Takakura, T. 1996. Germination and growth of spinach under hypobaric conditions. *Environmental Control in Biology* 34(3): 169-178.

Iwabuchi, K. and Kurata, K. 2003. Short-term and long-term effects of low total pressure on gas exchange rates of spinach. *Advances in Space Research* 31: 241-244.

Kaplan, D. 1988. *Environment of Mars, 1988.* NASA Technical Memorandum 100470, NASA Johnson Space Center, Houston, TX.

Kaplan, D.; Baird, R. S.; Flynn, H.F.; Ratliff, J.E.; Baraona, C.R.; Jenkins, P.P.; Landis G.A.; Scheimann, D.A.; Johnson K.R.; and Karlmann, P.B. 2001. The 2001 Mars in-situ-propellant-production precursor (MIP) flight demonstration: Project objectives and qualification test results. *Space 2000 Conference and Exposition.* AIAA-2000-5145. Long Beach, CA.

Kennedy, K. J. 1999. Inflatable habitats & greenhouse design: Technology & development for Mars implementation. In: R.M. Wheeler and C. Martin-Brennan (eds.) *Mars greenhouses: Concepts and challenges.* NASA Technical Memorandum 208577. NASA Kennedy Space Center, FL.

Lacey, R.; Drew, M.; and Spanarkel, R. 2000. Low pressure systems for plant growth. In: R.M. Wheeler and C. Martin-Brennan (eds.) *Mars greenhouses: Concepts and challenges.* NASA Technical Memorandum 208577. NASA Kennedy Space Center, FL.

Langhans, R.W. and Tibbitts, T.W. 1997. *Plant growth chamber handbook.* North Central Regional Research Publication No. 340. Iowa Agriculture and Home Economics Experimental Station Special Report No. 99.

Mu, Y. 2005. *A distributed control system for low pressure plant growth chambers.* Ph.D. Dissertation. University of Florida.

Musgrave M.E.; Gerth W.A.; Scheld H.W. and Strain B.R. 1988. Growth and mitochondrial respiration of mungbeans (*Phaseolus aureus* Roxb.) germinated at low pressure. *Plant Physiology* 86: 19-22.

National Aeronautics and Space Administration (NASA). 2002. *Advanced life support project plan.* JSC-39168 (CTSD-ADV-348, Revision C). National Aeronautics and Space Administration, Lyndon B. Johnson Space Center, Houston, TX.

National Aeronautics and Space Administration (NASA). 2004. *Mars fact sheet.* Accessed online 22 January 2005: http://nssdc.gsfc.nasa.gov/planetary/factsheet/marsfact.html

Quebedeaux, B. and Hardy, R.W.F. 1973. Oxygen as a new factor controlling reproductive growth. *Nature* 243: 477–479.

Rettberg, P.; Rabbow, E; Panitz, C. and Horneck, G. 2004. Biological space experiments for the simulation of Martian conditions: UV radiation and Martian soil analogues. *Advances in Space Research* 33: 1294–1301.

Rygalov, V.Y.; Bucklin, R.A.; Fowler, P.A. and Wheeler, R.M. 2000. Preliminary estimates of possibilities for deployable greenhouse for a planetary surface (Mars). In: R.M. Wheeler and C. Martin-Brennan (eds.) *Mars greenhouses: Concepts and challenges.* NASA Technical Memorandum 208577. NASA Kennedy Space Center, FL.

Rygalov, V.Y.; Fowler, P.A.; Metz, J.M.; Wheeler, R.M. and Bucklin, R.A. 2002. Water cycles in closed ecological systems: Effects of atmospheric pressure. *Life Support & Biosphere Sciences* 8(3/4): 125-135.

Shallcross, D.C. 1997. *Handbook of psychrometric charts*. Humidity diagrams for engineers. Black Academic and Professional. London, UK.

Schwartzkopf, S.H. and Mancinelli, R.L. 1991, Germination and growth of wheat in simulated Martian atmospheres. *Acta Astronautica* 25: 245-247.

Spanarkel, R. and Drew, M.C. 2002. Germination and growth of lettuce *(Lactuca sativa)* at low atmospheric pressure. *Physiologia Plantarum* 116: 468-477.

Tibbitts, T. W. 1979. Humidity and plants. *BioScience* 29(6): 358-363.

Wheeler, R.M. 2000. Can CO_2 be used as a pressurizing gas for Mars greenhouses? In: R.M. Wheeler and C. Martin-Brennan (eds.) *Mars greenhouses: Concepts and challenges.* NASA Technical Memorandum 208577. NASA Kennedy Space Center, FL.

Wheeler, R.M.; G.W. Stutte; G.V. Subbarao and N.C. Yorio. 2001. Plant growth and human life support for space travel. In: M. Pessarakli (ed.) *Handbook of plant and crop physiology*. 2nd Edition: 925-941.

Wilkerson, E.G. 2005. *Plant evapotranspiration in a greenhouse on Mars.* Ph.D. Dissertation. University of Florida.

BIOGRAPHICAL SKETCH

Inka Hublitz was born on August 2nd, 1975, in Bavaria's Capital "München" (Munich), Germany. In 1994 she enrolled in mechanical engineering at the Technical University of Munich (TUM). While studying in Munich she participated in the LunarSat Project, the ambitious plan to send a micro orbiter, built by various universities, to the Moon. As Inka was always interested in other cultures and languages she studied two semesters as an exchange student at the University of Córdoba, Argentina.

Inka did the research for her master's thesis on "Engineering Concepts for Inflatable Mars Surface Greenhouses" during a six month stay at NASA's Johnson Space Center in Houston, Texas. During her research she met her Ph.D. advisor, Prof. Ray A. Bucklin. In 2000 she graduated with a "Diplom Ingenieur" degree (equivalent to US bachelor and master's Degree) in mechanical engineering.

After her graduation, Inka accepted a position at the Brazilian Space Research Institute INPE in São Paulo, Brazil, where she worked in the thermal division of the satellite integration and test laboratory.

In 2001 she decided to venture back to the United States and to pursue a Ph.D. degree in Agricultural and Biological Engineering at the University of Florida. During her Ph.D. program she was the leader of University of Florida's team participating in NASA's MarsPort engineering competition. Her team won an award for being one of six finalists in the nationwide competition.

In 2004 she was awarded a scholarship by the German and European Space Agency to participate at the Summer Session Program of the International Space University in Adelaide, Australia.

After the completion of her Ph.D. degree, Inka is looking forward to new adventures and challenges, hopefully adding numerous countries and new fields of interest to her long list.